INFORMATION TO USERS

This manuscript has been reproduced from the microfilm master. UMI films the text directly from the original or copy submitted. Thus, some thesis and dissertation copies are in typewriter face, while others may be from any type of computer printer.

The quality of this reproduction is dependent upon the quality of the copy submitted. Broken or indistinct print, colored or poor quality illustrations and photographs, print bleedthrough, substandard margins, and improper alignment can adversely affect reproduction.

In the unlikely event that the author did not send UMI a complete manuscript and there are missing pages, these will be noted. Also, if unauthorized copyright material had to be removed, a note will indicate the deletion.

Oversize materials (e.g., maps, drawings, charts) are reproduced by sectioning the original, beginning at the upper left-hand corner and continuing from left to right in equal sections with small overlaps. Each original is also photographed in one exposure and is included in reduced form at the back of the book.

Photographs included in the original manuscript have been reproduced xerographically in this copy. Higher quality 6" x 9" black and white photographic prints are available for any photographs or illustrations appearing in this copy for an additional charge. Contact UMI directly to order.

UMI®

Bell & Howell Information and Learning
300 North Zeeb Road, Ann Arbor, MI 48106-1346 USA
800-521-0600

Dynamics and Modelling of the Oceanic Surface Boundary Layer

by

Konstantin Zahariev

B.Sc., University of Sofia, 1992

A Dissertation Submitted in Partial Fulfillment of the
Requirements for the Degree of
DOCTOR OF PHILOSOPHY
in the School of Earth and Ocean Sciences

We accept this dissertation as conforming
to the required standard

Dr. Chris Garrett
Supervisor (School of Earth and Ocean Sciences)

Dr. Ken Denman
Departmental Member (School of Earth and Ocean Sciences)

Dr. Andrew Weaver
Departmental Member (School of Earth and Ocean Sciences)

Dr. Norm McFarlane
Outside Member (Canadian Centre for Climate Modelling and Analysis)

Dr. Eric D'Asaro
External Examiner (University of Washington)

Abstract

The oceanic surface boundary layer is of great importance and interest as its dynamics provides for the exchange of energy, momentum, heat and matter between the atmosphere and the ocean. It is crucial to have a thorough understanding of physical processes that might have a significant influence on its properties and variability. In this study I consider several different facets of mixed layer/boundary layer dynamics.

One aspects concerns the consequences of the nonlinearity of the equation of state in mixed layer models. The nonlinearity of the equation of state gives rise to a term in the averaged surface buoyancy flux which can be comparable in magnitude to other terms. Its magnitude is shown to be proportional to the area enclosed by the seasonal cycle of sea-surface temperature T_s versus the oceanic heat content $\mathcal{H}$. The term always represents a buoyancy input into the ocean and is compensated exactly by the buoyancy loss via cabbeling (densification on mixing) whenever the mixed layer entrains water with different properties from below.

Another problem of interest is the role of the coherent wind-induced vortices, commonly known as Langmuir circulation, in generating the surface mixed layer. A simple parameterization of the mixing due to Langmuir circulation is examined in the light of an oceanic dataset. Some evidence for the validity of the parameterization is found, thus drawing attention to Langmuir's assertion that Langmuir circulation is one of the key physical processes in the oceanic boundary layer.

The third aspect of surface boundary layer dynamics explored is the mean effect on mixed layer entrainment of periodic vertical movement of isopycnals in the thermocline due to non-breaking internal waves (referred to as heaving). Seasonal model runs incorporating idealized heaving show that heaving can produce significant seasonal differences in sea-surface temperature compared to a reference case without heaving. It is inferred that by periodically stretching and compressing the mixed layer, heaving causes instabilities that result in additional entrainment of colder water from below. A heaving number R_H is proposed, and two parameterizations of heaving for use in mixed layer models are suggested.

Dr. Chris Garrett
Supervisor (School of Earth and Ocean Sciences)

Dr. Ken Denman
Departmental Member (School of Earth and Ocean Sciences)

Dr. Andrew Weaver
Departmental Member (School of Earth and Ocean Sciences)

Dr. Norm McFarlane
Outside Member (Canadian Centre for Climate Modelling and Analysis)

Dr. Eric D'Asaro
External Examiner (University of Washington)

Table of Contents

List of Tables vii

List of Figures viii

Acknowledgments xv

Dedication xvi

Chapter 1. Introduction 1

1.1 Motivation and outline 1

1.2 The oceanic surface boundary layer 3

1.2.1 Overview 3

1.2.2 Forcing 4

1.2.3 Processes 9

1.3 Observations 19

1.3.1 OWS Papa 19

1.3.2 LOTUS 20

1.3.3 MILE 20

1.3.4 PATCHEX 21

1.3.5 GATE, phase III 21

Chapter 2. Mixed layer models 23

2.1 Equations 23

2.2 The Price-Weller-Pinkel model 26

2.3 The Mellor-Yamada Level 2 model 31

2.4 Other models 33

Chapter 3. Nonlinear equation of state and apparent buoyancy flux 39

3.1 Introduction 39

3.2 Theory 41

3.2.1 Representation of the term involving $\overline{\alpha' Q'}$ 41

3.2.2 General properties of the seasonal cycle of T_s versus $\mathcal{H}$ 47

3.3 Seasonal cycle modelling – a test case 50

3.4 Calculation of the NES term from OWS Papa data 55

3.5 Discussion and conclusions 57

Chapter 4. Langmuir circulation and mixed layer deepening 61

4.1 Introduction 61

4.2 The LC criterion for ML deepening 63

4.3 Verification of the LC criterion using LOTUS data 66

4.4 Implications for upper ocean restratification 78

Chapter 5. Isopycnal heaving and its effect on entrainment 80

5.1 Introduction 80

5.2 Models and sensitivities to the background diffusivity K_{bg} . . . 81

5.2.1 A relationship between background diffusion and entrainment 83

5.2.2 Seasonal runs with a MY-2 model 86

5.3 Effects of isopycnal heaving on entrainment 91
5.3.1 A model with isopycnal heaving 91
5.3.2 Seasonal runs with different heaving parameters 98
5.3.3 A detailed look at a three-day period in the summer . . 104
5.3.4 Heaving number 110
5.4 Parameterizing heaving for use in mixed layer models 115
5.4.1 Heaving as an equivalent K_{bg} 115
5.4.2 Heaving as a correction to the dynamic stability criterion 119
5.5 Summary and conclusions 124

Chapter 6. Outlook 126

References 131

List of Tables

List of Figures

1.1 Some of the mechanisms affecting the turbulence in the oceanic surface boundary layer: Langmuir circulation, breaking surface waves, shear-induced turbulence, convection, breaking internal waves (redrawn from Thorpe (1985)). 10

1.2 A schematic of the nonlinear dependence of density of seawater on temperature. Warm water expands more than cool water contracts. If water with temperature $T1$, density $D1$, mixes with water with temperature $T2 > T1$, density $D2 < D1$, in equal volumes, the mixture, while of temperature $Tm = (T1+T2)/2$, will have density $D(Tm)$ larger than the mean density $Dm = (D1 + D2)/2$. 12

1.3 A schematic representation of Langmuir circulation (redrawn from Pollard (1977)). 14

1.4 Ten-day time series of isotherms versus depth and time, taken from the LOTUS dataset (Briscoe and Weller 1984; Bowers *et al.* 1986). The high-frequency variability in the isotherms' position in and below the seasonal thermocline at 20 metres depth is indicative of internal wave activity 17

3.1 A schematic of mixed layer deepening due to mechanical stirring and associated entrainment. A well mixed surface layer of depth h, temperature T, and a temperature jump ΔT across its base deepens, in time δt, to a depth $h + \delta h$, lowering its temperature by δT to $T - \delta T$. 44

3.2 The annual cycle of T_s versus $\mathcal{H}$ at OWS Echo (35°N, 48°W), modified from Gill and Turner (1976). 48

3.3 Idealized forcing with zero mean annual heat flux. Top: insolation Q_s, total heat loss Q_L (the sum of sensible, latent, and longwave), and net heat flux Q. Bottom: eastward wind stress τ_x. 51

3.4 The annual cycle of T_s versus $\mathcal{H}$ from model output, if the NES is excluded (upper solid lines), and including it (dashed lines). The pairs of lines for each case delineate the diurnal ranges. The lower curve shows the loop, with the NES but when the diurnal cycle is not resolved. The minimum annual heat content is a free parameter which does not enter the calculations of the NES term, and is set to zero. Each circle corresponds to the middle of a month. 53

3.5 (top) The daily range (i.e. daily minimum and daily maximum values) of mixed-layer depth h if the NES is excluded (solid lines) and including it (dashed lines); h is slightly larger on average in the NES case. (bottom) The daily range of sea-surface temperature T_s if the NES is excluded. Its inclusion results in slightly lower average T_s (not shown). 54

3.6 The annual cycle of T_s versus $\mathcal{H}$ for the year 1972 from OWS Papa data. The minimum annual heat content is set to zero. Each circle corresponds to the middle of a month. 58

4.1 A schematic diagram showing the interaction between Langmuir circulation and pre-existing stratification. I: the general problem, II: starting from a linear stratification, and III: starting from a two-layer stratification. Redrawn from LG97. 64

4.2 Time-series of the difference between the temperature at a depth of 0.6 m (considered a sea-surface temperature), and the temperature at a depth of 5 metres. The surface temperature is consistently lower by about $0.06^{\circ}C$ even at night when the upper ocean appeared well mixed. 68

4.3 Top (right) panel: an example of temperature contours and corresponding estimates of h (upper thick line) and h_{tr} (lower thick line); Bottom (left) panel: Forcing (wind speed and insolation) for the same period. 69

4.4 Comparison of the heat content estimates for the upper 51 metres of ocean as derived from temperature profiles (shaded) and as implied from the local surface heat fluxes (thick black). 71

4.5 The caption is on page 70 74

4.6 The caption is on page 70 75

4.7 The caption is on page 70 76

4.8 The caption is on page 70 77

5.1 Temperature profiles after 50-day runs with the MY-2 model for different background diffusivity values, and for forcing with zero mean total heat flux, constant eastward wind stress of 0.1 Pa. From right to left at the surface: initial profile; 50th day final profiles for $K_{bg} = 0; 1 \times 10^{-5}; 5 \times 10^{-5} m^2 s^{-1}$. 87

5.2 Idealized forcing with zero mean annual heat flux. Top: insolation Q_s, total heat loss Q_L (the sum of sensible, latent, and longwave), and total heat flux Q_T. Bottom: eastward wind stress τ_x. 89

5.3 Seasonal runs with MY-2 model for two different background diffusivity values: $1 \times 10^{-5} m^2 s^{-1}$ (middle), and $5 \times 10^{-5} m^2 s^{-1}$ (bottom). Compare the maximum seasonal SST at the end of summer with the reference ($K_{bg} = 0$ (top) case). 90

5.4 Ten-day time series isopycnal plot of depth versus time, from the LOTUS dataset. Note the coherent heaving movement of isopycnals regardless of depth. Also shown is the estimated mixed layer depth. 92

5.5 Seasonal runs with the PWP model for three different background diffusivity values: $0.7 \times 10^{-5} m^2 s^{-1}$ (1), $1 \times 10^{-5} m^2 s^{-1}$ (2), and $1.5 \times 10^{-5} m^2 s^{-1}$ (3). Also shown for comparison is the reference ($K_{bg} = 0$ (top) case). 95

5.6 One-day (year-day 202) modified PWP model output showing heaving isopycnals (thin lines) and mixed layer depth (thick black line). 97

5.7 Seasonal runs with a modified PWP model for two different amplitudes of isopycnal heaving: $A_w = 2.0m$ (1), and $A_w = 5.0m$ (2), with a fixed wave period T_w of 1.6 h. Those are compared to the reference (top) no-heaving case. 100

5.8 Mixed layer depth from a modified PWP model for two different amplitudes of isopycnal heaving: $A_w = 2.0m$ (top panel), and $A_w = 5.0m$ (bottom panel), with a fixed wave period T_w of 1.6 h. Those are compared to the mixed layer depth (daily range) for the reference case. 102

5.9 Seasonal runs with a modified PWP model for three different periods of isopycnal heaving: $T_w = 2.4\ h$ (1), $T_w = 1.2\ h$ (2), and $T_w = 0.4\ h$ (3), with a fixed wave amplitude of A_w of $2.0m$. Those are compared to the reference (top) no-heaving case. 103

5.10 Mixed layer depth from a modified PWP model for two different periods of isopycnal heaving: $T_w = 1.2\ h$ (top panel), and $T_w = 0.4\ h$ (bottom panel), with a fixed wave amplitude A_w of 2.0 m. Those are compared to the mixed layer depth (daily range) for the reference case. 105

5.11 Contour plots of depth versus time, for days 200-202. Top panel: mean (over a heaving period) temperature contours for the reference case (no heaving). Bottom panel: mean temperature contours for a heaving case with an amplitude of 2 metres and a period of 1.6 hours. The plots show the upper 20 metres of model ocean. . . 107

5.12 Contour plot of depth versus time, for days 200-202, of the mean temperature difference (over a heaving period) between the reference case (no heaving) and a heaving case with an amplitude of 2 metres and a period of 1.6 hours. The plot shows the upper 20 metres of model ocean. The mixed layer depth for the reference case is shown in white. 108

5.13 Seasonal runs with a modified PWP model for a heaving with $A_w = 2.0\ m$ and $T_w = 1.6\ h$: original run with continuous heaving (1) and a run with heaving switched off from 8:00am to 4:00pm each day (2). The no-heaving case is also shown for reference. 111

5.14 Values of ΔT_s^{max} for pairs of data-points with the same heaving number R_H but different nondimensional frequency T_D/T_w. Pairs of points are denoted by the same symbol. Pairs: "o", $R_H = 1.64$; "+", $R_H = 2.22$; "$\triangle$", $R_H = 2.82$; "$*$", $R_H = 4.47$; "$\square$", $R_H = 7.69$. 114

5.15 Dependence of the scaled maximum seasonal SST difference $\zeta_{\Delta T}$ on the heaving number R_H (top panel), and on the scaled background diffusivity R_K (bottom panel), with corresponding interpolated values (dashed lines; in the top panel the dashed line indicates a crude piece-wise linear interpolation). 116

5.16 Correspondence between the scaled background diffusivity R_K and the heaving number R_H (top panel), and equivalent background diffusivity K_{bg} (in $m^2 s^{-1}$) as a function of R_H (bottom panel), with corresponding interpolated values (dashed lines, indicating a crude piece-wise linear interpolation). 118

5.17 Dependence of the scaled maximum seasonal SST difference $\zeta_{\Delta T}$ on the critical Richardson number Rb_{cr} (top panel), and a correspondence between the stability adjustment factor ξ_{Rb} and the heaving number R_{H} (bottom panel), with corresponding interpolated values (dashed lines; in the bottom panel the dashed line indicates a crude piece-wise linear interpolation). 121

5.18 A comparison between seasonal $\mathcal{H} - T_s$ curves for a heaving run (black line) with $R_{\mathrm{H}} = 3.0$ and a diffusivity run with an equivalent background diffusivity of $K_{\mathrm{bg}} = 0.8 \times 10^{-5} m^2 s^{-1}$ (top panel). The bottom panel shows a comparison between the same heaving run (black line) and an adjusted critical Richardson number run with the equivalent stability adjustment factor of $\xi_{\mathrm{Rb}} = 3.6$. 123

Acknowledgments

I would like to thank my supervisor Dr. Chris Garrett for his guidance and generous support. I also thank my external examiner, Dr. Eric D'Asaro, and the members of my committee, Dr. Ken Denman, Dr. Andrew Weaver, and Dr. Norm McFarlane, for their support and for valuable comments and suggestions. I thank my family for their love and support. I would also like to thank the University of Victoria for a Graduate Fellowship.

Dedication

To my grandfather, Kiril Georgiev Tsenoff.

Chapter 1

Introduction

1.1 Motivation and outline

Oceanic and atmospheric variability fascinates with its complexity on any temporal and spatial scale. The oceanic surface boundary layer[1] is of particular importance and interest, as its dynamics provides for the exchange of energy, momentum, heat and matter between the atmosphere and the ocean. Its seasonal variability controls the exchange of heat with the thermocline. The properties and dynamics of the mixed layer influence chemical and biological processes in the ocean; almost all biological activity takes place in the upper layer of the ocean. Mixed layer dynamics governs the sea-surface temperature and thus the fluxes of heat, moisture, and gases to the atmosphere; it is one of the most important factors determining climate.

Consequently, it is crucial to have a thorough understanding of physical processes that might have a significant influence on the properties and variability of the surface boundary layer. In this study I consider several different facets of mixed layer/boundary layer dynamics.

[1] The terms "oceanic surface boundary layer", "surface boundary layer", "surface mixed layer", and "mixed layer" may be used interchangeably in this study. They denote the surface layer of water of quasi-uniform temperature, salinity, and buoyancy/density, but may also include the underlying thermocline depending on context. In the latter case, the term "boundary layer" is usually preferred.

One of the aspects I look at pertains to the consequences of the nonlinearity of the equation of state in mixed layer models. As noted by Garrett *et al.* (1993) for the Mediterranean Sea, the nonlinearity of the equation of state gives rise to an additional term in the averaged surface buoyancy flux which can be comparable in magnitude to the other terms. The term always represents a buoyancy input into the ocean even when the annual mean heat flux is zero, so a compensating buoyancy loss over the seasonal cycle must occur, via cabbeling (densification on mixing) whenever the mixed layer entrains water with different properties from below. A simple representation of the magnitude of this term is derived, relating it to the the seasonal cycle of sea-surface temperature T_s versus the oceanic heat content $\mathcal{H}$, and general properties of the seasonal cycle of T_s versus $\mathcal{H}$ are discussed[2].

Another problem in this area of interest is the role of the coherent wind-induced vortices, commonly known as Langmuir circulation, in establishing and maintaining the surface mixed layer. Following up work by Li and Garrett (1997) on a simple parameterization of the mixing due to Langmuir circulation from which a Langmuir circulation criterion was derived for use in bulk mixed layer models, I collaborated with the authors to verify their formulation by directly examining an oceanic dataset, looking for mixed layer deepening events that did not appear to be caused by shear instability at the base of the mixed layer but were predicted with the new criterion. Implications for seasonal and daytime ocean restratification are also discussed[3].

[2]This research was published as Zahariev and Garrett (1997).

[3]This research was published as Li, Zahariev, and Garrett (1995).

The third aspect of surface boundary layer dynamics I explore is the mean effect on mixed layer entrainment of periodic isopycnal up-down movement in the thermocline due to non-breaking internal waves (henceforth referred to as "heaving"). Model output, such as sea-surface temperature, from one-dimensional mixed layer models shows that models are sensitive to the value of background diffusivity K_{bg} used below the mixed layer, in the thermocline. It is thus important to establish whether K_{bg} represents mixing processes in the thermocline or is a proxy for processes omitted from the models. One such process is isopycnal heaving. I examine the sensitivity of the mean entrainment rate to the heaving at the base of the mixed layer by considering a modification of the Price *et al.* (1986) mixed layer model that allows for periodic isopycnal displacement superimposed on the other variability. Results from seasonal runs with this model and idealized forcing are presented, along with estimates of the equivalent background diffusivity. A heaving number R_H to characterize heaving is proposed, and two parameterizations of heaving for use in mixed layer models are suggested.

1.2 The oceanic surface boundary layer

1.2.1 Overview

The ocean typically manifests a surface boundary layer in which turbulent mixing driven from above by surface fluxes of buoyancy and momentum and from below by shear at the base of the layer creates a quasi-uniform stratification within it. Thus it is conventionally referred to as a "mixed layer", although observations frequently reveal the existence of velocity shear within the layer (e.g. Davis *et*

al. (1981a), Weller and Plueddemann (1996)) indicating imperfect mixing and/or the presence of organized structures (e.g. Smith *et al.* (1987)).

Throughout the course of a year, the mixed layer executes a characteristic seasonal cycle, varying its thickness in response to the forcing. In the winter, it deepens because of heat loss at the surface; in the spring progressively shallower mixed layers are formed under conditions of net ocean heating until a new seasonal thermocline is formed for the year. On top of this variability, each diurnal period a shallow mixed layer may be formed in the daytime because of strong penetrating solar heating, deepening at night back to its seasonal depth. The depth of mixing can also vary with geographical location. Especially in the winter, it could be as little as 50 metres in the subtropics and as much as 500 metres or more in the northern North Atlantic ocean.

This study focuses on the mid-latitude mixed layer, away from equatorial and polar regions. Moreover, it considers open ocean conditions away from lateral boundaries and horizontal variability, so that a one-dimensional (1-D) model in the vertical of local forcing and response can be adequately applied. In addition, salinity/freshwater variability is not considered.

1.2.2 Forcing

The oceanic surface boundary layer is forced by fluxes of heat, momentum, and freshwater.

The upper ocean gains heat by absorption of solar radiation in the daytime, and (normally) loses heat from the surface due to turbulent transfer via sensible and latent heat heat fluxes, and due to long-wave radiation.

The sensible heat flux

$$Q_h = \rho_a C_{pa} \overline{w'T'}, \tag{1.1}$$

where ρ_a, C_{pa} are air density and specific heat, respectively, results from a turbulent transfer of heat to/from the atmosphere, depending on the sign of the surface temperature difference between the atmosphere and the ocean. Since the air turbulence near the surface is largely caused by shear, the rate of sensible heat transfer depends also on wind speed. Thus, on dimensional grounds, Q_h is parameterized by a "bulk" (i.e. involving averaged quantities) formula (Smith 1980; Large and Pond 1982; Smith 1988)

$$Q_h = \rho_a C_{pa} c_{\mathrm{H}} U_{10} (T_s - T_a), \tag{1.2}$$

where c_{H} is a dimensionless coefficient, U_{10} the wind speed at 10 metres height, T_s the sea-surface temperature, T_a the 10-meter air temperature. Under moderate wind conditions with wind speeds of $5 - 25\ ms^{-1}$, which often prevail over the ocean, the atmospheric boundary layer is nearly neutrally stratified. Different values/formulae for the neutral c_{H} have been suggested; e.g. Smith *et al.* (1980) suggests

$$10^3 c_{\mathrm{H}} = \begin{cases} 0.83 & \text{for stable conditions } (T_s < T_a), \\ 1.10 & \text{for unstable conditions } (T_s > T_a). \end{cases} \tag{1.3}$$

Typical mean values of Q_h are in the range $10 - 20\ Wm^{-2}$ (Nurser 1996), and could constitute heat loss or heat gain by the ocean depending on the sign of the air-sea temperature difference.

The latent heat flux

$$Q_e = L_{\mathrm{V}}\overline{w'q'}, \tag{1.4}$$

where L_{V} is the latent heat of vaporization and q is humidity, results from evaporation of water, taking heat away from the ocean. Again on dimensional grounds the evaporation rate is parameterized as

$$E = \rho_a c_{\mathrm{E}} U_{10}(q_s - q_a), \tag{1.5}$$

where c_{E} is a dimensionless coefficient, q_s is the saturation value of the specific humidity at temperature T_s, q_a is the specific humidity of air at 10 metres. Smith (1980) suggests for the neutral c_{E}

$$10^3 c_{\mathrm{E}} = 1.5 \tag{1.6}$$

but later revises it to

$$c_{\mathrm{E}} = 1.2 c_{\mathrm{H}} \tag{1.7}$$

(Smith 1988). The latent heat of vaporization is

$$L_{\mathrm{V}} = 2.5008 \times 10^{6} - 2.3 \times 10^{3} T \ [Jkg^{-1}] \tag{1.8}$$

where T is the water temperature (Gill 1982). Thus the latent heat flux is

$$Q_e = L_{\mathrm{V}} E = L_{\mathrm{V}} \rho_a c_{\mathrm{E}} U_{10} (q_s - q_a). \tag{1.9}$$

A typical mean value of Q_e is 100 Wm^{-2} or more (Nurser 1996), and constitutes heat loss by the ocean.

The long-wave radiation heat flux is the result of emission of infrared radiation by the ocean. It is parameterized as a flux emitted by a black body, corrected for the departure of the ocean from a black body behaviour, for atmosphere moisture, and for cloudiness. An example is

$$Q_b = \epsilon \sigma {T_s}^4 (0.39 - 0.05 {e_a}^{1/2})(1 - 0.6 {n_c}^2), \tag{1.10}$$

where $\epsilon = 0.985$ is the estimated ocean emissivity, σ is Stefan's constant, e_a is the 10-metre vapour pressure, n_c is the fraction of sky covered by clouds (Gill 1982). Typical mean values of Q_b are in the range $30 - 70$ Wm^{-2}, and always represent heat loss by the ocean.

Solar radiation is a source of heat for the ocean. The incoming solar radiation can be estimated by empirical formulae involving the solar constant and corrections for atmospheric scattering, oceanic reflection, and cloudiness (Reed 1977;

Dobson and Smith 1988). Furthermore, the insolation is absorbed with depth depending on water clarity, with the red spectral components absorbed within the upper 1 metre of ocean, and the rest penetrating deeper. Parameterizations of this absorption profile involve an exponential depth dependence. This can be a single exponential fit (Ivanoff 1977), the more commonly used 2-exponent fit (Paulson and Simpson 1977), 3-exponent fit (Woods *et al.*1984) or a fit with even more exponents (Simpson and Dickey 1981; Woods 1980). Using more exponents would typically improve the accuracy of the fit near the surface, in the top 5 metres of ocean.

The ocean surface gains momentum by turbulent transfer from the atmosphere via the wind stress

$$\tau = -\rho_a \overline{w' \mathrm{u}'}, \tag{1.11}$$

virtually all of which goes into driving the mean current (Richman and Garrett 1977), imparting a "friction velocity"

$$u_* = \left(\frac{|\tau|}{\rho_w}\right)^{1/2} \tag{1.12}$$

where ρ_w is the density of water. Starting with Taylor (1916), the drag of the atmosphere against the sea surface is conventionally parameterized as

$$|\tau| = \rho_a c_D U_{10}^{\ 2}, \tag{1.13}$$

where c_D is a dimensionless drag coefficient dependent on wind speed and on atmospheric stability. Different formulae for the neutral c_D have been suggested, e.g. Smith (1980) suggests

$$10^3 c_D = 0.61 + 0.063 U_{10} \quad \text{for } 6 ms^{-1} < U_{10} < 22 ms^{-1} \tag{1.14}$$

which is very close to a more recent formula by Yelland and Taylor (1996). A typical wind stress value is 0.1 Nm^{-2} for U_{10} of $8 - 9\ ms^{-1}$.

The upper ocean is also forced by a freshwater flux, with rain and ice melting being a freshwater source, and evaporation and freezing being a freshwater sink for the ocean.

1.2.3 Processes

The upper ocean is host to a variety of processes, some of which are schematically depicted in Fig. 1.1. Here I will describe briefly only the processes considered in subsequent chapters.

Cabbeling

The equation of state for seawater is nonlinear, that is to say the density ρ is a nonlinear function of temperature T, salinity s, and pressure p (Millero and Poisson 1981). For the upper ocean at temperate latitudes the temperature dependence is the most important one. The temperature expansion coefficient increases with T, so warm water expands more than cool water contracts. This

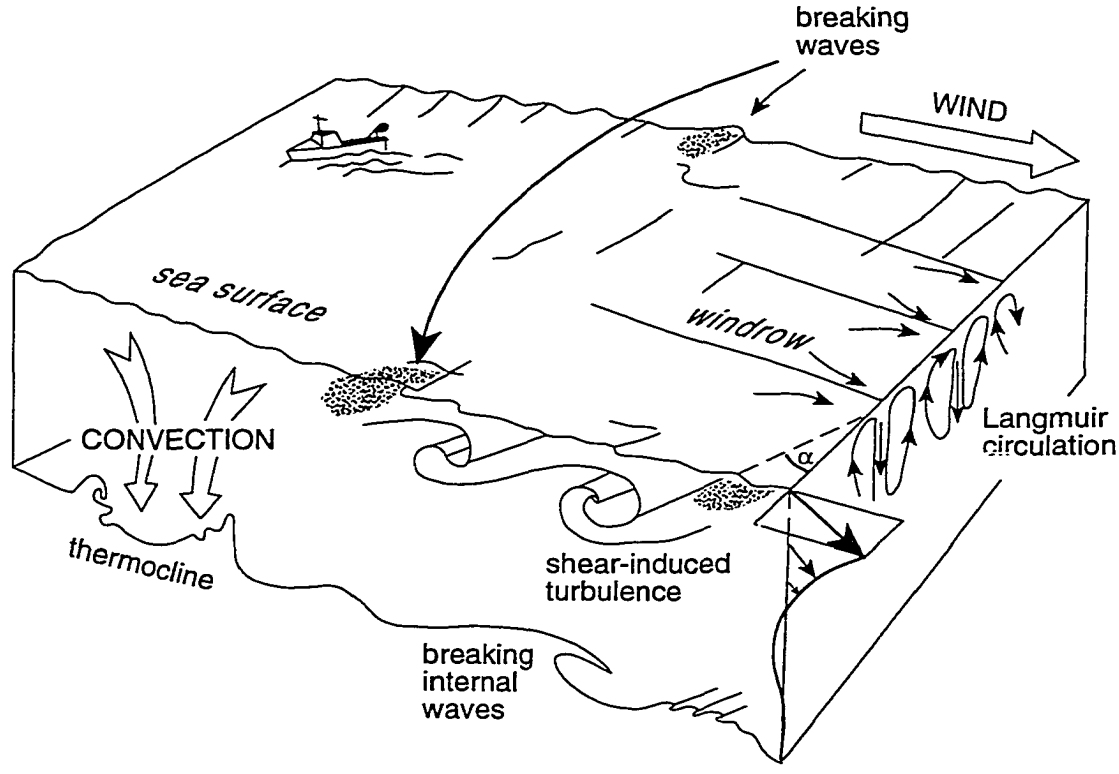

Fig. 1.1. Some of the mechanisms affecting the turbulence in the oceanic surface boundary layer: Langmuir circulation, breaking surface waves, shear-induced turbulence, convection, breaking internal waves (redrawn from Thorpe (1985)).

nonlinearity means that if equal volumes of two water masses of different properties are mixed, the resulting mixture, while having their mean temperature, will have a density larger than their mean density (Fig. 1.2). In the special case when the two water masses have different salinities and temperatures but the same or nearly the same density, the resulting mixture will be heavier than both and will tend to sink. Apparently Witte (1902) was the first to recognize the possible importance of this phenomenon (Foster 1972), visualizing a frontal situation when the two water masses are juxtaposed and lateral mixing occurs, causing sinking in a narrow region between them. The same setup was considered also by Garrett and Horne (1978). However, cabbeling need not occur only in horizontal fronts. Indeed, it occurs whenever there is mixing of water of different properties, e.g. whenever the mixed layer entrains colder water from below. Cabbeling might be important for the formation of the densest ocean water, e.g. in the formation of the Atlantic Bottom Water in the Weddell Sea (Foster 1972). The salinity contribution to cabbeling opposes that of temperature, but is typically 2 orders of magnitude smaller (Kilmatov and Kuzmin 1991).

Langmuir circulation

In 1927, while crossing the Atlantic Ocean, the chemist Irwing Langmuir observed floating seaweed arranged in streaks roughly parallel to the wind direction, and with a spacing of 100 to 200 metres between them. In subsequent years he made a series of experiments in a lake, and showed (Langmuir 1938) that these streaks are manifestations of a subsurface organized structure — pairs of counter-rotating vortices with axes nearly parallel to the wind direction, and with

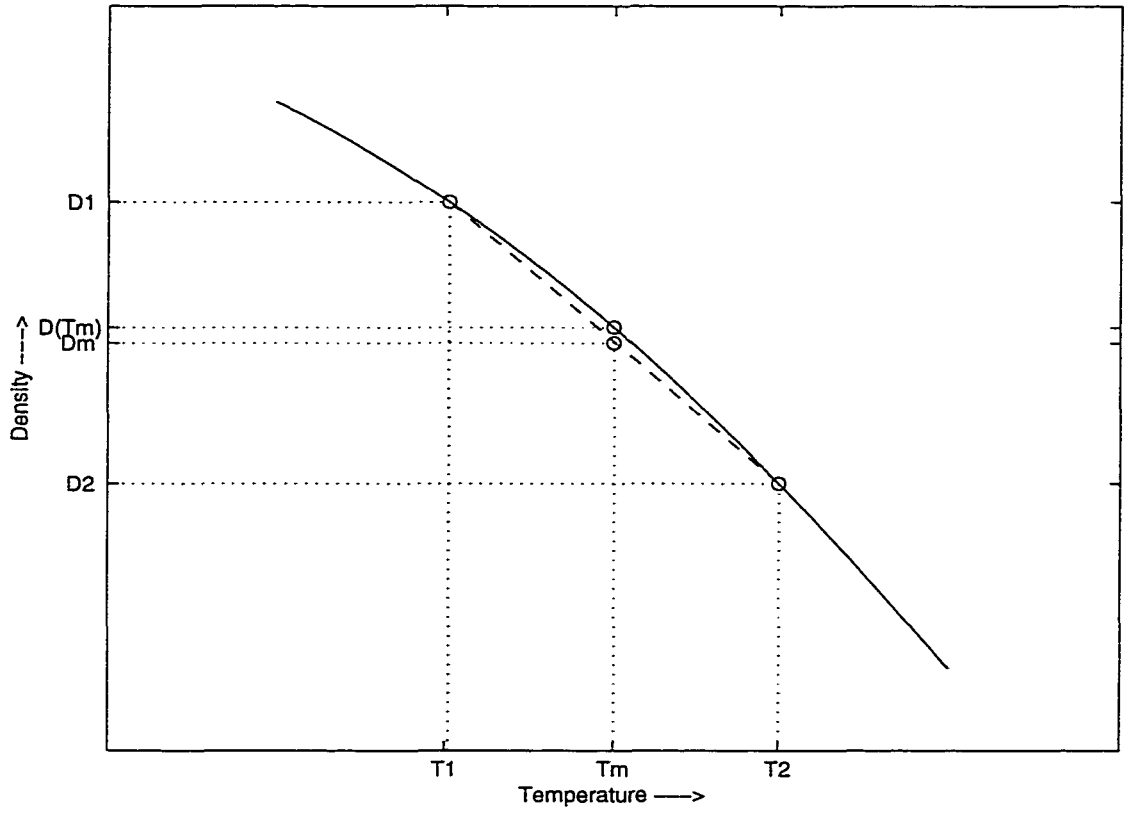

Fig. 1.2. A schematic of the nonlinear dependence of density of seawater on temperature. Warm water expands more than cool water contracts. If water with temperature $T1$, density $D1$, mixes with water with temperature $T2 > T1$, density $D2 < D1$, in equal volumes, the mixture, while of temperature $Tm = (T1+T2)/2$, will have density $D(Tm)$ larger than the mean density $Dm = (D1 + D2)/2$.

downwelling regions between the rolls (hence surface convergences and streaks of flotsam above them). Langmuir concluded from his experiments that these vortices, later named after him, "apparently constitute the essential mechanism by which the [mixed layer] is produced". Furthermore, envisioning mixed layer entrainment due to this Langmuir circulation (LC), he stated that the "currents thus set up at the bottom of the [mixed layer] may sweep off the upper part of the thermocline, making it thin and of increased gradient".

After many years of observations (in lakes and in the ocean, more recently in 1982 and 1990 off the coast of California (Smith 1992; Plueddemann *et al.*1996)), the conceptual picture for these subsurface vortices has remained largely as described by Langmuir. Fig. 1.3 presents a schematic diagram of LC by Pollard (1977). The spacing between streaklines, or "windrows", can range from 2 to hundreds of meters (Leibovich 1983). Observations (e.g. Weller and Price (1988)) and modelling (e.g. Skyllingstad and Denbo (1995)) suggest that, as time progresses, smaller-scale cells are swept into the larger scale, while at the same time new small-scale cells form. The horizontal scale for the spacing, at least of the largest cells, is generally assumed to correlate with the depth of the thermocline, i.e. the cells have an aspect ratio of O(1) and penetrate to the base of the mixed layer (ML). Some observations (e.g. Smith (1992)) have confirmed this, while others (e.g. Weller and Price (1988)) have found that LC is confined to the upper half of the ML. The localized downwelling velocities below the streaks are from 0.03 to 0.20 ms^{-1} (Weller and Price 1988), sometimes more (Pollard and Thomas 1989). The upwelling is significantly slower and broader. There is a characteristic downwind surface horizontal jet. LC is always nearly aligned with the wind, and if the

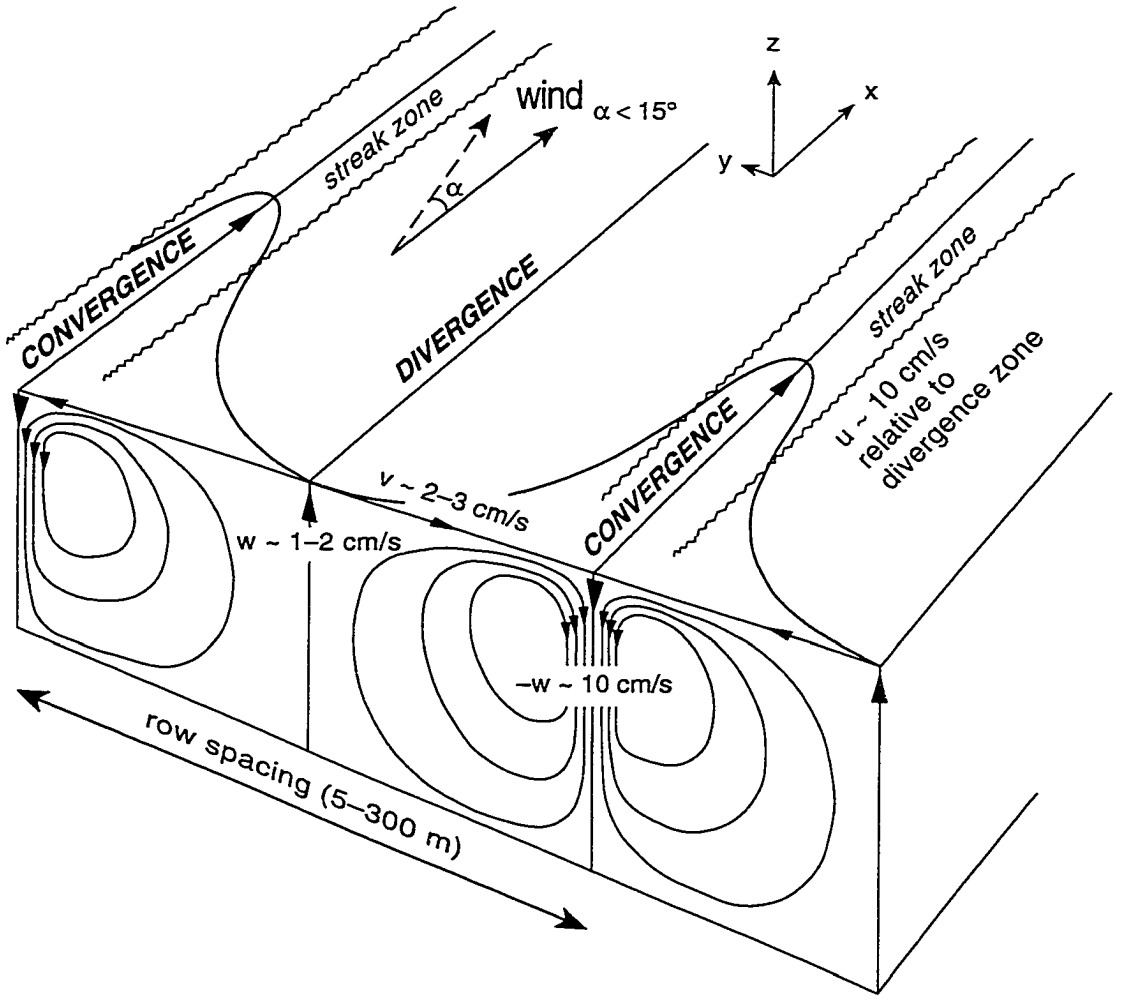

Fig. 1.3. A schematic representation of Langmuir circulation (redrawn from Pollard (1977)).

wind suddenly changes direction, LC gets reoriented in the new direction within a few minutes to about half an hour, with smaller scale LC reorienting more quickly than larger scale LC. These times are also indicative of the formation times for LC (Leibovich 1983).

Many theories for the formation of LC have been proposed, but the commonly accepted theory is that of Craik (1977) and Leibovich (1977a). It relies on an interaction between a sheared horizontal current and the surface waves, and involves an instability of an infinitesimal downwind jet with its induced vertical vorticity of alternating sign on both sides. The Stokes drift, which decays vertically with depth, tilts these vorticities and thus creates the pairs of rolls with downwelling in between. This pattern gets reinforced, as water moving towards the surface convergence line gets accelerated by the wind stress which in turn leads to more downwelling, intensification of the circulation, and stronger horizontal surface jet.

Internal waves

Gravity waves in the interior of the ocean are commonplace. In analogy to surface gravity waves, one can think of a disturbance of an interface between two layers of slightly different densities which will feel the restoring force of gravity (although much reduced because of the similar densities) and reverse direction, overshoot its equilibrium position, and so on, resulting in wave propagation. However, internal waves can be supported in any continuously varying stable stratification. Because the restoring force is much weaker than in the case of surface waves, internal waves have spatial scales and time scales which are typically much

larger. Away from the upper ocean, typical internal waves have vertical displacements of the order of tens of meters and periods from tens of minutes to many hours (Garrett and Munk 1979). In the upper ocean, internal waves typically have smaller amplitudes and shorter periods (Pinkel 1975; Käse and Clarke 1978; Dillon and Caldwell 1980; Levine *et al.*1983), but are still large compared with surface waves (Fig. 1.4). Internal waves are commonly manifested in single-sensor observations as short period fluctuations in the temperature (Munk 1981). Nansen (1902) might have been the first to report them. Attributing these temperature fluctuations to internal waves, and thus estimating their instantaneous vertical velocity by $w = -(\partial T/\partial t)/(\partial T/\partial z)$ assumes no significant horizontal advection and/or diffusion (Briscoe 1975).

The equations for a Boussinesq fluid (Boussinesq 1903; Spiegel and Veronis 1960) of varying stratification with buoyancy frequency $N(z)$ lead to the dispersion relation (Phillips 1977)

$$\omega^2 = N^2 \cos^2\theta + f^2 \sin^2\theta, \tag{1.15}$$

where ω is the internal wave frequency, f is the local inertial frequency, θ is the angle to the horizontal of the vector wavenumber. Varying θ from 0 to $\pi/2$, thus internal waves can exist only in the range of frequencies

$$f \leq \omega \leq N. \tag{1.16}$$

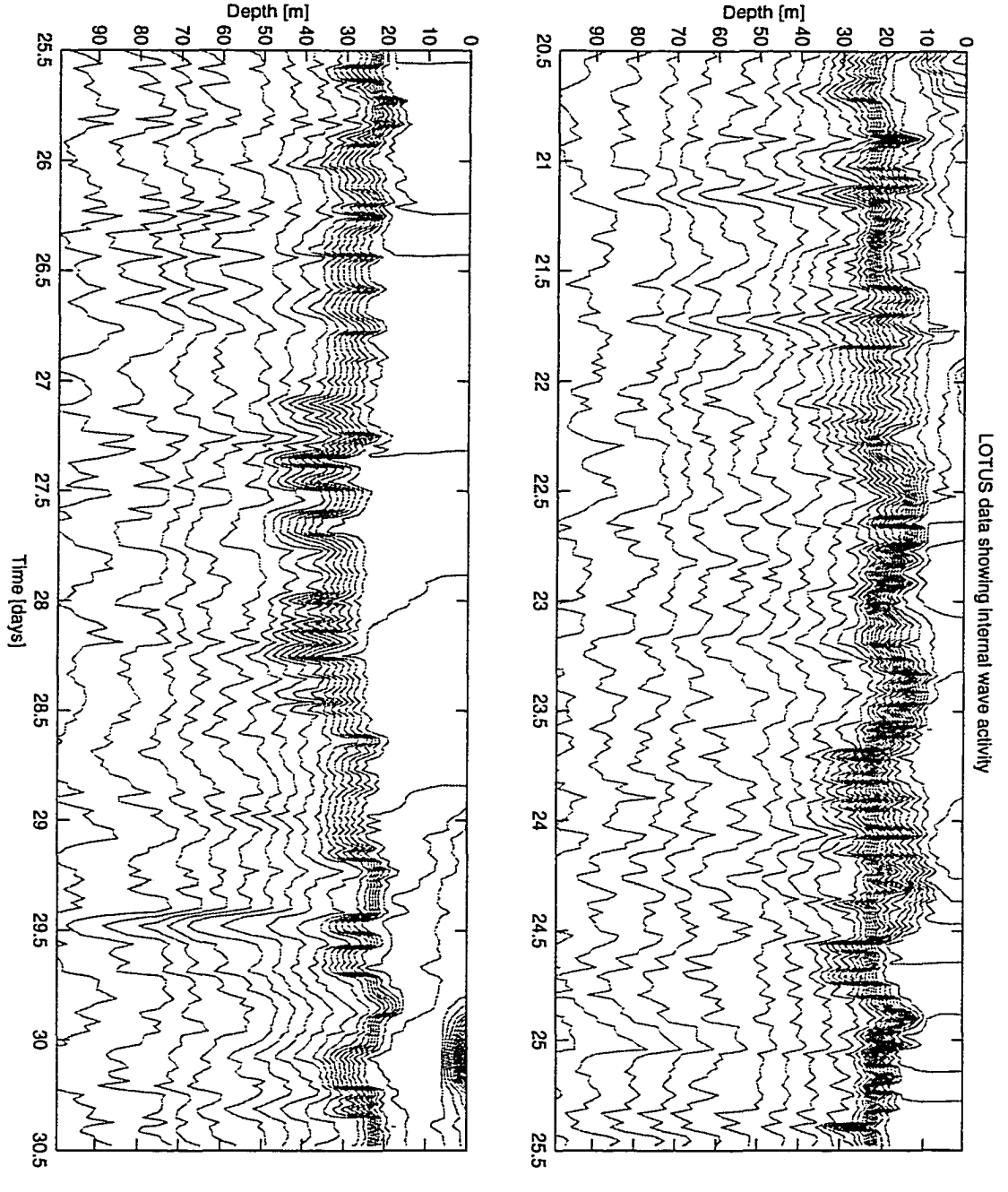

Fig. 1.4. Ten-day time series of isotherms versus depth and time, taken from the LOTUS dataset (Briscoe and Weller 1984; Bowers *et al.* 1986). The high-frequency variability in the isotherms' position in and below the seasonal thermocline at 20 metres depth is indicative of internal wave activity

Garrett and Munk (1975), using many different observations of internal wave activity in the ocean away from the upper layer, compiled a representation of the distribution of internal wave energy in wavenumber and frequency space, subsequently called the GM spectrum. After tests and refinements it was concluded that the observed characteristics of deep-ocean internal waves are nearly universal in space and time, thus the GM spectrum can be regarded as a universal equilibrium spectrum, the result of a dynamic balance between wave generation, interaction, and dissipation. In the upper ocean, where such an equilibrium is not to be expected due to the forcing and variability, the internal wave field of higher frequencies deviates from the GM spectrum, and exhibits high coherence with depth (Fig. 1.4).

Internal waves can be generated by a variety of mechanisms. Surface generation by the atmosphere could involve travelling pressure fields/fronts (Keller and Munk 1970; Polyanskaya 1969; Leonov and Miropolsky 1973), a travelling buoyancy flux (Magaard 1973), and a travelling wind stress field (Tomczak 1966; Tomczak 1967; Krauss 1972a; Krauss 1972b), the latter being the most plausible source (Thorpe 1975). Surface generation by interaction of pairs of surface waves with similar wavenumbers and frequencies is also possible (Thorpe 1966; Nesterov 1972; Brekhovskikh *et al.*1972). The steady flow of the stratified ocean over bottom topography is another source (Huppert and Miles 1969; Bell 1975), generating standing internal waves analogous to lee waves in the atmosphere. Tidal (barotropic) currents over topography can also generate internal waves of tidal frequency (Cox and Sandstrom 1962; Baines 1973; Bell 1975; Baines 1982). In the

ocean interior, internal waves can be generated and/or modified by wave-wave interactions (Olbers 1976; McComas and Bretherton 1977; Pomphrey *et al.*1980). Dissipation of internal waves could occur through shear instability (Thorpe 1973) and wave breaking (Orlanski and Bryan 1969; Orlanski and Ross 1973; Gargett and Holloway 1984), and also through viscous attenuation (LeBlond 1966).

1.3 Observations

I will briefly describe the sets of observations of the upper ocean which are referred to in subsequent chapters.

1.3.1 OWS Papa

Since 1952 (Tabata 1965), extensive oceanographic observations of the upper ocean were made by Canadian weatherships at Ocean Weather Station (OWS) "P" (50°N, 145°W) in the northeast Pacific Ocean, until the weatherships were retired in 1981. The data consist of meteorological observations and bathythermograph (BT) temperature records over many years at 3-hour intervals (the BT records are at 3-hour intervals since 1965). The meteorological observations consist of wind speed, wind direction, sea-surface temperature, air temperature, wet-bulb and dew-point temperatures, cloud cover, and surface air pressure. The BT temperature data are generally at 5-metre intervals from the surface to 295 m.

1.3.2 LOTUS

The Long-Term Upper-Ocean Study (LOTUS) experiment was conducted from May 1982 to May 1984 at 34°N, 70°W in the deep water over the Hatteras abyssal plane in the Sargasso Sea in the western subtropical Atlantic Ocean. The data consist of meteorological observations, temperature and current meter records (Briscoe and Weller 1984; Stramma *et al.*1986). These are divided into four periods of several months each, with gaps in between when the moorings were replaced and with other gaps caused by data losses. The meteorological observations consist of wind speed, wind direction, sea-surface temperature (at a depth of 0.6 m), air temperature, barometric air pressure, and directly measured insolation. The humidity measurements were unreliable. Mooring data consist of temperature and east and north currents generally at depths of 5, 10, 15, 20, 25, 35, 50, 65, 75, 100 metres and some in deeper water. Data are available at 15-minute intervals.

1.3.3 MILE

The MIxed Layer Experiment (MILE) was conducted from August 19 to September 6, 1977, at 49°37′N, 145°6′W, in the vicinity of OWS Papa. The data consist of meteorological observations, temperature and current meter records (Davis *et al.*1981a), and also two series of casts through the upper 200 metres of ocean with a microstructure profiler (Dillon and Caldwell 1980). The meteorological observations consist of wind speed, wind direction, sea-surface temperature, air temperature, wet-bulb and dew-point temperatures, surface air pressure, cloud cover, made every 3 hours, and solar radiation measurements made every 1 hour.

The MILE-1 mooring has complete 19-day records of temperature and east and north currents at depths of 11, 23, 26, 29, 32, 35, 41, 44, 47, 50, 75, 92, 125 and 175 metres and 16-day records at 20 and 38 metres. The MILE-2 mooring has complete records of temperature and east and north currents at depths of 5, 10, 15, 20, 42 and 54 metres. The data are available at 112.5-second intervals.

1.3.4 PATCHEX

The PATCHes EXperiment (PATCHEX) was conducted in October 1986 around 34°N, 127°W, 800 km west of Point Conception, off the coast of California. The data include meteorological observations, temperature and horizontal velocity records (Brainerd and Gregg 1993). The meteorological observations consist of wind speed, wind direction, sea-surface temperature, air temperature, wet-bulb and dew-point temperatures, cloud cover, surface air pressure, and insolation. An Advanced Microstructure Profiler recorded 11 days of temperature, conductivity, temperature gradient, and velocity fluctuations profiles down to 300 m, at an average rate of 2.4 profiles per hour. Relative current velocities were measured using an acoustic current meter, at a rate of 4 drops per day for the last 7 days.

1.3.5 GATE, phase III

The GARP Atlantic Tropical Experiment (GATE), phase III, was conducted from August 30 to September 19, 1974, at 9°N, 23°W in the Atlantic Ocean, to study internal waves in the upper ocean (Käse and Clarke 1978). The data consist of a triangular horizontal array of moorings, recording temperature and currents, and CTD profiles from a drifting ship. The CTD profiles reached

down to 500 m, at 3-hour intervals, and there were also some short-term CTD series from 20 to 70 m, at 108-second intervals. The data at the moorings are at 225-second intervals.

Chapter 2

Mixed layer models

I will present the approximate and simplified governing equations that are adequate for use in 1-D models of the upper ocean, and describe in more detail models referred to in subsequent chapters.

2.1 Equations

The full equations governing the evolution of the ocean are (Gill 1982):

The mass conservation equation

$$\rho^{-1}\frac{D\rho}{Dt} + \nabla \cdot \mathbf{u} = 0, \tag{2.1}$$

where $D/Dt \equiv \partial/\partial t + \mathbf{u} \cdot \nabla$ is the material derivative, $\mathbf{u}$ is the fluid's (vector) velocity, and ρ the density of the fluid.

The momentum equation

$$\frac{D\mathbf{u}}{Dt} + f(\mathbf{k} \times \mathbf{u}) = \rho^{-1}\nabla p - \mathbf{g} + \nu\nabla^2\mathbf{u}, \tag{2.2}$$

where f is the Coriolis parameter/inertial frequency, $\mathbf{k}$ the vertical coordinate unit vector, p the pressure, $\mathbf{g}$ the gravitational acceleration, ν the kinematic viscosity of the fluid.

The heat equation

$$\rho C_p \frac{DT}{Dt} - \alpha T \frac{Dp}{Dt} = \nabla \cdot (\chi \nabla T - F^{rad}) + \mathcal{Q}_H, \tag{2.3}$$

where T is the temperature, C_p the specific heat at constant pressure, $\alpha = -1/\rho(\partial\rho/\partial T)$ the temperature expansion coefficient at constant salinity and pressure, χ the thermal conductivity, F^{rad} the radiative flux, $\mathcal{Q}_H$ the heating due to a change of phase, chemical reaction, and viscous dissipation.

The salinity equation

$$\rho \frac{Ds}{Dt} = \nabla \cdot (\kappa_D \nabla s), \tag{2.4}$$

where s is the salinity, and κ_D is the salinity diffusivity.

The equation of state

$$\rho = \rho(p, s, T). \tag{2.5}$$

We can simplify these equations by making a number of approximations and/or assumptions based on the context in which they will be used, that is, for upper ocean modelling. Because both particle and phase speeds of disturbances are much smaller than the speed of sound, and also because the vertical scale of the motion is small compared to the scale height of the ocean, we assume incompressibility (Batchelor 1967), so $D\rho/Dt = 0$ and therefore (2.1) reduces to the continuity equation $\nabla \cdot \mathbf{u} = 0$; we also ignore pressure variations in the heat equation, and assume $C_p = const.$ Because the reference hydrostatically balanced

density varies little around its mean, and also because the motion-induced density variations are much smaller than the reference state density, we can make the Boussinesq approximation (Boussinesq 1903; Spiegel and Veronis 1960) and replace density in the equations with a constant reference density ρ_0 except when it gives rise to buoyancy ($b = -g\rho_0^{-1}(\rho - \rho_0)$) forces in the gravitational acceleration term. In addition, we make the boundary layer approximation that vertical gradients are much greater than horizontal gradients, and in fact completely drop horizontal gradients, assuming a local balance in the vertical as 1-D ML models do (Niiler and Kraus 1977). We are interested in the evolution of mean properties, and how they are affected in a mean sense by turbulence, so we perform Reynolds decomposition of all variables into mean and fluctuation parts. Molecular terms are also neglected as small compared with the other terms. Finally, the averaged equations for mean quantities are

$$\frac{\partial \overline{T}}{\partial t} = -\frac{\partial}{\partial z}\left(\overline{w'T'}\right) - \frac{1}{\rho_0 C_p}\frac{\partial I}{\partial z} \tag{2.6}$$

$$\frac{\partial \overline{s}}{\partial t} = -\frac{\partial}{\partial z}\left(\overline{w's'}\right) \tag{2.7}$$

$$\frac{\partial \overline{\mathbf{U}}}{\partial t} = -f(\mathbf{k} \times \overline{\mathbf{U}}) - \frac{\partial}{\partial z}\left(\overline{w'\mathbf{u}'}\right) \tag{2.8}$$

$$\rho = \rho(\overline{s}, \overline{T}), \tag{2.9}$$

where overlines denote averaging and mean quantities, and primes denote turbulent fluctuations. $I(z)$ is the vertical absorption profile for the insolation. In addition to these equations, the equation for the averaged turbulent kinetic energy (TKE) is also often used for calculating the amount of mixing and/or the entrainment

rate for a mixed layer. It is, under the same assumptions and approximations as above (Kraus 1972),

$$\frac{1}{2}\frac{\partial(q^2)}{\partial t} = -\overline{w'\mathbf{u}'}\cdot\frac{\partial\overline{\mathbf{U}}}{\partial z} + \overline{w'b'} - \frac{\partial}{\partial z}\overline{w'(q^2/2 + p'/\rho_0)} - \epsilon, \tag{2.10}$$

where $q^2 = \mathbf{u}'^2 + w'^2$ is twice the TKE per unit mass. The first term on the right-hand side of (2.10) is the rate of work by the Reynolds stress $\overline{w'\mathbf{u}'}$ on the mean shearing flow $\partial\overline{\mathbf{U}}/\partial z$; the second term is the rate of work of buoyancy forces; the third term is the convergence of the turbulent vertical flux; the fourth term is the dissipation rate of TKE. Henceforth overlines denoting mean quantities will be dropped, but implied.

2.2 The Price-Weller-Pinkel model

The model of Price, Weller, and Pinkel (1986), henceforth the PWP model, is a 1-D bulk mixed layer model, i.e. it assumes the existence of a well-mixed surface layer. The model solves equations (2.6 — 2.9) on a fine uniform vertical grid (e.g. with $\Delta z = 1\ m$), and employs stability criteria to establish, maintain, and evolve a mixed layer of uniform temperature, salinity, momentum, and density. In accord with the scope of this study, let us consider the salinity to be constant. The surface boundary conditions are

$$\overline{w'T'}(0) = -\frac{Q_L}{\rho_0 C_p}, \tag{2.11}$$

$$I(0) = -Q_s, \tag{2.12}$$

$$\overline{w'\mathbf{u}'}(0) = -\frac{\boldsymbol{\tau}}{\rho_0}, \tag{2.13}$$

where $Q_L = Q_b + Q_e + Q_h$ is the net heat flux (loss) from long-wave radiation, latent, and sensible fluxes, respectively; Q_s is the incoming solar radiation; τ is the vector wind stress. The turbulent fluxes at depth are not explicitly calculated, but are implicitly accounted for as a result of the adjustments by stability criteria. The absorption profile $I(z)$ for the penetration of solar radiation at depth is assumed to have a double exponent dependence (Paulson and Simpson 1977), i.e.

$$I(z) = I(0)\left[r\exp(z/\beta_1) + (1-r)\exp(z/\beta_2)\right], \tag{2.14}$$

so the radiation is divided into a long-wave and a short-wave spectral component with attenuation depths of β_1 and β_2, respectively. The attenuation depths change with water turbidity. Jerlov (1976) designated several water types based on water chlorophyll concentrations. For a fairly clear, mid-ocean water of type IA the values are $r = 0.62; \beta_1 = 0.6m; \beta_2 = 20m$.

For each time-step, the PWP model proceeds as follows.

(i) Insolation Q_s is absorbed in the water column, and net heat loss Q_L occurs from the top grid-point, or layer, thus changing the temperature profile. Density is calculated (from a linear or nonlinear equation of state, depending on implementation).

(ii) A static stability criterion

$$\frac{\partial \rho}{\partial z} \geq 0 \tag{2.15}$$

is evaluated, and complete mixing of temperature, momentum, and density occurs from the surface downwards, iteratively, until a statically stable stratification with a mixed layer on top is achieved. Mixing at this stage is equivalent to that caused by free, non-penetrative convection.

(iii) The wind stress is applied to the top grid-point, and momentum is distributed uniformly through the mixed layer. Horizontal currents are rotated inertially.

(iv) Overall mixed layer shear instability versus buoyancy stability is evaluated at the base of the mixed layer by a bulk Richardson number criterion

$$Rb = \frac{g\Delta\rho h}{\rho_0 |\Delta \mathbf{U}|^2} \geq 0.65 \tag{2.16}$$

where h is the mixed layer depth, 0.65 is the critical Rb value, $\Delta\rho$ and $|\Delta \mathbf{u}|$ are the density and velocity differences, respectively, between the ML and just below it. If $Rb < 0.65$, the mixed layer deepens by one grid-point and properties are mixed completely within the new ML. The new Rb number is then evaluated, and entrainment and mixing proceed iteratively until the criterion is satisfied. This type of dynamic stability criterion, implying that the ML is always either stable or in a state of marginal stability, has also been implemented by others (Pollard *et al.*1973; Price *et al.*1978; Kronenburg 1985). Although no sound theoretical evidence that a true critical Richardson number exists for a turbulent mixed layer (Phillips 1977), laboratory experiments by Ellison and Turner (1959) show that entrainment by a surface half-jet decreases by a full order of magnitude as Rb increases from 0.4 to 0.8, suggesting an approximate critical bulk Richardson number in that range.

(v) Local shear flow stability is evaluated below the mixed layer with a gradient Richardson number criterion

$$Rg = \frac{g\partial\rho/\partial z}{\rho_0(\partial \mathrm{U}/\partial z)^2} \geq 0.25 \tag{2.17}$$

where 0.25 is the critical Rg value; gradients are evaluated by taking first differences over neighbouring grid-points. If Rg is found to be less than 0.25 at a given pair of grid-points, partial mixing of properties occurs between them. If densities prior to the partial mixing are ρ_1 and ρ_2, the density exchanged is e.g.

$$\left(1 - \frac{Rg}{0.3}\right)(\rho_1 - \rho_2)/2, \tag{2.18}$$

with a complete mixing for $Rg = 0$; a constant (0.3) slightly larger than 0.25 is used to hasten convergence, the larger value having no appreciable effect in the solutions (Price *et al.*1986). Then the Rg array is recalculated, reevaluated, and new adjustments are made, until $Rg \geq 0.25$ everywhere.

The motivation for adding gradient Richardson number dependent mixing below the mixed layer was to smooth out sharp temperature jumps at the ML base, making model profiles more like the profiles from observations, and also to relieve local shear instabilities in the stratified fluid below the ML. However, the implementation of this criterion in the model leads to "unmixing" of the mixed layer established with the bulk Richardson number criterion, as partial mixing adjusts the temperature at the bottom ML grid-point as well. As a result, the final ML depth diagnosed by the model is not the ML depth established by overall

mixed layer stability, as evident e.g. from Fig. 2 of Schudlich and Price (1992) and the accompanying figure caption. Thus, the *Rg* procedure seems to deliver more than it was designed to do; this does not seem to be commonly recognized, as the model has been described or implied by others as setting its ML depth with a bulk criterion, with *Rg* mixing only resolving instabilities below such a mixed layer (Archer *et al.*1993; Kantha and Clayson 1994; Large *et al.*1994; Large and Crawford 1995).

Model diagnostics (not shown) revealed that to satisfy $Rg \geq 0.25$ everywhere, up to tens of thousands of adjustments at each time-step might be needed for a region with a few tens of grid-points. In addition, while looking on occasion at spikes in the PWP model output such as ML depth and sea-surface temperature, I was able to trace them back to the *Rg* criterion procedure. It appears that, after many small adjustments, the final ML depth might incorporate a more or less arbitrary fluctuation. Apparently, the problem of maximizing *Rg*, by overshooting discrete-step adjustments, to achieve $Rg \geq 0.25$ everywhere for an array of grid-points, does not have a unique solution. So the final ML depth may not be consistent from one time-step to the next as different "solutions" are realized. The spikes disappear, however, if the ML depth achieved from overall mixed layer stability with the bulk Richardson number criterion is enforced, while still allowing for adjustments in the thermocline below it[1]. Therefore, the mixed layer depth

[1]This can be done as follows. For each iterative adjustment due to the gradient Richardson number criterion, if partial mixing affected the bottom grid-point of the mixed layer established by the *Rb* criterion, a complete mixing is performed within this layer to restore its homogeneity before the next iteration is attempted.

based on overall stability is consistent in time, and in fact it seems difficult to justify modifications of this depth via the gradient Richardson number criterion.

2.3 The Mellor-Yamada Level 2 model

A hierarchy of turbulent closure models, based on an order-of-magnitude analysis of small deviations of the Reynolds stresses and heat fluxes from local isotropy, was described by Mellor and Yamada (1974), refined by them later (Mellor and Yamada 1982), and reexamined by Galperin *et al.* (1988). In the limiting case of near isotropy, algebraic relations are obtained for all turbulent quantities. The resulting model, classified as Level 2 closure (MY-2), is attractive because of its simplicity and robustness (Galperin *et al.*1988), and has been applied in various situations (Martin 1985; Martin 1986; Kantha and Clayson 1994; Large *et al.*1994). The equations, in terms of buoyancy instead of temperature and salinity separately, are

$$\frac{\partial b}{\partial t} = -\frac{\partial}{\partial z}\left(\overline{w'b'}\right) - \frac{g\alpha}{\rho_0 C_p}\frac{\partial I}{\partial z} \tag{2.19}$$

$$\frac{\partial \mathbf{U}}{\partial t} = -f(\mathbf{k}\times\mathbf{U}) - \frac{\partial}{\partial z}\left(\overline{w'\mathbf{u}'}\right) \tag{2.20}$$

$$\frac{q^3}{\Lambda_1} = -\overline{w'\mathbf{u}'}\cdot\frac{\partial \overline{\mathbf{U}}}{\partial z} + \overline{w'b'} \tag{2.21}$$

where (2.21) is the averaged TKE equation (2.10), simplified by neglecting the convergence of the turbulent vertical flux, and assuming a balance between shear production, buoyancy forcing, and dissipation. The dissipation is assumed to be of the form q^3/Λ_1 (Kolmogoroff 1941), where $\Lambda_1 = B_1 l$. The length scale l is a

"master length scale" of turbulence, to which all other relevant length scales are proportional. This master scale is calculated from Blackadar's (1962) interpolation formula

$$l = \frac{l_0 \kappa |z|}{l_0 + \kappa |z|}, \tag{2.22}$$

where z is distance from a boundary, $\kappa \approx 0.4$ is von Karman's constant, l_0 is a measure of the extent of the turbulent field. The formula interpolates between $l \longrightarrow \kappa |z|$ as $|z|/l_0 \longrightarrow 0$, and $l \longrightarrow l_0$ as $|z|/l_0 \longrightarrow \infty$; l_0 is calculated from

$$l_0 = 0.2 \frac{\int |z| q \, dz}{\int q \, dz}, \tag{2.23}$$

where q is rms turbulent velocity, and 0.2 is the chosen value of the empirical constant in agreement with results from higher level MY models (Mofjeld and Lavelle 1984; Martin 1985).

The turbulent fluxes in (2.19 — 2.21) are parameterized by eddy diffusivity K_{H} and eddy viscosity K_{M}

$$\overline{w'b'} = -K_{\mathrm{H}}(z) \frac{\partial b}{\partial z} = -lqS_{\mathrm{H}} \frac{\partial b}{\partial z} \tag{2.24}$$

$$\overline{w'\mathbf{u}'} = -K_{\mathrm{M}}(z) \frac{\partial \mathbf{U}}{\partial z} = -lqS_{\mathrm{M}} \frac{\partial \mathbf{U}}{\partial z}, \tag{2.25}$$

where the vertically-varying eddy coefficients are products of the master length scale $l(z)$, rms turbulent velocity $q(z)$, and a gradient Richardson number Rg dependent stability functions $S_{\mathrm{H}}, S_{\mathrm{M}}$ involving more proportionality constants. After

substituting the values of the proportionality constants taken from Mellor and Yamada (1982), wherever needed, the final equations are

$$\frac{\partial b}{\partial t} = \frac{\partial}{\partial z}\left(lqS_{\mathrm{H}}\frac{\partial b}{\partial z}\right) - \frac{g\alpha}{\rho_0 C_p}\frac{\partial I}{\partial z} \tag{2.26}$$

$$\frac{\partial \mathbf{U}}{\partial t} = -f(\mathrm{k}\times\mathbf{U}) + \frac{\partial}{\partial z}\left(lqS_{\mathrm{M}}\frac{\partial \mathbf{U}}{\partial z}\right) \tag{2.27}$$

$$q^2 = 16.6\, l^2\left(\frac{\partial \mathbf{U}}{\partial z}\right)^2\left(S_{\mathrm{M}} - S_{\mathrm{H}}Rg\right) \tag{2.28}$$

$$S_{\mathrm{H}} = \frac{0.49}{1-34.68G_{\mathrm{H}}} \tag{2.29}$$

$$S_{\mathrm{M}} = \frac{0.40-3.08G_{\mathrm{H}}}{(1-34.68G_{\mathrm{H}})(1-6.13G_{\mathrm{H}})} \tag{2.30}$$

where $G_{\mathrm{H}} = -(l/q)^2\partial b/\partial z$, and l and l_0 are calculated from (2.22) and (2.23) above. It can be shown that $S_{\mathrm{H}} \geq 0, S_{\mathrm{M}} \geq 0$, and that they are zero for $Rg \geq 0.19$.

2.4 Other models

One-dimensional models of the mixed layer generally fall into two classes. Turbulence closure ML models (also called K-theory models) can be organized and classified as parts of a single hierarchy (Mellor and Yamada 1974; Mellor and Yamada 1982; Galperin *et al.*1988) based on an order of magnitude analysis of small deviations of the second moments of turbulence from the state of local isotropy. These models employ vertically-varying eddy diffusivity and eddy viscosity. The Mellor-Yamada Level 2 model described in the previous section is an example of a K-theory model. Details on other K-theory models will not be given here; the reader is referred to the three papers cited above. Bulk ML models assume the existence and evolution of a well-mixed surface layer. They employ two approaches

to the parameterization of ML deepening (however one can be viewed as a limiting case of the other), and can subsequently be subdivided into finite entrainment rate models (FER models) and dynamic instability models (DI models). FER models have an evolution equation for the ML depth, and DI models are defined in terms of a critical bulk number of the ML. The Price-Weller-Pinkel model described in section 2.2 is an example of a DI bulk model. In addition, there is the hybrid model of Large *et al.* (1994) which is a K-theory model but determines its boundary layer depth from a bulk Richardson number stability criterion.

The traditional theory of the processes in the boundary layer of the ocean and the atmosphere has led to the identification of three possible mechanisms which can cause entrainment (Deardorff 1983). They are near-surface shear stress with velocity scale the friction velocity u_*; near-surface buoyancy flux with free convection velocity scale $(B_0 h)^{1/3}$; entrainment-zone shear stress associated with velocity jump at the ML base $|\Delta \mathbf{u}|$. The only mechanism opposing entrainment is associated with the stable buoyancy jump at the ML base at depth h, with velocity scale $(h\Delta b)^{1/2}$. If dh/dt describes the evolution of the ML depth, with $dh/dt > 0$ corresponding to mixed layer deepening, then the entrainment rate w_e is defined as

$$w_e = \begin{cases} \frac{dh}{dt}, & \frac{dh}{dt} > 0 \\ 0, & \frac{dh}{dt} < 0. \end{cases} \tag{2.31}$$

FER models solve equations (2.6 — 2.9) below the mixed layer; in addition the 1-D equations for scalars and horizontal momentum are integrated across the mixed layer. Using the surface boundary conditions (2.11) and (2.12) and the

boundary condition for the turbulent flux across the ML base

$$\overline{w'T'}(-h) = -w_e \Delta T \tag{2.32}$$

(Niiler and Kraus 1977), we get e.g. for the ML temperature T_m

$$\frac{dT_m}{dt} = -\frac{w_e \Delta T}{h} + \frac{Q}{\rho_0 C_p h}, \tag{2.33}$$

where T_m is equal to the sea-surface temperature T_s, and the term involving the insolation penetrating below the ML is neglected.

An additional relation involving w_e is needed and is provided from the steady state of the integrated across the mixed layer turbulent kinetic energy equation (2.10). We make all simplifying assumptions and parameterizations of the various terms as in Niiler and Kraus (1977), not giving further consideration to the contributions from the surface buoyancy flux and the penetrating part of the insolation to the integrated TKE equation. Thus we get

$$\frac{1}{2} w_e \left(h\Delta b - s|\Delta \mathbf{u}|^2 \right) = m u_*^3 \tag{2.34}$$

where s, m are constants to be identified later. $1/2\ w_e h \Delta b$ is the power needed to lift denser water and mix it through the layer h; $1/2\ s w_e |\Delta \mathbf{u}|^2$ is the rate of reduction of the mean flow energy by mixing across the ML base – it is a parameterization of the shear production term as being proportional to the entrainment

rate and the square of the velocity difference at the ML base; mu_*^3 parameterizes the rate of working by the wind due to the turbulent velocity and pressure correlations at the surface.

We define bulk Richardson numbers based on u_* and Δu as

$$Rb_\tau = \frac{h\Delta b}{u_*^2}, \tag{2.35}$$

$$Rb_{\Delta u} = \frac{h\Delta b}{|\Delta \mathbf{u}|^2}. \tag{2.36}$$

Then (2.34) can be written as

$$\frac{w_e}{u_*} = \frac{2mRb_\tau^{-1}}{1 - sRb_{\Delta u}^{-1}}. \tag{2.37}$$

This entrainment formulation is used in the bulk FER models of Niiler (1975), Niiler and Kraus (1977), Garwood (1977), and Davis *et al.* (1981b). The values for the constants s and m are chosen differently in each model and are regarded as tunable parameters to optimize the model's performance.

In bulk DI models (Pollard *et al.*1973; Price *et al.*1978; Price *et al.*1986), taking advantage of the results of the experiments by Ellison and Turner (1959) showing a negligible entrainment beyond a critical $Rb_{\Delta u}$, it is postulated that the mixed layer is always stable or marginally stable, adjusting itself so that a bulk Richardson number based on $|\Delta \mathbf{u}|$ is a constant s of O(1). This is equivalent to

ignoring the dependence on Rb_τ in (2.37) and crudely approximating (2.37) with

$$w_e = \begin{cases} \infty, & Rb_{\Delta u} < s \\ 0, & Rb_{\Delta u} > s \end{cases} \tag{2.38}$$

Note that $s = 1.0$ in the model of Pollard *et al.*, and $s = 0.65$ in the PWP model.

To recover the formulation of the historically first bulk ML models which were FER models without a shear term, we ignore the contribution of the mean velocity shear at the ML base, and obtain from (2.34)

$$\frac{w_e}{u_*} = 2mRb_\tau^{-1}. \tag{2.39}$$

This is the entrainment formulation of the bulk FER models of Kraus and Turner (1967) and Denman and Miyake (1973). They typically use a value of $m = 1.0$.

All finite entrainment rate formulations presented so far are scaled with u_*. In order to derive the formulation for the models that have Δu scaling, we have to go back to the parameterization of the shear production term in the TKE equation at the base of the ML. Stull (1976), somewhat arbitrarily, assumed this term to be proportional to $|\Delta \mathbf{u}|^3$ instead. Assuming that the shear at the ML base dominates the deepening

$$\frac{w_e}{|\Delta \mathbf{u}|} = 2nRb_{\Delta u}^{-1}. \tag{2.40}$$

where n is another adjustable constant. This formulation is formally equivalent to the rescaled with Δu entrainment formula of Kraus and Turner (1967). The

models by Price (1979a) and the rescaling arguments of Price (1979b) are thus equivalent to the approach taken in Stull (1976).

The hybrid model of Large *et al.* (1994) (called the KPP model as in K-profile parameterization) is a K-theory model with a non-local counter-gradient term, and with a vertically-varying eddy diffusivity and eddy viscosity proportional to the boundary layer depth. The boundary layer depth (the boundary layer includes the mixed layer as well as the upper part of the underlying thermocline) is determined from a bulk Richardson number stability criterion as in a bulk model, with an additional term parameterizing turbulent shear to account for penetrative convection.

All afore-mentioned 1-D mixed layer models, as well as other ML models, are described in detail and discussed in depth in the excellent review by Nurser (1996).

Chapter 3

Nonlinear equation of state and apparent buoyancy flux

3.1 Introduction

The surface buoyancy flux B_0 per unit area of the sea surface is given by:

$$B_0 = -C_p^{-1}\rho_0^{-1}g\alpha Q + \rho_0^{-1}g\beta s(E-P) = B_{0T} + B_{0S}, \tag{3.1}$$

where C_p is the specific heat of water, ρ_0 is a reference density, $\alpha = -1/\rho(\partial\rho/\partial T)_{s,p}$ is the surface value of the temperature expansion coefficient of water at fixed salinity s and pressure p, Q is the net heat flux into the ocean, $\beta = 1/\rho(\partial\rho/\partial S)_{T,p}$ is the salinity expansion coefficient, E is the evaporation rate and P is the rainfall rate (Gill 1982). In (3.1) it is assumed that the insolation is absorbed by water of the same temperature as the sea surface; we will return to this later. Positive B_0 corresponds to a buoyancy loss by the ocean. In many models of the upper ocean α and β are taken as constants, i.e. a linear equation of state is used. In reality, the density of seawater depends in a nonlinear way on the pressure and on the temperature and salinity of water. For the surface mixed layer the temperature dependence is the most important one and can give rise to the interesting and potentially misleading existence of a net annual buoyancy flux into the sea even in a situation where the net annual heat flux is zero.

This is easily seen by inspection of (3.1). The relevant nonlinearity in the equation of state (NES) arises from the temperature dependence of the expansion coefficient α. The annual average buoyancy flux, $\overline{B_0}$, includes a term $-C_p^{-1}\rho_0^{-1}g\overline{\alpha' Q'}$, where α', Q' are departures from the respective annual means. Evidence for the importance of this term (henceforth called NES term) has been found in the Mediterranean Sea (Garrett *et al.*1993), where it is comparable to the other buoyancy flux terms and equivalent to a heat input of 6 W m^{-2}, i.e. there is a positive correlation between α' and Q'. This, of course, does not mean that the ocean is becoming steadily less dense even if $\overline{Q} = 0$. The temperature dependence of α is also responsible for a compensating buoyancy loss via cabbeling, or densification on mixing (Foster 1972; Garrett and Horne 1978; McDougall 1984), whenever the mixed layer entrains colder water from below.

We derive a convenient representation of the term involving $\overline{\alpha' Q'}$ and discuss some general properties of the seasonal cycle of the sea-surface temperature T_s versus the total heat content $\mathcal{H}$. Then we discuss results from a one-dimensional mixed-layer model, run over a seasonal cycle with idealized forcing. Data analysis from Ocean Weather Station Papa (OWS P) in the Northeast Pacific Ocean is presented, and used to infer the importance of the term at that location. Discussion and conclusions follow.

3.2 Theory

3.2.1 Representation of the term involving $\overline{\alpha' Q'}$

We will examine the 1-D heat and buoyancy budgets of an ocean of constant depth D, neglecting changes due to salinity and pressure. Let us assume that, instead of being a constant, the temperature expansion coefficient α varies linearly with temperature

$$\alpha = \alpha_0 + \frac{\partial \alpha}{\partial T}(T - T_0) = \frac{-1}{\rho_0}\frac{\partial \rho}{\partial T} \tag{3.2}$$

where $\partial\alpha/\partial T$ is assumed constant, thus ignoring further small corrections involving higher derivatives. Then

$$\frac{\partial b}{\partial t} = g\alpha\frac{\partial T}{\partial t}, \tag{3.3}$$

where the buoyancy b, defined with respect to ρ_0, is

$$b = -g{\rho_0}^{-1}(\rho - \rho_0). \tag{3.4}$$

Neglecting horizontal variability, the equations for T and b thus are

$$\frac{\partial T}{\partial t} + \frac{\partial}{\partial z}\left(\overline{w'T'}\right) = -\frac{1}{\rho_0 C_p}\frac{\partial I}{\partial z}, \tag{3.5}$$

$$\frac{\partial b}{\partial t} + g\alpha\frac{\partial}{\partial z}\left(\overline{w'T'}\right) = -\frac{g\alpha}{\rho_0 C_p}\frac{\partial I}{\partial z}, \tag{3.6}$$

where $\partial/\partial z\left(\overline{w'T'}\right)$ is the divergence of the turbulent heat flux and $I(z)$ is the flux profile for the penetrating part of the insolation. Let us define the total heat content $\mathcal{H}$ and the total buoyancy content $\mathcal{B}$ per unit area of the ocean as:

$$\mathcal{H}(t) = \int_{-D}^{0} T(z,t)\, dz, \qquad \mathcal{B}(t) = \int_{-D}^{0} b(z,t)\, dz, \tag{3.7}$$

where D = constant is the total depth of the ocean. Neglecting advection and compressibility, and assuming that the insolation is absorbed by water of the same temperature as the sea surface, we integrate (3.5) and (3.6)

$$\frac{d\mathcal{H}}{dt} = \frac{1}{\rho_0 C_p} Q, \tag{3.8}$$

$$\frac{d\mathcal{B}}{dt} = \frac{g}{\rho_0 C_p}\alpha Q + g\frac{\partial \alpha}{\partial T}\int_{-D}^{0} \overline{w'T'}\frac{\partial T}{\partial z}\, dz \tag{3.9}$$

using the boundary conditions

$$\overline{w'T'}(0) = -\frac{Q_{\mathrm{L}}}{\rho_0 C_p}, \tag{3.10}$$

$$I(0) = -Q_s, \tag{3.11}$$

$$\overline{w'T'}(-D) \approx 0, \tag{3.12}$$

$$I(-D) \approx 0, \tag{3.13}$$

and the identity $Q = Q_s + Q_{\mathrm{L}}$, where $Q_{\mathrm{L}} = Q_b + Q_e + Q_h$.

In the formulae above Q_s is the insolation, Q_L is the net surface heat flux due to heat loss from long-wave back radiation, latent, and sensible fluxes, respectively; α is evaluated at the ocean surface.

As $\partial T/\partial z$ is assumed to vanish within the ML, and $\overline{w'T'}$ is, presumably, negligible below the ML, we have to evaluate the integral in (3.9) at the ML base where a temperature difference ΔT is assumed to exist. Let the turbulent heat flux $\overline{w'T'}$ at the base of the ML be used up entirely to bring colder water across the temperature difference ΔT and mix it with the water in the ML so that the ML deepens at a rate w_e. Then, if h is the ML depth, we have

$$\overline{w'T'}\Big|_{-h} = -w_e \Delta T \tag{3.14}$$

e.g. Niiler and Kraus (1977), thereafter NK77. Finally we get

$$\frac{d\mathcal{B}}{dt} = \frac{g}{\rho_0 C_p}\alpha Q - g\frac{\partial \alpha}{\partial T} w_e (\Delta T)^2, \tag{3.15}$$

where α is evaluated at the sea-surface temperature T_s, and ΔT is the temperature jump at the base of the surface mixed layer, across which entrainment occurs at a rate w_e.

The first term on the right-hand side of (3.15) is, apart from a sign change, the B_{0T} term discussed in the introduction. The second term can also be derived (refer to Figure 3.1) by considering the change in buoyancy content after an entrainment event that conserves the heat content. To first order, $h\delta T = \Delta T \delta h$,

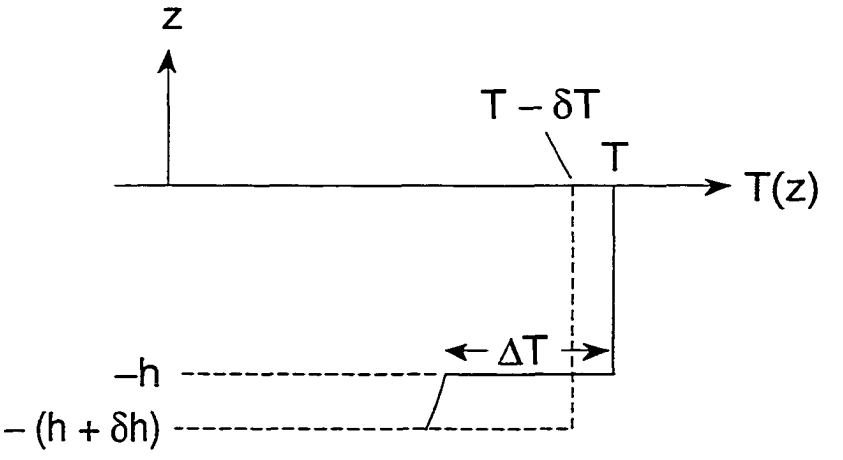

Fig. 3.1. A schematic of mixed layer deepening due to mechanical stirring and associated entrainment. A well mixed surface layer of depth h, temperature T, and a temperature jump ΔT across its base deepens, in time δt, to a depth $h + \delta h$, lowering its temperature by δT to $T - \delta T$.

so

$$\delta T = \frac{\delta h}{h}\Delta T. \tag{3.16}$$

Before the entrainment, the buoyancy content down to a depth $-(h+\delta h)$ is

$$\mathcal{B}_{\mathrm{B}} = \int_{-h}^{0} gT\alpha\, dz + \int_{-(h+\delta h)}^{-h} g\,(T-\Delta T)\,\alpha(T-\Delta T)\, dz. \tag{3.17}$$

After the entrainment it becomes

$$\mathcal{B}_{\mathrm{A}} = \int_{-(h+\delta h)}^{0} g\,(T-\delta T)\,\alpha(T-\delta T)\, dz. \tag{3.18}$$

Then

$$\delta\mathcal{B} = \mathcal{B}_{\mathrm{A}} - \mathcal{B}_{\mathrm{B}} = g\left[(h+\delta h)(T-\delta T)\alpha(T-\delta T)\right] - g\left[hT\alpha(T) + \delta h(T-\Delta T)\alpha(T-\Delta T)\right] \tag{3.19}$$

Using (3.16) and the linear dependence on temperature of the temperature expansion coefficient

$$\alpha(T-\delta T) = \alpha(T) - \delta T\,\alpha'(T), \tag{3.20}$$

$$\alpha(T-\Delta T) = \alpha(T) - \Delta T\,\alpha'(T), \tag{3.21}$$

we obtain, after rearrangement and simplifications

$$\delta\mathcal{B} = -g\delta h(\Delta T)^2\alpha'(T). \tag{3.22}$$

Therefore

$$\frac{\delta \mathcal{B}}{\delta t} = -g\frac{\delta h}{\delta t}(\Delta T)^2 \alpha'(T) = -g\frac{\partial \alpha}{\partial T} w_e (\Delta T)^2 \tag{3.23}$$

This term describes a buoyancy loss by cabbeling. We have ignored a very small contribution from changes in salinity and have retained only terms involving $\partial\alpha/\partial T$, ignoring further small corrections involving higher derivatives.

Assuming $\overline{Q} = 0$, the annual average of (3.15) is

$$\overline{\frac{d\mathcal{B}}{dt}} = -\overline{B_{0T}} - g\frac{\partial \alpha}{\partial T}\overline{w_e(\Delta T)^2}. \tag{3.24}$$

If $\overline{\mathcal{B}}$ does not change, we see that the buoyancy gain from $-\overline{B_{0T}} = C_p^{-1}\rho_0^{-1} g\alpha' \overline{Q'}$ must be exactly compensated by the annual average of the cabbeling term.

We call $\overline{B_{0T}}$ the NES term. Multiplying (3.8) by α and averaging, and assuming $\overline{Q} = 0$, we obtain

$$\overline{B_{0T}} = -g\frac{\partial \alpha}{\partial T}\overline{T_s \frac{d\mathcal{H}}{dt}}. \tag{3.25}$$

But

$$\overline{T_s \frac{d\mathcal{H}}{dt}} = \frac{1}{t_0}\oint T_s \, d\mathcal{H}, \tag{3.26}$$

where the integral proceeds around the $\mathcal{H}-T_s$ curve in the direction corresponding to increasing time t; t_0 is 1 year. Finally we get

$$\overline{B_{0T}} = -t_0^{-1} g \frac{\partial \alpha}{\partial T} A, \tag{3.27}$$

so the magnitude of the NES term is simply proportional to the area A inside the hysteresis loop of the seasonal cycle of T_s versus $\mathcal{H}$. Note that a linear equation of state does not cause the hysteresis loop to collapse onto a single curve; the area A can be finite but give no contribution to $\overline{B_{0T}}$ if $\partial\alpha/\partial T = 0$. The NES term corresponds to a buoyancy gain by the ocean if the integration is clockwise in a plane with $\mathcal{H}$ on the x-axis, and T_s on the y-axis. This must be the case since the cabbeling term corresponds to a buoyancy loss regardless of the sign of ΔT, but the following arguments also demonstrate the sign.

3.2.2 General properties of the seasonal cycle of T_s versus $\mathcal{H}$

Figure 3.2 shows the annual cycle of T_s versus $\mathcal{H}$ at OWS Echo (35°N, 48°W), modified from Gill and Turner (1976). It can be seen that the minima of $\mathcal{H}$ and T_s are achieved simultaneously. This occurs when the daily averaged Q is zero, the mixed layer depth is maximum, and T_s a minimum. On either side of the minimum of T_s and $\mathcal{H}$, from January to June, there are separate "heating" (upper) and "cooling" (lower) branches due to a shallower mixed layer and more rapid variation of the sea-surface temperature in the former. Thus

$$\left[\frac{dT_s}{d\mathcal{H}}\right]_{\text{heating branch}} > \left[\frac{dT_s}{d\mathcal{H}}\right]_{\text{cooling branch}} \tag{3.28}$$

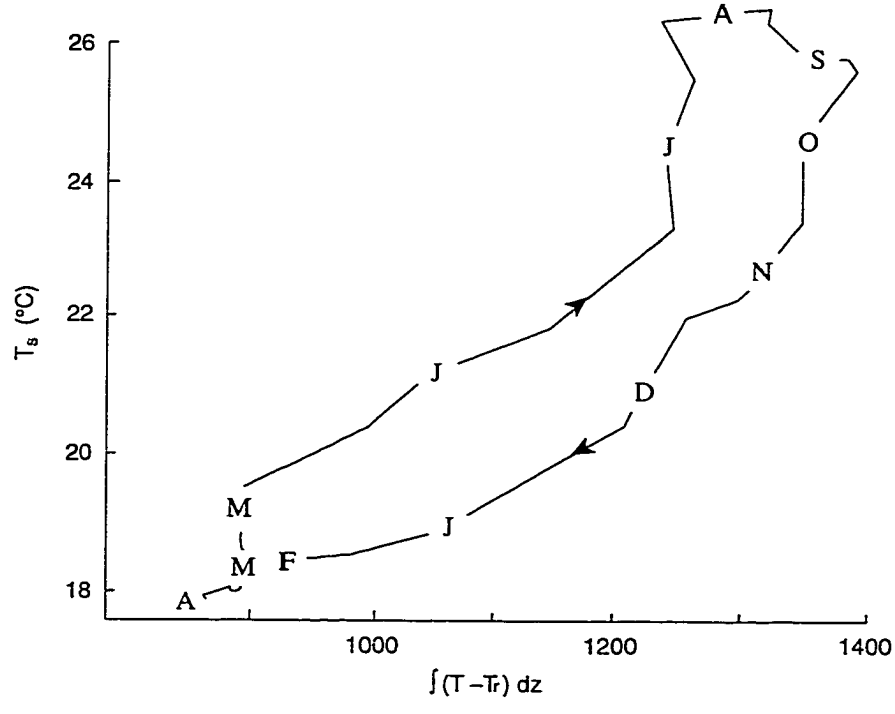

Fig. 3.2. The annual cycle of T_s versus $\mathcal{H}$ at OWS Echo (35°N, 48°W), modified from Gill and Turner (1976).

on average. The inequality can be explained in terms of the different physics of heating and cooling the ocean. As the heating season starts, the mixed-layer depth decreases rapidly and, for a given heat content, the mixed layer is shallow in the spring, but deep in the winter. If the ocean were of constant mixed-layer depth h, then $T_s \propto \mathcal{H}$, resulting in a single straight line instead of hysteresis, and, subsequently, from (3.27), $\overline{B_{0T}} = 0$. Similarly, a symmetric variation of h would result in a single curve with varying slope.

Another feature shown by Figure 3.2 is T_s achieving its maximum two to three weeks before the maximum of $\mathcal{H}$. This is because the mixed layer deepens before the point with zero net Q, thus moving the T_s maximum before that of $\mathcal{H}$ as entraining colder water from below decreases T_s. Two processes can cause the shift. First, as $Q = Q_s + (Q_b + Q_e + Q_h)$, i.e. insolation minus heat loss from long-wave back radiation, latent, and sensible fluxes, respectively, at some point where Q is still positive, instabilities can occur due to heat loss at the surface since Q_s is absorbed with depth according to some exponential depth dependence (e.g. Paulson and Simpson (1977)). Second, as the stratifying effect of Q becomes weaker and the winds become stronger on average with the approach of autumn, the destabilizing influence of the momentum input from the wind causes the mixed layer to deepen. From model runs (not shown) we conclude that the latter process is overwhelmingly more important.

From the above properties of the $\mathcal{H} - T_s$ loop, it is obvious that the loop is traced clockwise. It follows that the NES term always represents a buoyancy gain by the ocean.

3.3 Seasonal cycle modelling – a test case

We have chosen a one-dimensional mixed layer model as the simplest possible type. The Price et al. (1986) model (PWP) has been modified to allow for a nonlinear equation of state. We have not attempted to force the model with real data, nor have we tried to estimate and parameterize horizontal advection. The goal has been to examine the sensitivity of the model to the inclusion of the nonlinearity in the equation of state by running it with a nonlinear (N case) and linear (L case) equation of state.

We integrated the model for two years with a time step of one hour and surface forcing varying sinusoidally over one year. The insolation also varied over half a sinusoid during daylight hours each day. In the second year of integration we obtained a closed curve, in $\mathcal{H}$–T_s space, which was repeated in subsequent years. Figure 3.3 presents the idealized forcing used to drive the model. The values for the forcing functions (daily averages for the insolation) are

$$\begin{aligned} &\text{Insolation:} && Q_s = 180 - 141\cos\left(\tfrac{2\pi}{365}t\right)\ \text{W m}^{-2} \\ &\text{Heat loss:} && Q_H = -180 - 24\cos\left(\tfrac{2\pi}{365}t\right)\ \text{W m}^{-2} \\ &\text{Net heat flux:} && Q = -165\cos\left(\tfrac{2\pi}{365}t\right)\ \text{W m}^{-2} \end{aligned} \tag{3.29}$$

where $Q = Q_s + Q_H$; $Q_H = Q_b + Q_e + Q_h$, t is time in days, and the wind stress is

$$(\tau_x, \tau_y) = \left(0.12 + 0.09\cos\left(\frac{2\pi}{365}t\right), 0\right)\ \text{N m}^{-2} \tag{3.30}$$

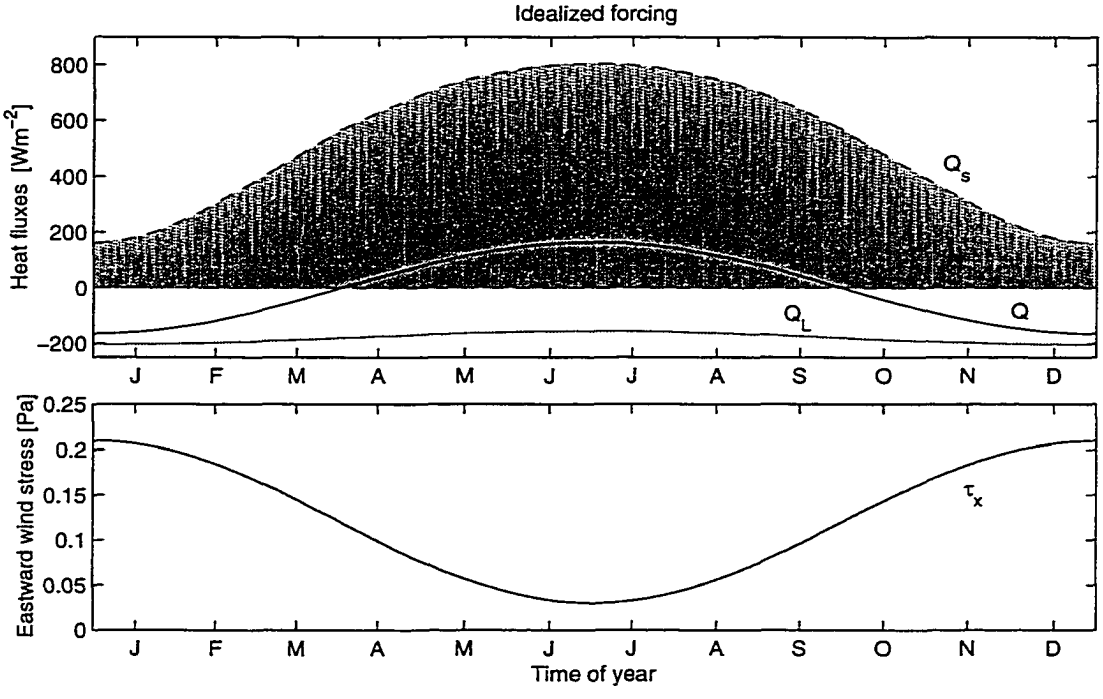

Fig. 3.3. Idealized forcing with zero mean annual heat flux. Top: insolation Q_s, total heat loss Q_L (the sum of sensible, latent, and longwave), and net heat flux Q. Bottom: eastward wind stress τ_x.

which corresponds to wind speeds from 4 to 11 $\mathrm{m\,s^{-1}}$. Note that $\overline{Q} = 0$. The net heat flux and wind stress have been chosen to approximate the range of values observed in the Mediterranean. Salinity $s = 38$ psu, C_p is 3980 $\mathrm{J\,kg^{-1}\,K^{-1}}$, and the latitude is taken to be 37°N. The dependence of α on temperature has been derived from a linear fit with values for α obtained using the International Equation of State (Millero and Poisson 1981), and is

$$\alpha = 7.788 \times 10^{-5} + 8.446 \times 10^{-6} T, \tag{3.31}$$

where T is in degrees Celsius.

First the N case was run with a reference temperature for α of 21.61°C, matching the actual $\overline{T_s}$, calculated from the model output, to assure proper calculation of the perturbation α'. The L case was run next. The resulting $\mathcal{H}$–T_s curves are shown in Figure 3.4. It is evident that the essential features have been reproduced, namely, the hysteresis, the relative phases of $\mathcal{H}$ and T_s, and the clockwise direction of the loop. There is only a weak sensitivity of the output to the inclusion of nonlinearity, as seen also in Figure 3.5 showing T_s and h in the N and L cases. The asymmetric variation of T_s and h has been reproduced. The range of values for the sea-surface temperature in general agrees with that observed in the Mediterranean (15–32°C). Apparently most of the compensation for the NES term, by densification on mixing, occurs in the winter and spring months as intensive mixing takes place. For the NES term in the N case we find $-C_p^{-1}\rho_0^{-1}g\overline{\alpha' Q'} = -4.05 \times 10^{-9}\ \mathrm{m^2\,s^{-3}}$, thus, incidentally, close to the value of $-3.32 \times 10^{-9}\ \mathrm{m^2\,s^{-3}}$ implied from Garrett et al.'s (1993) calculations from COADS

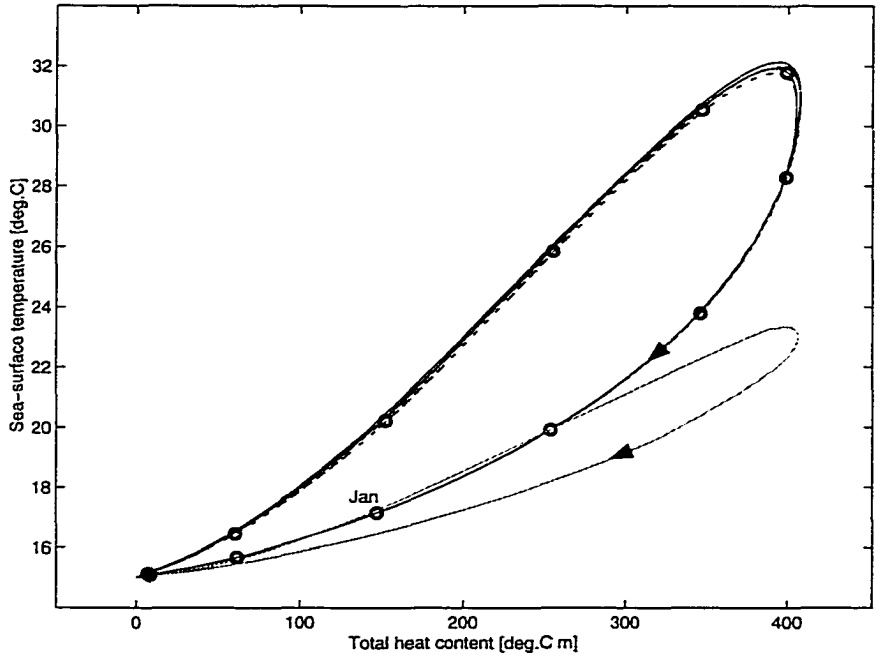

Fig. 3.4. The annual cycle of T_s versus $\mathcal{H}$ from model output, if the NES is excluded (upper solid lines), and including it (dashed lines). The pairs of lines for each case delineate the diurnal ranges. The lower curve shows the loop, with the NES but when the diurnal cycle is not resolved. The minimum annual heat content is a free parameter which does not enter the calculations of the NES term, and is set to zero. Each circle corresponds to the middle of a month.

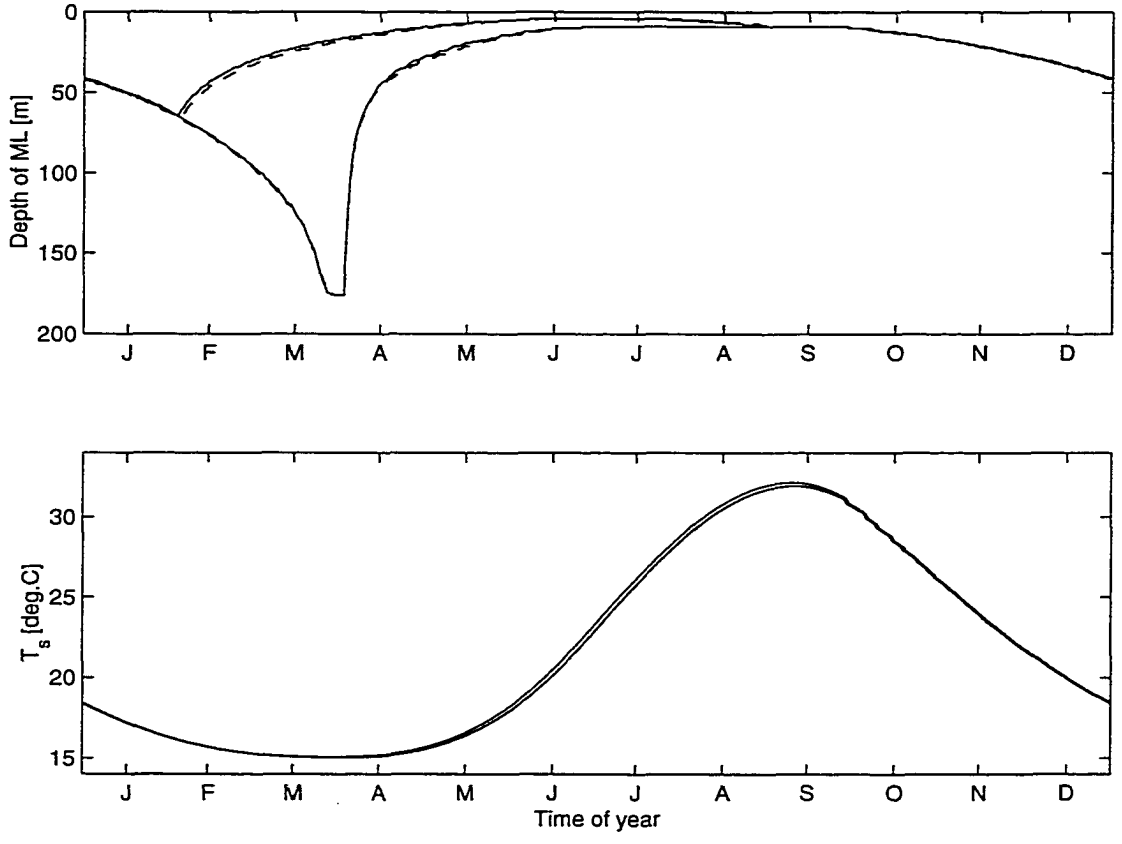

Fig. 3.5. (top) The daily range (i.e. daily minimum and daily maximum values) of mixed-layer depth h if the NES is excluded (solid lines) and including it (dashed lines); h is slightly larger on average in the NES case. (bottom) The daily range of sea-surface temperature T_s if the NES is excluded. Its inclusion results in slightly lower average T_s (not shown).

data. We remark that if the area A is calculated from the hysteresis curve, the right-hand side of (3.27) also gives -4.05×10^{-9} m^2 s^{-3}. Because of the large specific heat of water, the diurnal variation of Q_s causes rather small daily loops compared with the annual variation even though the mixed-layer depth h shows large diurnal changes.

The lower-most curve in Fig. 3.4 is the result of a model run with the same forcing as before, but with a time step of 24 h, thus not resolving the diurnal cycle. There is a large difference in the seasonal loop. This is because, in the heating season, convection is quenched around midday (Woods 1980) as the insolation has a much higher value than the average for the day. The small h at that time allows heat to be trapped in a shallow surface layer, causing T_s to increase more rapidly, and giving a higher daily-averaged T_s than if the diurnal cycle is not resolved (Woods and Barkmann 1986). In contrast, because of the lack of a diurnal cycle in the cooling season, heat is distributed more evenly in the water column. This demonstrates the importance of running models with the diurnal cycle resolved.

3.4 Calculation of the NES term from OWS Papa data

We have examined time series of sea-surface temperature measurements and forcing functions for the years 1970 to 1975 at OWS P (50°N, 145°W) with a time step of 3 h. We did not run a model, but, in order to construct the $\mathcal{H}$–T_s curve, we needed an estimate of the heat content. As temperature profiles were not available, we inferred $\mathcal{H}$ from the heat fluxes. However, OWS P is known to have an annual mean heat flux $\overline{Q}$ of around 30 W m^{-2}. As discussed by Large et al. (1986), this

net heating is compensated mainly by episodic horizontal advection of colder water in the autumn and early winter which, presumably, takes place above $h_{\max}$ in order to affect T_s. We can represent this effect as an effective heat flux Q_{adv} which is not constant but has an annual mean exactly balancing the annual mean positive heat flux Q. Then (3.8) and (3.15) become, respectively,

$$\frac{d\mathcal{H}}{dt} = \frac{1}{\rho_0 C_p}[Q + Q_{\text{adv}}], \tag{3.32}$$

$$\frac{d\mathcal{B}}{dt} = \frac{g}{\rho_0 C_p}[\alpha Q + \alpha Q_{\text{adv}}] - g\frac{\partial \alpha}{\partial T} w_e (\Delta T)^2. \tag{3.33}$$

The averaged buoyancy content equation now becomes

$$\overline{\frac{d\mathcal{B}}{dt}} = \frac{g}{\rho_0 C_p}[\overline{\alpha' Q'} + \overline{\alpha' Q'_{\text{adv}}}] - g\frac{\partial \alpha}{\partial T}\overline{w_e (\Delta T)^2}, \tag{3.34}$$

and the equation analogous to (3.25) is

$$-\frac{g}{\rho_0 C_p}[\overline{\alpha' Q'} + \overline{\alpha' Q'_{\text{adv}}}] = -g\frac{\partial \alpha}{\partial T}\overline{T_s \frac{d\mathcal{H}}{dt}}. \tag{3.35}$$

Then the NES term is

$$-\frac{g}{\rho_0 C_p}[\overline{\alpha' Q'} + \overline{\alpha' Q'_{adv}}] = -t_0^{-1} g\frac{\partial \alpha}{\partial T} A, \tag{3.36}$$

i.e., as in (3.27), it is still proportional to the the area under the hysteresis curve of the seasonal cycle of T_s versus $\mathcal{H}$.

If there is a constant advection throughout the year, $Q'_{\text{adv}} = 0$ and (3.36), (3.35), and (3.34) reduce to (3.27), (3.25), and (3.24), respectively. If, however, as in the case of OWS Papa, the advection is present only in the autumn and early winter, then $\overline{\alpha' Q'_{\text{adv}}}$ is negative.

For each of the years 1970 to 1975, we introduced Q_{adv} as a constant negative heat flux for October, November, and December, and zero otherwise, such that $\overline{Q_{\text{adv}}} = -\overline{Q}$ for that year. Then, via the heat content equation (3.32), a time series of the heat content $\mathcal{H}$ was produced. Figure 3.6 shows the hysteresis curve for 1972. From the area and from the now-known function Q_{adv} we can calculate the terms from the left-hand side of (3.36). The first term gives -2.18×10^{-9} m^2 s^{-3}. The second, about seven times smaller, is 0.30×10^{-9} m^2 s^{-3}, so the NES term is -1.88×10^{-9} m^2 s^{-3}. The second term need not be that small: the calculation for 1974 gives the second term as 0.33×10^{-9} m^2 s^{-3}, about a third of the magnitude of the first term for that year. Nevertheless, in any of the years considered, the NES term is not any larger than about -2.0×10^{-9} m^2 s^{-3}, which is equivalent to a heat flux of no more than 6 W m^{-2}. It is rather small compared to an annual mean heat flux of 30 W m^{-2}, which is typical for OWS Papa.

3.5 Discussion and conclusions

The nonlinearity of the equation of state gives rise to an additional term, $-C_p^{-1}\rho_0^{-1}g\overline{\alpha' Q'}$, in the averaged surface buoyancy flux B_0, which can be comparable in magnitude to the other terms. Evidence for its importance has been found in the Mediterranean where it is equivalent to a heat flux of 6 W m^{-2}, compared

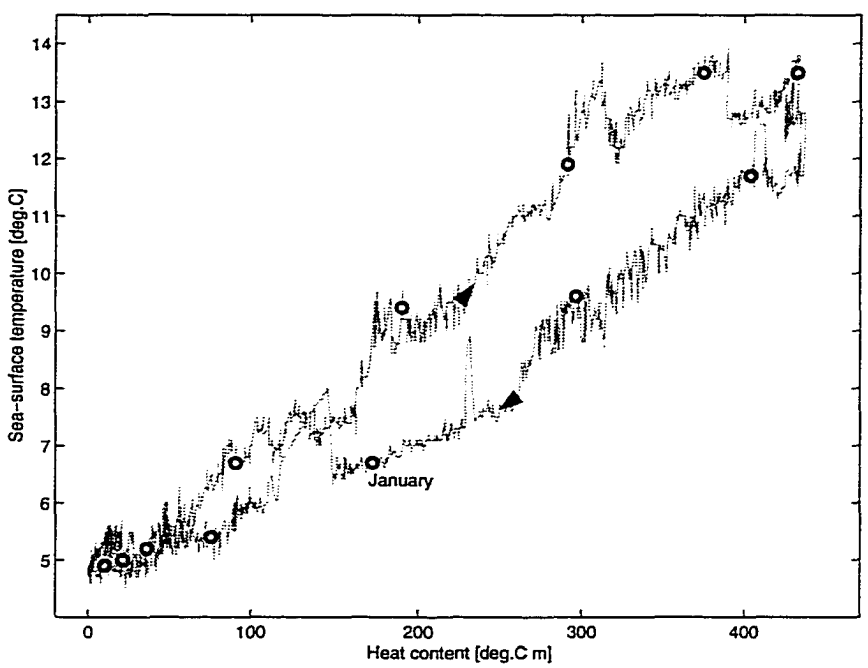

Fig. 3.6. The annual cycle of T_s versus $\mathcal{H}$ for the year 1972 from OWS Papa data. The minimum annual heat content is set to zero. Each circle corresponds to the middle of a month.

with an annual mean heat flux of -5 W m^{-2} (Macdonald *et al.*1994). This term, referred to as the NES term, has been shown to be simply proportional to the area enclosed by the hysteresis curve of the sea-surface temperature T_s versus the heat content $\mathcal{H}$. The characteristic features of the curve have been explained with the thermodynamics and dynamics of the upper ocean. This loop is always traced clockwise, so that the NES term is always negative, representing a buoyancy input. It is compensated by cabbeling, or densification on mixing, whenever the mixed layer entrains water with different properties from below.

We have considered in detail only the case of a mixed layer entraining colder water from below. In places where salinity controls the mixing, as in polar regions, for example, a scenario can be envisioned with a colder mixed layer entraining warmer water from below. This, however, does not alter our conclusions, as cabbeling still results in a loss of buoyancy (ΔT is squared in (3.24)).

The output from a simple mixed-layer model gives reasonable agreement with the value for the NES term calculated from COADS data for the Mediterranean. The model shows only a weak sensitivity to the inclusion of a nonlinear equation of state. The time series of mixed-layer depth, obtained with the model, suggests that most of the compensation through cabbeling occurs in the winter and spring months when there is intensive mixing and entrainment.

We have assumed that the insolation is absorbed by water of the same temperature as the sea surface, thus neglecting a contribution from the term $\int_{-D}^{-h} I(z)(\partial\alpha/\partial T)(\partial T/\partial z)\, dz$ to the surface buoyancy flux and, subsequently, to the magnitude of the NES term. As seen in Fig. 3.4, on any given day the temperature difference within the water absorbing the insolation is indeed small compared

with the temperature difference, over the course of the year, which determines the area under the $\mathcal{H} - T_s$ curve, so that the neglected contribution is very small.

We have also estimated the NES term for the Northeast Pacific using data from OWS Papa. Horizontal advection terms were needed and have been included. The estimated NES term here is significant, but in contrast with the Mediterranean is rather small in comparison with the term involving the annual mean heat flux. However, the equivalent heat flux is roughly the same as in the Mediterranean Sea (6 W m^{-2}). In general, the form of the cabbeling term in (3.24) suggests that a large NES term in the surface buoyancy flux depends on a significant seasonal cycle in mixed layer depth and on storm events that lead to deepening with a significant ΔT.

In conclusion, we point out that if a model that has only buoyancy as a scalar variable (not temperature and salinity separately) is forced with the full surface buoyancy flux using a nonlinear equation of state, one would get a spurious buoyancy input. We emphasize the need for care in evaluating the thermodynamics and dynamics of the surface mixed layer.

Chapter 4

Langmuir circulation and mixed layer deepening

4.1 Introduction

Sixty years ago, in 1938, the chemist Irving Langmuir was the first to describe (Langmuir 1938) what is now considered a common feature in the surface mixed layer (ML) of the ocean. Whenever the wind blows over the sea surface, it induces subsurface vortices, combined in counter-rotating pairs generally aligned with the wind direction. After studying them, Langmuir concluded that these vortices (later named Langmuir circulation) must be an essential mechanism for mixing scalars and momentum in the surface layer and thus generating the commonly observed oceanic mixed layer.

One-dimensional (1-D) "bulk" ocean boundary layer (OBL) models have taken advantage of the concept of "mixed layer". They assume that buoyancy and horizontal velocity are reasonably well homogenized in the ML, with a sharp jump in properties at the ML base, and have either an evolution equation for the ML depth or a stability criterion that determines it. Consequently, the changes in ML depth, buoyancy, and horizontal velocity, are calculated in terms of the surface buoyancy flux B_0, the wind stress τ, and the differences in buoyancy and velocity between the ML and the water just below it. Nevertheless, despite Langmuir's pioneering work, these models, as well as more elaborate turbulence closure models

of the OBL, typically do not explicitly incorporate the effect of Langmuir circulation (LC) in their parameterizations of mixing. However, D'Alessio, Abdella, and McFarlane (1998) did include Langmuir circulation in their recent model of the oceanic mixed layer.

In the Price *et al.* (1986) model (PWP), for example, deepening of the mixed layer is accomplished in terms of a bulk Richardson number (Rb) criterion which states that deepening would occur if

$$\Delta b < \frac{0.65|\Delta \mathbf{u}|^2}{h} \tag{4.1}$$

where Δb, $|\Delta \mathbf{u}|$ are the buoyancy and velocity differences, respectively, between the ML and just below, h is ML depth, 0.65 is the assumed critical value of Rb for deepening. This criterion is based on a dimensional argument (Phillips 1977) relating the velocity scale $(h\Delta b)^{1/2}$ of the entrainment-zone shear stress associated with Δb, which hinders entrainment, with the velocity scale $|\Delta \mathbf{u}|$ of one of the available mechanisms facilitating entrainment – the entrainment-zone shear stress associated with shear at the bottom of the ML.

Despite their relative success in data simulations, PWP and other 1-D bulk models are known to sometimes predict too high sea-surface temperatures (SST) in the summer, possibly due to underprediction of the ML depth (Gaspar 1988), although it is possible that uncertainties and errors in the surface fluxes and episodic advection of water of different properties could also explain, at least in part, the discrepancies. Thus the *ad hoc* parameterizations in these models ultimately impose limits on their performance ability.

In an effort to establish the role of LC in ML deepening, Li and Garrett (1997) examined the interaction between LC and preexisting stratification using a numerical model. The results of the study are presented, along with their proposed stability criterion for deepening of the mixed layer from LC engulfment. Then, a verification of this LC criterion for deepening (and of the bulk Richardson number criterion of Price *et al* (1978), Price *et al* (1986)) is presented based on direct estimates of relevant quantities using data from the LOTUS experiment. Implications from the LC criterion for the seasonal and diurnal restratification of the upper ocean are discussed.

4.2 The LC criterion for ML deepening

Li and Garrett (1997), henceforth LG97, examined the interaction of LC with preexisting stratification. Using the 2-D model of Craik (1977) and Leibovich (1977a), henceforth CL, they solved numerically the equations

$$\frac{\partial u}{\partial t} + v\frac{\partial u}{\partial y} + w\frac{\partial u}{\partial z} = K_{\mathrm{M}}\nabla^2 u \tag{4.2}$$

$$\frac{\partial \Omega}{\partial t} + v\frac{\partial \Omega}{\partial y} + w\frac{\partial \Omega}{\partial z} = K_{\mathrm{M}}\nabla^2 \Omega - \frac{du_s}{dz}\frac{\partial u}{\partial y} + \alpha g\frac{\partial \theta}{\partial y} \tag{4.3}$$

$$\frac{\partial \theta}{\partial t} + v\frac{\partial \theta}{\partial y} + w\frac{\partial \theta}{\partial z} = K_{\mathrm{H}}\nabla^2 \theta, \tag{4.4}$$

where θ the temperature, u is the downwind current, $\Omega = \partial w/\partial y - \partial u/\partial z$ the downwind vorticity; K_{M} and K_{H} are constant eddy viscosity and diffusivity coefficients, respectively. $u_s(z)$ is the Stokes (mean particle) drift associated with surface

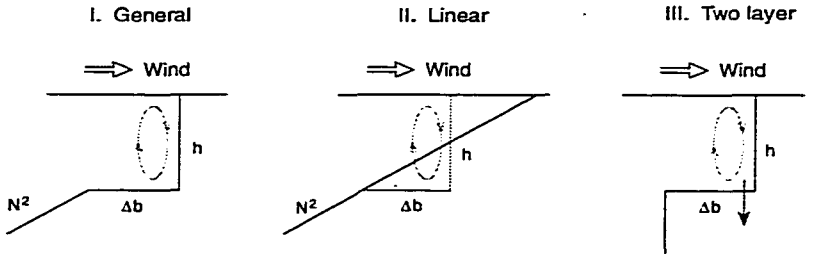

Fig. 4.1. A schematic diagram showing the interaction between Langmuir circulation and pre-existing stratification. I: the general problem, II: starting from a linear stratification, and III: starting from a two-layer stratification. Redrawn from LG97.

waves; $u_s(z) = 2S_0 \exp(2\beta z)$; the second term on the right-hand side of (4.3) is the CL vortex force.

The equations were non-dimensionalized and solved numerically for three kinds of pre-existing stratification (Figure 4.1). These numerical experiments showed that LC quickly develops and a surface mixed layer is created as growing Langmuir cells engulf water from below and homogenize the temperature within it. A temperature gradient develops at the ML base. For all cases of stratification considered, results suggest that the mixed layer rapidly deepens at first, but eventually stops its growth when the Froude number representing competition between vertical penetration and the stratification inhibiting it

$$Fr = \frac{w_{dn}}{(h\Delta b)^{1/2}} \tag{4.5}$$

reaches a value of about 0.9. In (4.5), w_{dn} is the maximum downwelling velocity generated by Langmuir cells in homogeneous water; Δb is the buoyancy jump at the base of the ML of depth h.

Li and Garrett (1993) related w_{dn} to the friction velocity u_* by

$$w_{dn} = 0.72 \left(\frac{S_0}{u_*}\right)^{1/3} La^{-1/3} u_*, \tag{4.6}$$

where

$$La = \left(\frac{K_M \beta}{u_*}\right)^{3/2} \left(\frac{S_0}{u_*}\right)^{-1/2} \tag{4.7}$$

is the Langmuir number (Leibovich 1977b) — the ratio of viscous to inertial forces, as one of the main nondimensional parameters characterizing LC. Taking a typical $La = 0.01$ results in an eddy viscosity K_M such that vertical velocities from the model match the observations (Li and Garrett 1993). Thus, the Froude number criterion for deepening (4.5) can be written as

$$\Delta b = c u_*^2 / h \tag{4.8}$$

i.e. LC will deepen the ML until the buoyancy jump at its base reaches a certain critical stability value. $c \approx 15.5 \left(S_0/u_*\right)^{2/3}$, and for fully developed seas $S_0/u_* = 5.75$ (Li and Garrett 1993), so then $c \approx 50$, and less in developing seas.

Thus LG97 proposed that, in addition to the bulk Richardson number criterion that the ML will deepen unless

$$\Delta b \geq 0.65 |\Delta \mathbf{u}|^2 / h, \tag{4.9}$$

a new LC criterion is used

$$\Delta b \geq 50 u_*^2 / h. \tag{4.10}$$

Comparison between (4.9) and (4.10) suggests that LC will dominate the deepening when

$$|\Delta \mathbf{u}| \lesssim 9 u_* \approx 0.01 U_w \tag{4.11}$$

i.e. if the velocity difference across the base of the ML is no greater than about 1% of the wind speed, or less in developing seas. This provides for a way to check the validity of the new criterion by examining a dataset directly – one can look for cases when $|\Delta \mathbf{u}|$ was small enough to allow restratification, but u_* was big enough to prevent it, and examine the actual evolution of the depth of the mixed layer.

4.3 Verification of the LC criterion using LOTUS data

We used data from the Long-Term Upper-Ocean Study (LOTUS) (Briscoe and Weller 1984; Stramma *et al.*1986; Price *et al.*1987) in the Sargasso Sea. In particular, we examined a continuous 68-day record of temperature and horizontal velocity profiles, available at 15-min intervals, starting in mid-May 1982, as it was the longest and had the best spatial resolution in the vertical. We needed to estimate u_*, h, Δb, and $|\Delta \mathbf{u}|$ from data.

We also obtained simultaneous meteorological measurements, as well as near sea-surface temperature estimates at 0.6 m. The latter were, however, increased

by about 0.06°C as a correction for an apparent instrument offset – even when the upper ocean appeared to be well mixed at night, the readings of this sensor were systematically lower than that of the 5-m sensor by this amount (Fig. 4.2). The data were then interpolated onto an equally-spaced grid with $\Delta z = 3m$ and filtered and resampled in time to have a cutoff frequency of 1 cycle per hour to avoid transient LC behaviour which occurs on a typical time-scale of less than an hour (Li and Garrett 1997), as the LC criterion was derived using results for well-established, quasi-steady LC.

We calculated the wind stress τ and therefore u_* from wind-velocity measurements at $3m$ above the ocean surface converted using Smith's (1988) tables. From each individual temperature profile we determined the depth of the ML h and the depth of the transition layer h_{tr}. Here h is defined as the depth above which the temperature variation is within $0.02^{\circ}C$, but below which the temperature shows a sharp jump. The transition layer is the layer of large temperature gradient below the mixed layer, with h_{tr} the depth below which the gradient becomes smaller (Fig. 4.3). These estimates are somewhat subjective, but were checked for consistency between successive profiles as well as in time in isotherms. Then we determined $|\Delta \mathbf{u}|$ and ΔT between h and h_{tr}. $|\Delta \mathbf{u}|$ is defined as the vector difference between the averaged velocity vector in the ML and the velocity vector at depth h_{tr}.

Using a linear equation of state, we determined the contribution to the buoyancy jump Δb from the temperature (ΔT) and salinity (ΔS). The latter was, subsequently, neglected as being estimated to be less than 1% that of ΔT. Thus we calculated Δb as $g\alpha\Delta T$, where g is the gravitational acceleration and

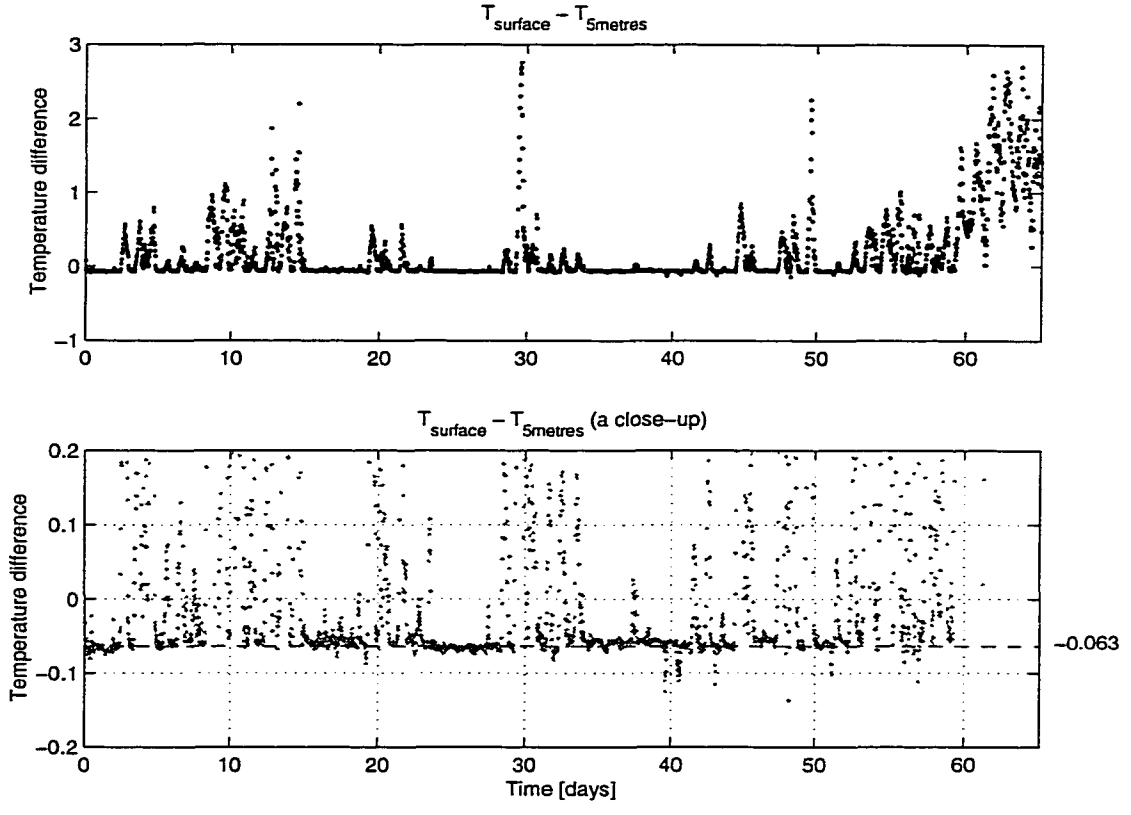

Fig. 4.2. Time-series of the difference between the temperature at a depth of 0.6 m (considered a sea-surface temperature), and the temperature at a depth of 5 metres. The surface temperature is consistently lower by about $0.06^{\circ}C$ even at night when the upper ocean appeared well mixed.

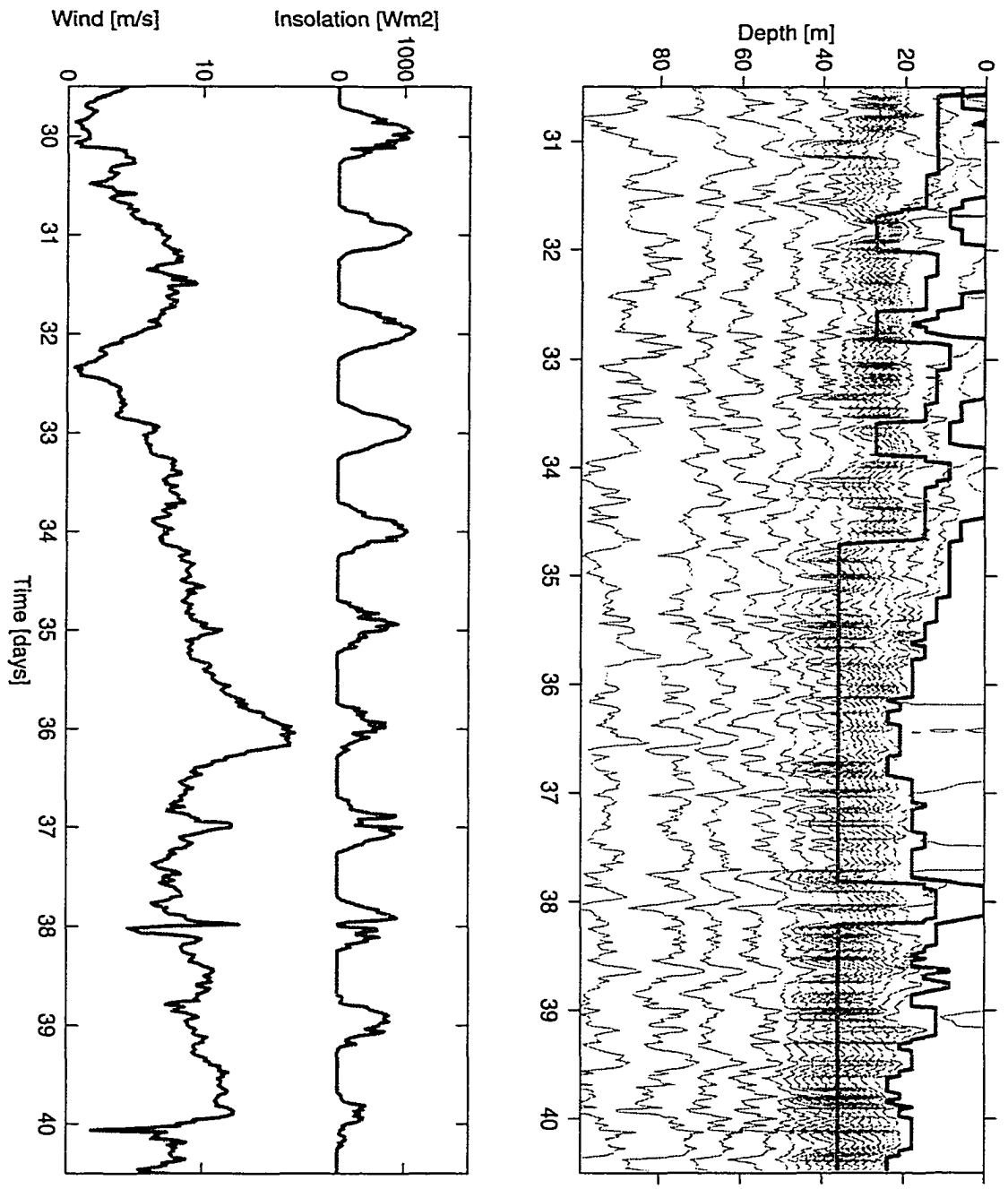

Fig. 4.3. Top (right) panel: an example of temperature contours and corresponding estimates of h (upper thick line) and h_{tr} (lower thick line); Bottom (left) panel: Forcing (wind speed and insolation) for the same period.

$\alpha = -1/\rho(\partial\rho/\partial T)$ is the temperature expansion coefficient. Before proceeding further, we identified periods when the 1-D heat balance could not be closed by comparing changes to the heat content of the upper $50m$ of ocean with those implied by the local surface heat flux (Fig. 4.4). For the latter we used a constant value of $-160\ Wm^{-2}$ for the combined heat loss flux Q_L because of unreliable humidity measurements (Price *et al.*1987). Despite this uncertainty, periods where the two estimates were grossly incompatible, perhaps due to horizontal advection or internal waves, were identified and avoided in the subsequent analysis.

We calculated the normalized quantities

$$Rb_n = \frac{0.65|\Delta \mathbf{u}|^2}{(h\Delta b)}, \qquad LC_n = \frac{50u_*^2}{(h\Delta b)}, \tag{4.12}$$

which, according to the criteria, suggest that deepening should occur if either Rb_n or LC_n exceeds 1. After examining the changes in the ML heat content to rule out deepening dominated by convection, we were able to identify several deepening cases.

The caption for Figures 4.5– 4.8 is as follows:

Four separate mixed layer deepening events: (A), (B), (C) and (D). (A) and (B) show deepening events dominated by Langmuir circulation, while (C) and (D) show deepening events mainly driven by shear instability. There are five panels vertically. (a) Isotherms constructed from conductivity-temperature-depth (CTD) measurements are shown as yellow contour lines for a two-day period. The red line shows the depth of the surface mixed layer while the blue line shows the depth of the

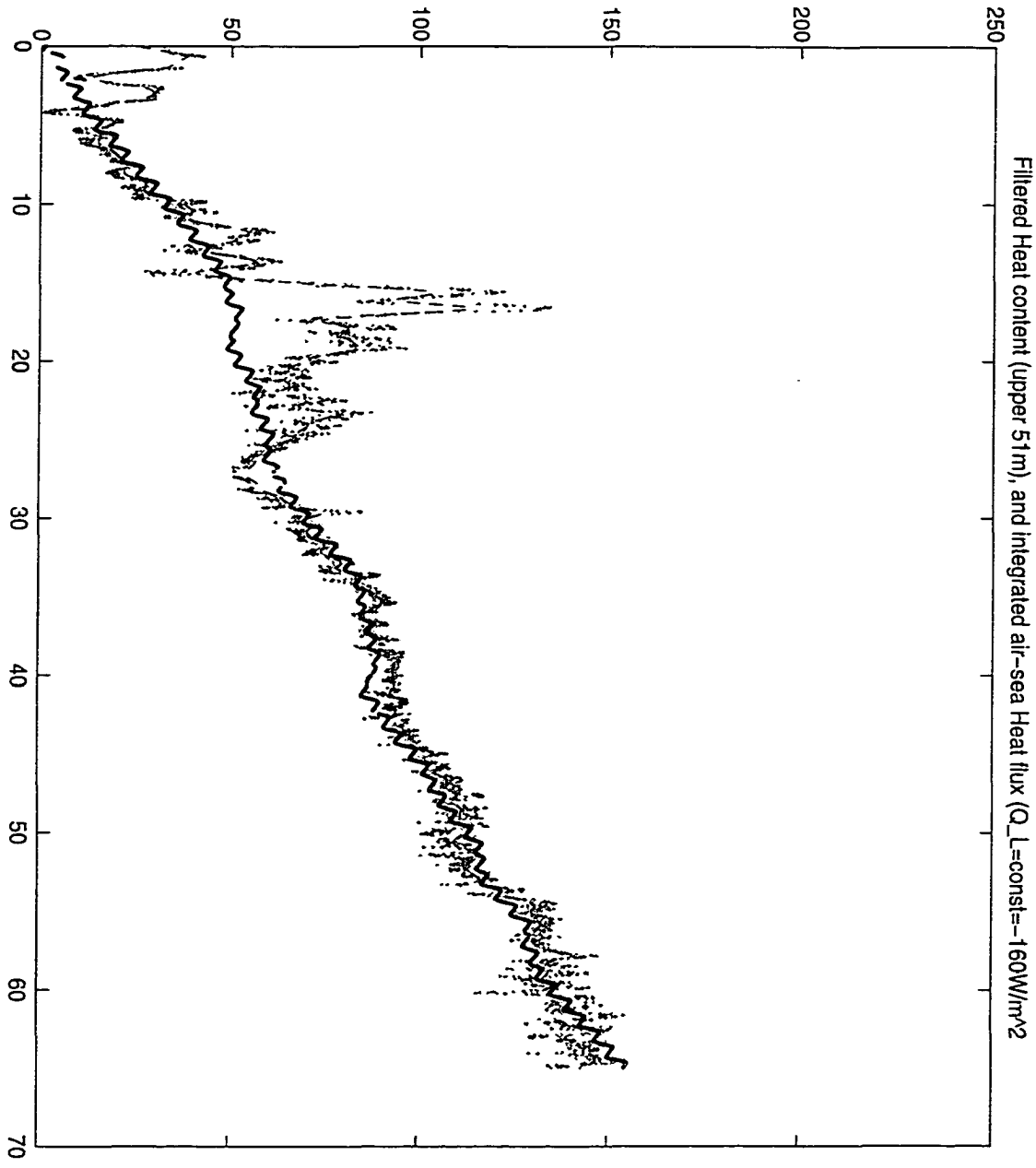

Fig. 4.4. Comparison of the heat content estimates for the upper 51 metres of ocean as derived from temperature profiles (shaded) and as implied from the local surface heat fluxes (thick black).

base of transition layer. Mixed layer depths shallower than 5 m cannot be resolved by the data and are drawn as red dashed lines at 5 m. They are excluded from the calculations of the flow indices. (b) Time series of the normalized stability indicators LC_n (light blue line) and Rb_n (plum line). $LC_n > 1$ should cause mixed-layer deepening due to Langmuir circulation whereas $Rb_n > 1$ should cause deepening due to shear instability. (c) Time series of the wind speed. (d) Successive vertical profiles of temperature during a deepening event. Corresponding depths of the mixed layer and the base of the transition layer are marked by short horizontal lines. Mixed layers shallower than 5 m and transition layers with bases lying outside the figure are not marked. (e) Corresponding indices LC_n ($\times$) and Rb_n (o). The color sequence used in the last two figures is yellow, green, blue, red and plum, representing profiles and indices at half-hour intervals.

The events illustrated in Fig. 4.5 (A) and Fig. 4.6 (B) are indicative of mixed-layer deepening caused by Langmuir circulation. During event (A) the wind was approximately constant at 5 ms^{-1} and the mixed-layer stayed shallow before 0300h (local time). Surface cooling caused the mixed layer to deepen from 6 to 9 m between 0300h and 0400h. It also greatly reduced the buoyancy jump at the mixed-layer base [compare the yellow and blue lines in (A) (Panel 4)]. This precipitated a rapid penetrative deepening [compare the blue and red lines in (A) (Panel 4)], although the heat content within the mixed layer was approximately conserved during this period. The Langmuir circulation index LC_n stayed close to 1 though decreasing slightly as the layer deepened. The second event, B, occurred in the afternoon when solar heating warmed the water. The index LC_n was initially larger than Rb_n and above the critical value of 1, suggesting that the mixed layer was unstable to Langmuir circulation deepening, possibly associated with a time lag in the response of the wave field to increasing wind. (Before this, the mixed layer depth was less than 5 m and so not resolvable.) Mixed-layer deepening, and a reduction in LC_n then occurred.

The deepening events in Fig. 4.7 (C) and Fig. 4.8 (D) involved Rb_n. In C, in the early morning, Rb_n relaxed from a supercritical value as the mixed layer deepened. In event (D), surface cooling initially reduced the temperature in a shallow surface layer [compare the yellow and green lines in (D) (Panel 4)]. The buoyancy jump Δb was thus reduced, causing both indices Rb_n and LC_n to be greater than 1. Subsequently the mixed layer rapidly deepened. Langmuir circulation and shear instability may both have contributed to the deepening.

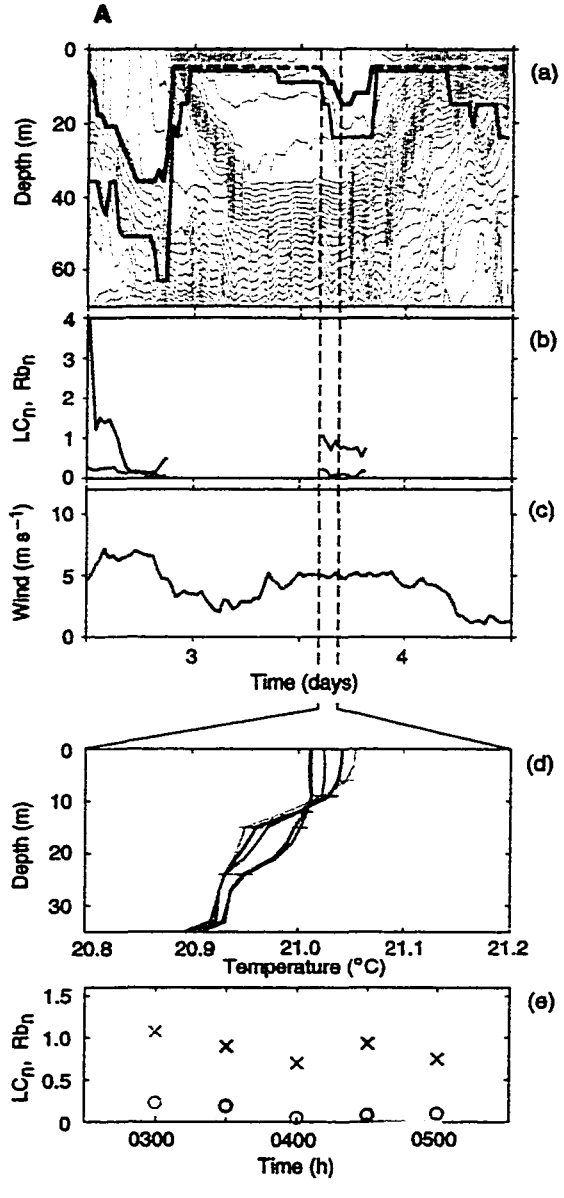

Fig. 4.5. The caption is on page 70

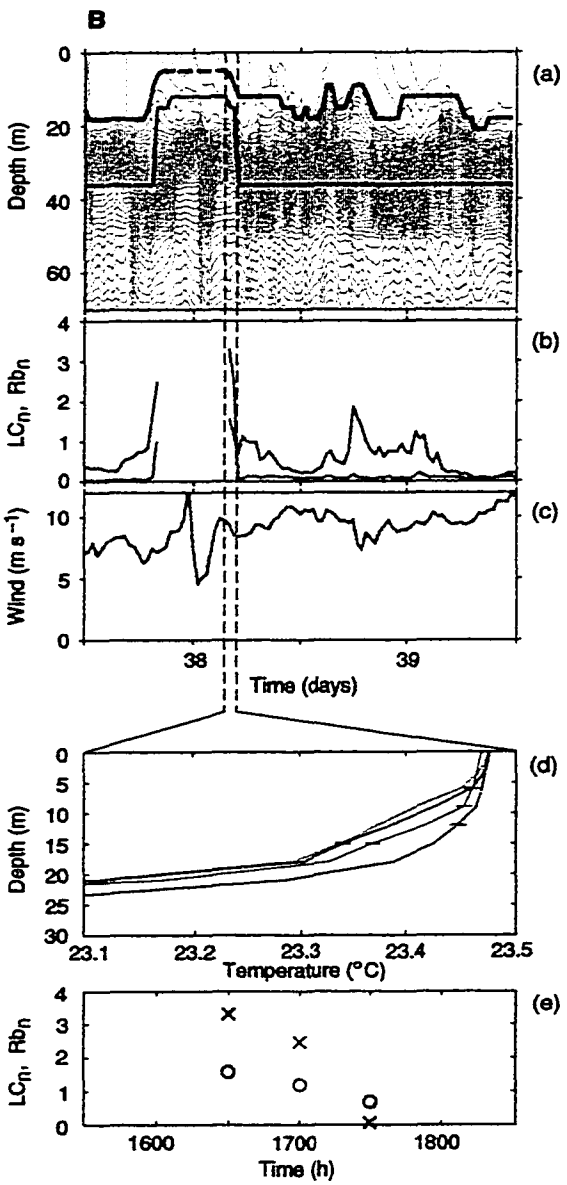

Fig. 4.6. The caption is on page 70

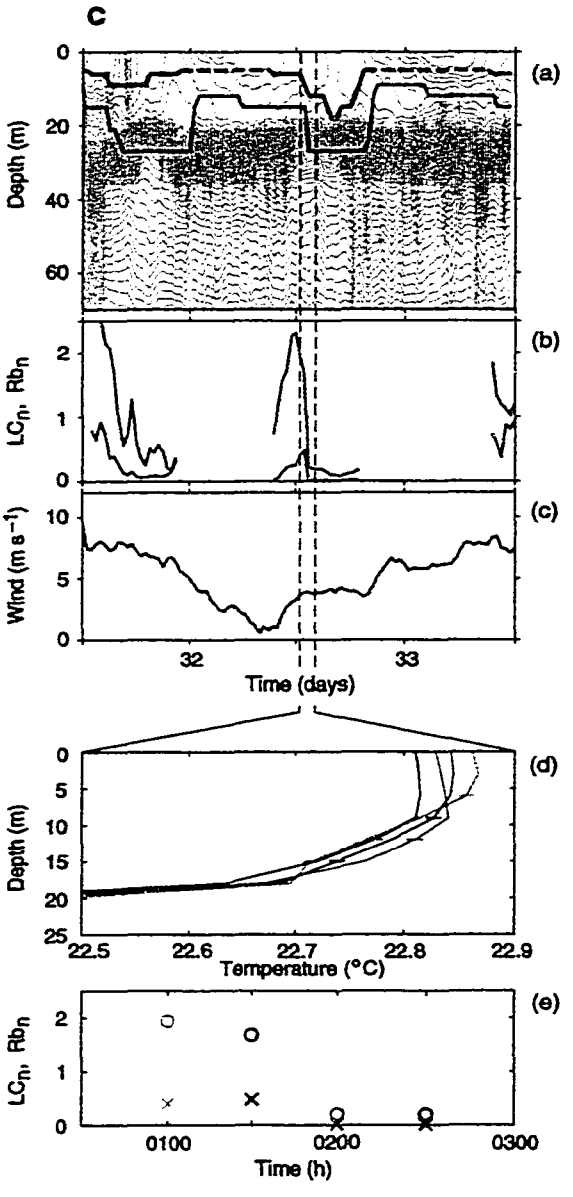

Fig. 4.7. The caption is on page 70

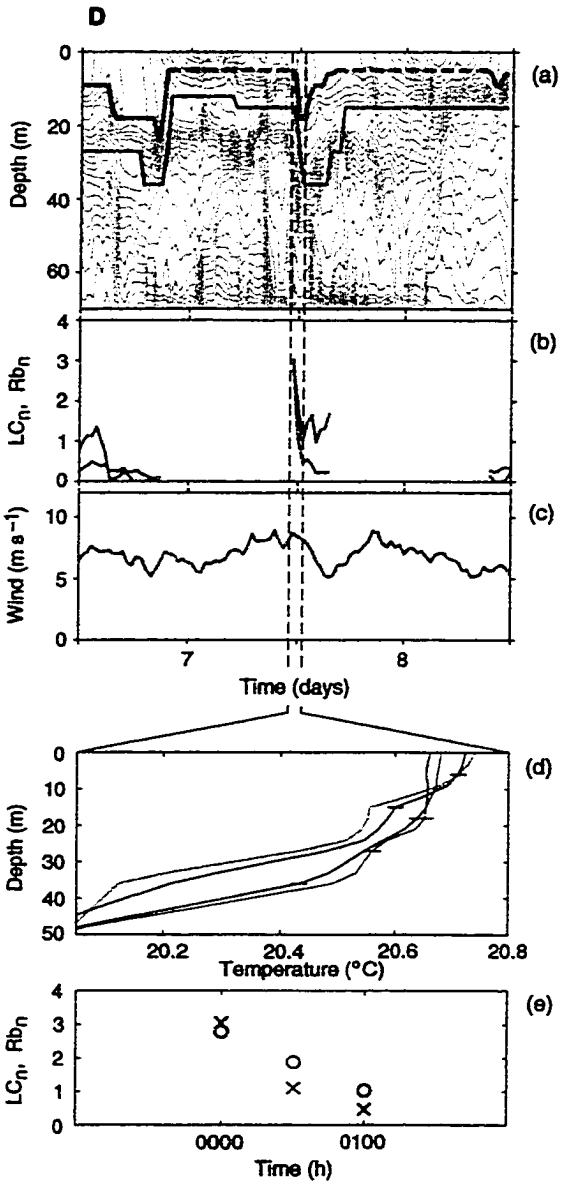

Fig. 4.8. The caption is on page 70

4.4 Implications for upper ocean restratification

Judging from the data analysis presented in the previous section, there is some evidence that LC may, though perhaps only occasionally, dominate the deepening of the surface mixed layer. Note that the LC criterion (4.10) does not depend on a velocity jump, but instead is a function of the friction velocity u_*, that is to say of the surface wind forcing. As such, it might be large enough to command ML deepening even when the buoyancy jump at the ML base is large enough to indicate a stable mixed layer according to the shear stability criterion (4.9). This has important implications for the formation of the thermocline on a seasonal and diurnal time-scale.

Consider a deep winter ML. When the heating season starts, increased insolation may cause a new, shallow ML to be formed if only the Rb shear criterion is used. Once formed, the ML can stabilize itself, as Rb of the mixed layer increases (the ML heat content $h\Delta b$ is conserved, but $|\Delta u|$ decreases) as ML deepens. However, according to the new criterion, if $h\Delta b < 50u_*^2$ initially, the new ML will not be able to stabilize at a new shallow depth as LC_n would not change as ML deepens - a new shallow ML cannot be formed. Therefore LC may prevent the formation of the seasonal thermocline in early spring unless the wind drops for a sufficient time to enable the establishment of a new ML with $h\Delta b$ large enough to overcome $50u_*^2$, where u_* is the friction velocity when the wind resumes. Taking the surface buoyancy flux $B_0 = 10^{-7} m^2 s^{-3}$ and $u_* = 0.01 ms^{-1}$, a typical time

would be

$$t = \frac{50u_*^{\ 2}}{g\alpha Q\rho_0^{\ -1}C_p^{\ -1}} \approx 15hrs. \tag{4.13}$$

where Q is the net heat flux, taken as $400Wm^{-2}$, ρ_0 is a typical water density, and C_p is the specific heat of water. Of course, t can be much shorter if u_* is less, Q is larger, and/or the sea state is not fully developed.

Several studies have examined or commented on the rapid transition from a deep winter ML to a shallow summer ML (Elsberry and Garwood 1978; Elsberry and Raney 1978; Plueddemann *et al.*1995). Data and modelling studies show that the transition takes place in a single diurnal cycle. Elsberry and Raney (1978) emphasize that the key synoptic feature is an extended period of low winds during a time of net downward (i.e. heating the ocean) heat flux, and that a period of several days with such conditions can establish a stable seasonal thermocline for that year.

Thus the form of the LC criterion suggests that LC may delay the formation of a shallow mixed layer and a shallow seasonal thermocline. From the same argument it follows that LC may also delay daytime restratification of ML and formation of a diurnal thermocline.

Chapter 5

Isopycnal heaving and its effect on entrainment

5.1 Introduction

The dynamics of the upper ocean determines the thickness of the relatively well-mixed surface layer (ML) and, consequently, the value and evolution of the sea-surface temperature (SST). It is important to be able to predict the correct SST given the surface forcing, as the sea-surface temperature provides for a feedback to the atmosphere.

One-dimensional models of the ML, whether employing the dynamical instability concept (e.g. the PWP model (Price *et al.*1986), as used in Archer *et al.* (1993)), or formulated in terms of a vertically-varying eddy diffusivity (K-theory models, e.g. Mellor and Yamada (1974; 1982), as used in Kantha and Clayson (1994), also the KPP model of Large *et al.* (1994)), have frequently added a small background, or ambient, vertical diffusivity K_{bg}. Here we will restrict the discussion to diffusion of heat only. This is to represent, for example, the effects of intermittent mixing in the thermocline associated with internal wave activity, molecular diffusion, and other processes not accounted for in models. Background diffusivity is usually taken as a constant, spatially and temporally (Martin 1985).

This chapter will first review previous findings on the sensitivity of model output to the value of K_{bg}, with the general trend being that an increase in K_{bg} leads to a decrease in SST and a deeper ML.

In order to explain this sensitivity it is shown that there is a relationship between K_{bg} and the rate of entrainment $w_e = dh/dt$ if $dh/dt > 0$, zero otherwise. Increasing K_{bg} results in (1) direct redistribution of heat from the ML to the thermocline below it; (2) facilitation of entrainment across the ML base, thus causing a decrease in SST. I infer from the formulae that it is expected that the term involving K_{bg} will be important in the summer months. Results for runs with a Level 2 Mellor-Yamada model with an added background diffusion are presented.

Next, the process of isopycnal heaving by non-breaking internal waves is examined, and its mean effect on entrainment. Seasonal model runs for different heaving parameters are presented. Then a three-day period in the summer months is examined to infer how heaving causes additional entrainment. A heaving number R_H to characterize heaving is proposed. A correspondence between heaving and K_{bg} model runs is presented, with the aim of parameterizing heaving by a background diffusivity. Equivalent background diffusivity values are calculated for the sites/datasets that previous ML model studies simulated with K_{bg}, showing that the internal wave heaving can explain a significant part of the need for K_{bg} in ML models. Next, another scheme for parameterizing heaving is suggested, involving scaling down the stability velocity scale $(h\Delta b)^{1/2}$. The resulting seasonal $\mathcal{H} - T_s$ curves appear to better simulate the seasonal evolution of SST in the heaving runs.

5.2 Models and sensitivities to the background diffusivity K_{bg}

Martin (1985) carried out a comparison of simulations at OWS P and OWS N using different 1-D ML models (MY2; MY2.5; Niiler, Garwood). He also performed sensitivity studies, one of which was to the value of ambient, or background,

diffusivity. For a range of K_{bg} from $2 \times 10^{-6} m^2 s^{-1}$ to $4 \times 10^{-5} m^2 s^{-1}$ he obtained a maximum change in SST at the end of summer of about 1.5°C (see his Table 3), and also noted that the effects of ambient diffusion are largest in the summer when the gradient at the ML base is strong and the ML is shallow.

Gaspar *et al.* (1988) compared bulk and K-theory models at OWS Papa. They investigated the effects of heat diffusion in the thermocline by performing runs with $K_{bg} = 0; 1 \times 10^{-5}; 5 \times 10^{-5} m^2 s^{-1}$. They remarked that $K_{bg} = 5 \times 10^{-5} m^2 s^{-1}$ gives a picture inconsistent with observations, with a lower SST than observed and a too diffuse thermocline (their Figs. 4, 5). Consequently the value for K_{bg} that they used was $1 \times 10^{-5} m^2 s^{-1}$.

Gaspar *et al.* (1990) test their K-theory model at LOTUS site and at OWS Papa. Their model has a background diffusivity proportional to the value of turbulent kinetic energy (TKE). They impose a minimum value of TKE $e_{min} = 1/2q^2 = 10^{-6} m^2 s^{-2}$, equivalent to $K_{bg} \approx 1 \times 10^{-5} m^2 s^{-1}$ below the ML. The model shows sensitivity to this value and they remark that using $e_{min} = 10^{-5} m^2 s^{-2}$ ($K_{bg}^{min} \approx 1 \times 10^{-4} m^2 s^{-1}$) "grossly underestimates the temperature gradient in the thermocline".

Kantha and Clayson (1994) make an attempt to correct the systematic underprediction of ML depth due to insufficient mixing in a MY model . They add a vertical diffusivity immediately below the ML, i.e. in the thermocline and below, utilizing the scheme for interior mixing from Large *et al.* (1994) who used a base value of $K_{bg} = 1 \times 10^{-5} m^2 s^{-1}$. They apply these diffusivities in the thermocline, below the base of the ML which is defined by the value of twice the TKE, q^2, dropping below $10^{-6} m^2 s^{-2}$. They remark that they needed to use a typical value

for the diffusivity below the ML of $5 \times 10^{-5} m^2 s^{-1}$, five times greater than the one used by Large *et al.* (1994), explaining their choice with the "necessity for the high values of mixing". In addition, they add a constant background diffusivity of $1 \times 10^{-5} m^2 s^{-1}$, so the effective increase over Large *et al.*'s values is six-fold.

This again can be interpreted as an indirect indication that their model's output was sensitive to the value of K_{bg} in the thermocline. In fact, when simulating two weeks worth of LOTUS data, they remark that without mixing in the thermocline their model would overestimate the sea-surface temperature by $1.0^{\circ} - 2.5^{\circ}$C.

All this seems to suggest that, although very small compared with the diffusion within the mixed layer, background diffusion in the thermocline below the mixed layer does have an appreciable effect on entrainment. The value required to give agreement between model predictions of SST and data varies from 1 to 6 $\times 10^{-5} m^2 s^{-1}$, and a typical value is $1 \times 10^{-5} m^2 s^{-1}$.

5.2.1 A relationship between background diffusion and entrainment

Neglecting horizontal variability and mean upwelling, the equation for the mean temperature T is:

$$\frac{\partial T}{\partial t} + \frac{\partial}{\partial z}\left(\overline{w'T'}\right) = -\frac{1}{\rho_0 C_p}\frac{\partial I}{\partial z}, \tag{5.1}$$

where $\partial/\partial z\left(\overline{w'T'}\right)$ is the divergence of the turbulent heat flux and $I(z)$ is the flux profile for the penetrating part of the insolation.

The concept of a relatively well-mixed surface layer of depth h, with a temperature (and velocity) difference ΔT (ΔU) across its base is utilized in the so called bulk ML models. Integrating (5.1) and using the usual boundary conditions as in Chapter 2, we get

$$h\frac{dT_s}{dt} = \overline{w'T'}(-h) + \frac{Q}{\rho_0 C_p} \tag{5.2}$$

where $\overline{w'T'}(-h)$ is the turbulent flux across the ML base.

Let $\overline{w'T'}$ be used up entirely to bring colder water across the temperature difference ΔT and mix it with the water in the ML so that the ML deepens at a rate w_e. Then in bulk model formulation the turbulent flux across the ML base is parameterized by

$$\overline{w'T'}(-h) = -w_e \Delta T \tag{5.3}$$

e.g. Niiler and Kraus (1977).

In K-theory models, alternatively, one assumes that mixing is accomplished as needed by a large vertical diffusivity $K_v(z)$, which is a function of the flow via, for example, the gradient Richardson number. The turbulent flux is parameterized as

$$\overline{w'T'}(z) = -K_v(z)\frac{\partial T}{\partial z}. \tag{5.4}$$

Let the K-theory model have a background diffusivity term as well. Then, integrated over the ML, the equation for the sea-surface temperature is

$$h\frac{dT_s}{dt} = -K_v(-h)\frac{\partial T}{\partial z}(-h) - K_{bg}\frac{\partial T}{\partial z}(-h) + \frac{Q}{\rho_0 C_p} \tag{5.5}$$

If both models produce identical results, we can formally write

$$w_e = \frac{K_v(-h)\frac{\partial T}{\partial z}(-h)}{\Delta T} + \frac{K_{bg}\frac{\partial T}{\partial z}(-h)}{\Delta T} \tag{5.6}$$

where w_e would be the entrainment rate for the model with background diffusion. Note that (5.6) does not imply that the entrainment rate w_e for the case of a model with background diffusivity is a summation of the entrainment rate term from a $K_v(z)$ model and from the term involving K_{bg}; the vertical temperature profile $\partial T/\partial z$ (and also ΔT) will be different when background diffusivity is added. Equation (5.6) simply relates w_e to K_{bg} and $K_v(z)$ without implying that w_e in the case with K_{bg} and $K_v(z)$ is larger than w_e in the case with $K_v(z)$ alone. Although we cannot prove with this analytical approach that K_{bg} will result in more entrainment, models demonstrate this to be the case.

When would we expect that the last term on the right-hand side of (5.6) is significant? We need to use the fact that $K_v(-h)$ depends on the flow, whereas K_{bg} does not. If the conditions are such that e.g. the local Richardson number is above its critical value, then $K_v(-h)$ would be identically zero. In addition, we seek a situation when $\frac{\partial T}{\partial z}(-h)$ is large, and ΔT is small, as this maximizes the second term on the right-hand side of (5.6).

All three requirements can be satisfied in the summer season, as then the ML is shallow, with a relatively small temperature difference, but with a large gradient at its base set mainly by mechanical stirring sharpening the interface. Thus the expectation is that background diffusivity might influence more noticeably ML entrainment under conditions of net heating. We turn to modelling next to confirm or rebut this hypothesis.

5.2.2 Seasonal runs with a MY-2 model

We use a standard version of the Mellor-Yamada level 2 (Mellor and Yamada 1974; Mellor and Yamada 1982) 1-D ML model. The variable vertical diffusivity at each depth level is a product of the length scale, the rms turbulent velocity, and a dimensionless function of the local Richardson number Rg. This function is positive when Rg is below the critical value, and zero otherwise.

First, three integrations were performed using different values for K_{bg}: $0; 1 \times 10^{-5}; 5 \times 10^{-5} m^2 s^{-1}$ — to check for the expected sensitivity to the value of background diffusion. These initial runs were for a duration of 50 days each. The forcing applied consisted of a constant wind stress of 0.1 Pa, and a diurnal heating/cooling cycle with a zero daily mean. The time-step $dt = 2$ seconds; grid-size $dz = 3$ metres. The lower part of the model domain has a linear temperature gradient of about $7.7 \times 10^{-3} K m^{-1}$.

Results from these three runs are combined in Figure 5.1, showing the initial and the three final temperature profiles. The SST decreases as K_{bg} increases, and the thermocline becomes more diffuse.

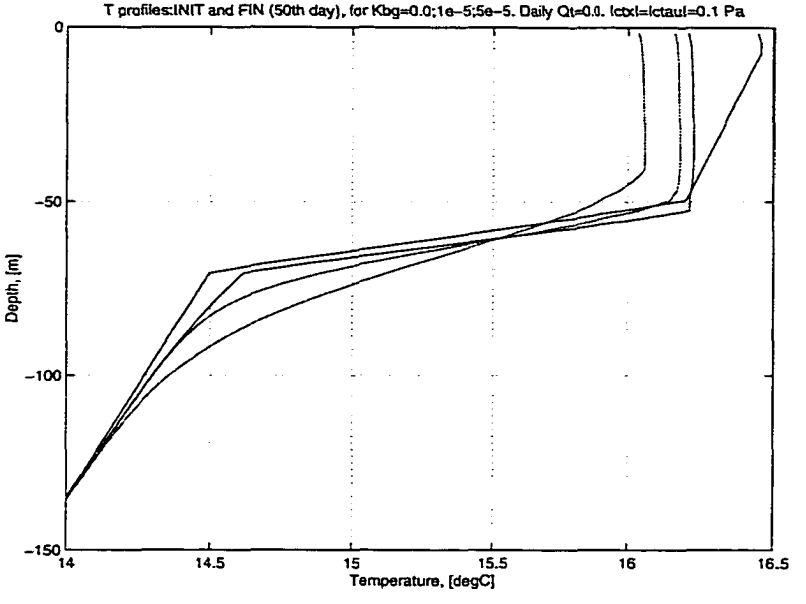

Fig. 5.1. Temperature profiles after 50-day runs with the MY-2 model for different background diffusivity values, and for forcing with zero mean total heat flux, constant eastward wind stress of 0.1 Pa. From right to left at the surface: initial profile; 50th day final profiles for $K_{bg} = 0; 1 \times 10^{-5}; 5 \times 10^{-5} m^2 s^{-1}$.

Next, we run the model over a seasonal cycle, with varying heat fluxes and winds (Fig. 5.2) as used in Chapter 3. Figure 5.3 shows the three hysteresis curves of SST T_s versus heat content $\mathcal{H}$, and the sensitivity to K_{bg} is obvious - there is more than 4 degrees difference in the seasonal SST maximum between runs with $K_{bg} = 1 \times 10^{-5} m^2 s^{-1}$ and $K_{bg} = 5 \times 10^{-5} m^2 s^{-1}$, for example. The loops are closed, ensuring that there is no appreciable net effect of the background diffusion on the model's ability to repeat the same values year after year.

The loops seem to diverge from one another during the summer months of June, July, and August, when there is a shallow ML, cycling up and down diurnally, with background diffusion influencing the ML depth (and SST) indirectly by weakening the temperature jump at the base of the mixed layer, thus facilitating instability and entrainment.

There are a few sharp slumps in SST towards the end of the summer for all three model loops. Those reflect sudden deepenings of the mixed layer. A close look at these events (not shown) reveals that at these points in time the mixed layer is very shallow, only 2 grid-points, and so the SST is extremely sensitive to it, as ML deepening by another grid-point is equivalent to a 50% increase in ML depth. The characteristic shape of the diffusivity profile is not resolved at all at those shallow depths. Thus it seems quite likely that these events do not reflect real physics but are artefacts of the inability to resolve the vertical diffusivity profile properly.

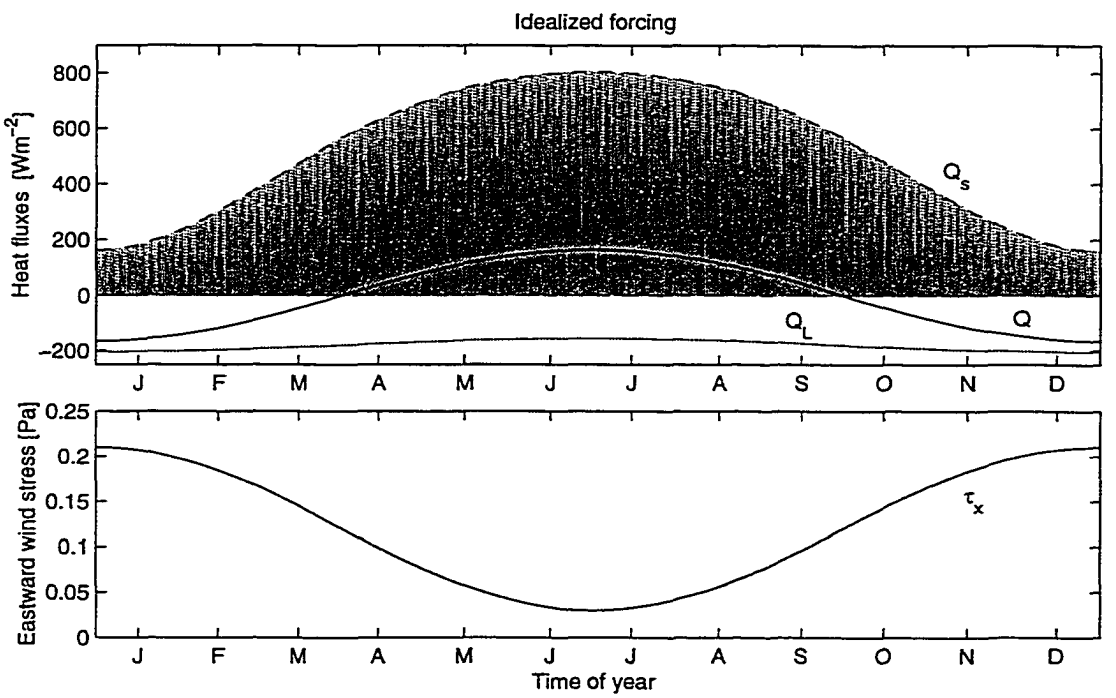

Fig. 5.2. Idealized forcing with zero mean annual heat flux. Top: insolation Q_S, total heat loss Q_L (the sum of sensible, latent, and longwave), and total heat flux Q_T. Bottom: eastward wind stress τ_x.

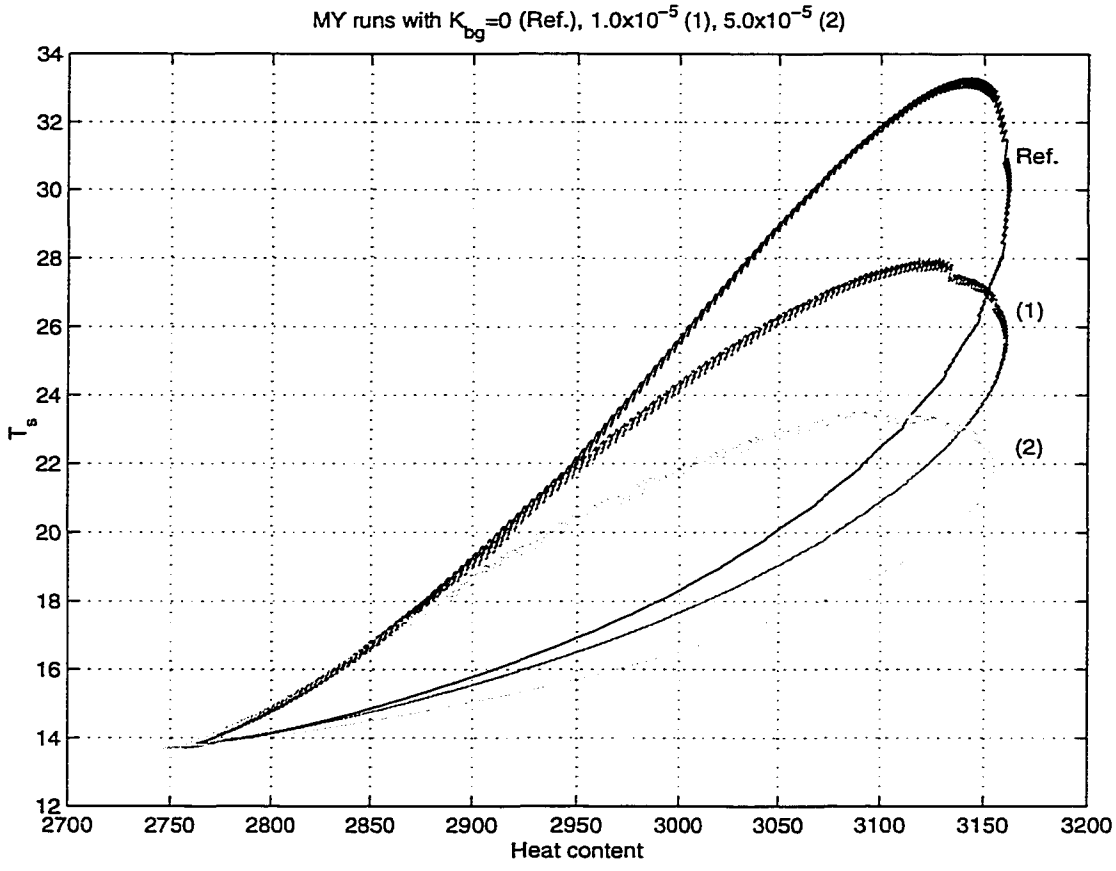

Fig. 5.3. Seasonal runs with MY-2 model for two different background diffusivity values: $1 \times 10^{-5} m^2 s^{-1}$ (middle), and $5 \times 10^{-5} m^2 s^{-1}$ (bottom). Compare the maximum seasonal SST at the end of summer with the reference ($K_{bg} = 0$ (top) case).

5.3 Effects of isopycnal heaving on entrainment

All quoted studies seem to suggest that models are sensitive to the value of background diffusivity. It is thus important to establish whether K_{bg} represents mixing processes in the thermocline or is a proxy for processes omitted from the models.

One such process is isopycnal heaving in the thermocline due to non-breaking internal waves. This refers to the periodic up-down movement of isopycnals, which leads to stretching and compressing of the mixed layer. I examine the sensitivity of the mean entrainment rate to the heaving at the base of the mixed layer by considering a modification of the PWP ML model that allows for periodic isopycnal displacement superimposed on the other variability. Results from seasonal runs with this model and idealized forcing are presented, along with estimates of the equivalent background diffusivity.

5.3.1 A model with isopycnal heaving

Isopycnal heaving is a ubiquitous feature below the mixed layer, as evident from time-series of temperature profiles e.g. from the LOTUS experiment in the Sargasso Sea (Fig. 5.4). It is interesting to note that the periods and amplitudes of the oscillations do not vary appreciably with depth, and are more or less the same throughout the thermocline and below it.

Theoretically, the frequency of the internal waves can range from the local inertial frequency f to the local buoyancy frequency N. In the deeper ocean,

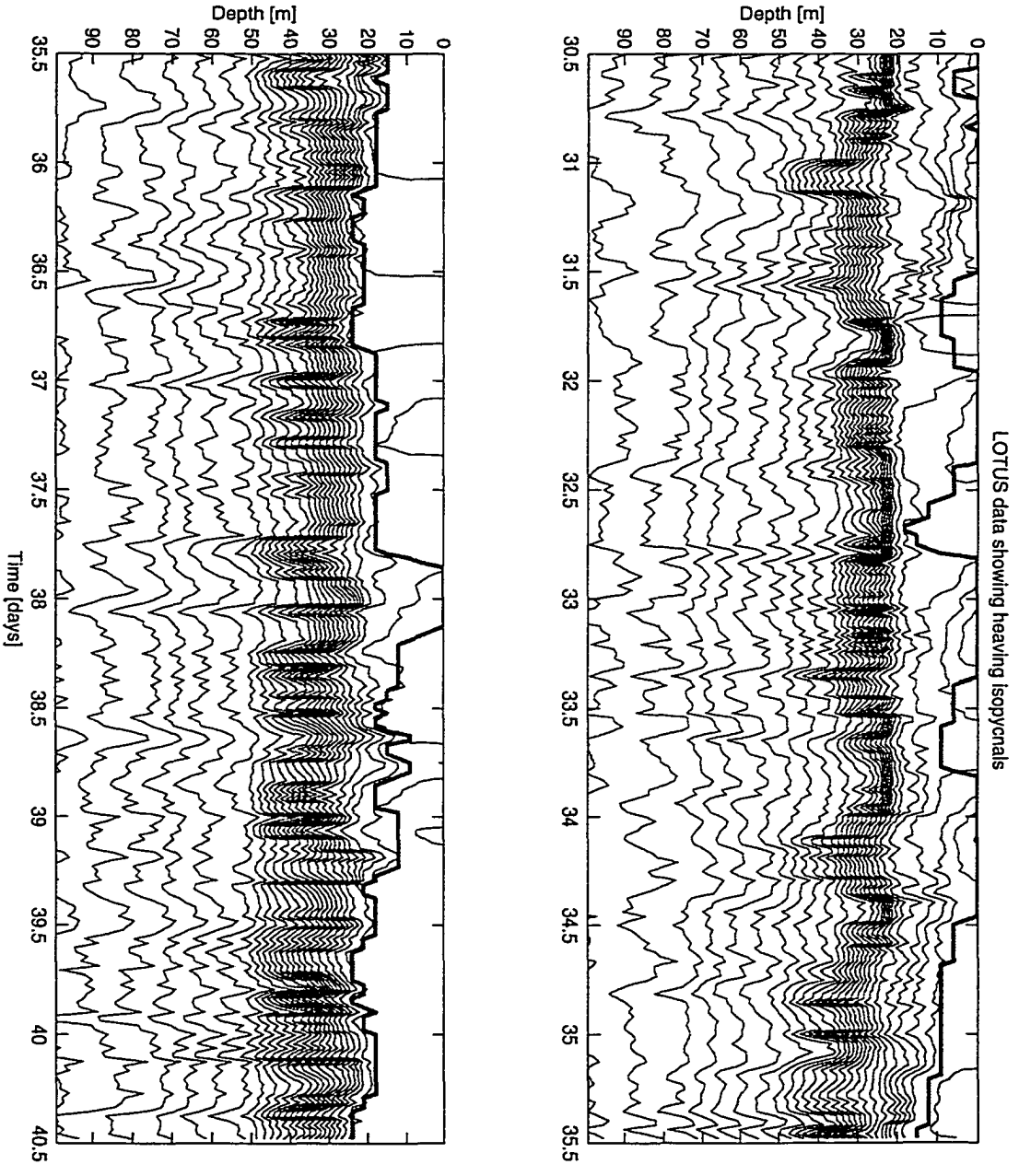

Fig. 5.4. Ten-day time series isopycnal plot of depth versus time, from the LOTUS dataset. Note the coherent heaving movement of isopycnals regardless of depth. Also shown is the estimated mixed layer depth.

where the stratification is usually weak compared to the seasonal thermocline, typical internal waves have vertical displacements (amplitudes) of the order of tens of meters and periods from tens of minutes to many hours (Garrett and Munk 1979). In the upper ocean, however, internal waves have smaller amplitudes and shorter periods. Dillon and Caldwell (1980) observed internal waves in the upper 200 metres at OWS Papa, as part of the MILE experiment (Davis *et al.*1981a). They report a range of frequencies from 2.5 to 4 cph, with amplitudes from 0.7 to 2.5 metres (Levine *et al.*1983). Burenkov and Vasilkov (1987) observed internal waves in the vicinity of the Mascarene Ridge in the upper 150 metres of ocean, with amplitudes ranging from 2 to 4 metres and frequencies of up to 6 cph. Käse and Clarke (1978) made measurements in the upper 60 metres at the GATE experiment, and found internal waves with frequencies in the 2–5 cph range and amplitudes from 1 to 2 metres. Pinkel and Anderson (1992) looked at data from the PATCHEX experiment (Brainerd and Gregg 1993) and found internal waves, very coherent with depth, of 1–2 cph frequency and amplitude of up to 5 metres. LOTUS data (Briscoe and Weller 1984) presented in Figure 5.4 show internal waves with frequencies less than 1 cph and typical amplitudes of 5 metres or less.

In order to examine the mean effect of isopycnal heaving on entrainment in more detail, I have chosen to switch from the MY model to a simpler and computationally faster model — the Price-Weller-Pinkel (PWP) model, and use better vertical resolution.

The Price-Weller-Pinkel model, as discussed in Chapter 2, is a simple 1-D mixed layer model which relies on static and dynamic stability criteria for mixing. Despite its simplicity, it is known to perform adequately under a wide range

of conditions, as attested in various model inter-comparison and simulation studies (Martin 1986; Schudlich and Price 1992; Crawford 1993; Kantha and Clayson 1994; Large and Crawford 1995; Plueddemann *et al.*1995). Its partial mixing below the mixed layer, dependent on the gradient Richardson number Rg, is an attempt to simulate the effect of unresolved processes in the thermocline, and to achieve more realistic-looking profiles without a sharp jump at the ML base. Since this chapter deals with process studies in the thermocline and in view of the questions about the implementation of the gradient Richardson number criterion, as discussed in Chapter 2, it seems prudent to switch off the Rg criterion for thermocline mixing and instead either add a background diffusivity, as done e.g. in Archer *et al.* (1993), or add a heaving routine, as required.

Before going into model studies of heaving using the PWP model, we have to establish the sensitivity of its output to background diffusion in the manner in which it was done previously with the MY model. Recall from MY model runs that increasing K_{bg} had the effect of lowering the seasonal SST maximum. Running a PWP model with different background diffusivities, not surprisingly, produces a similar picture. Figure 5.5 presents seasonal model runs for three K_{bg} values: $0.7 \times 10^{-5} m^2 s^{-1}$ (1), $1 \times 10^{-5} m^2 s^{-1}$ (2), and $5 \times 10^{-5} m^2 s^{-1}$ (3). Those are compared with the reference (top) case.

Thus the modified PWP model with added background diffusivity exhibits sensitivity to the value of K_{bg} consistent with previous studies and other models (compare Figs. 5.3 and 5.5). Hence we proceed with a process study of isopycnal heaving using this model.

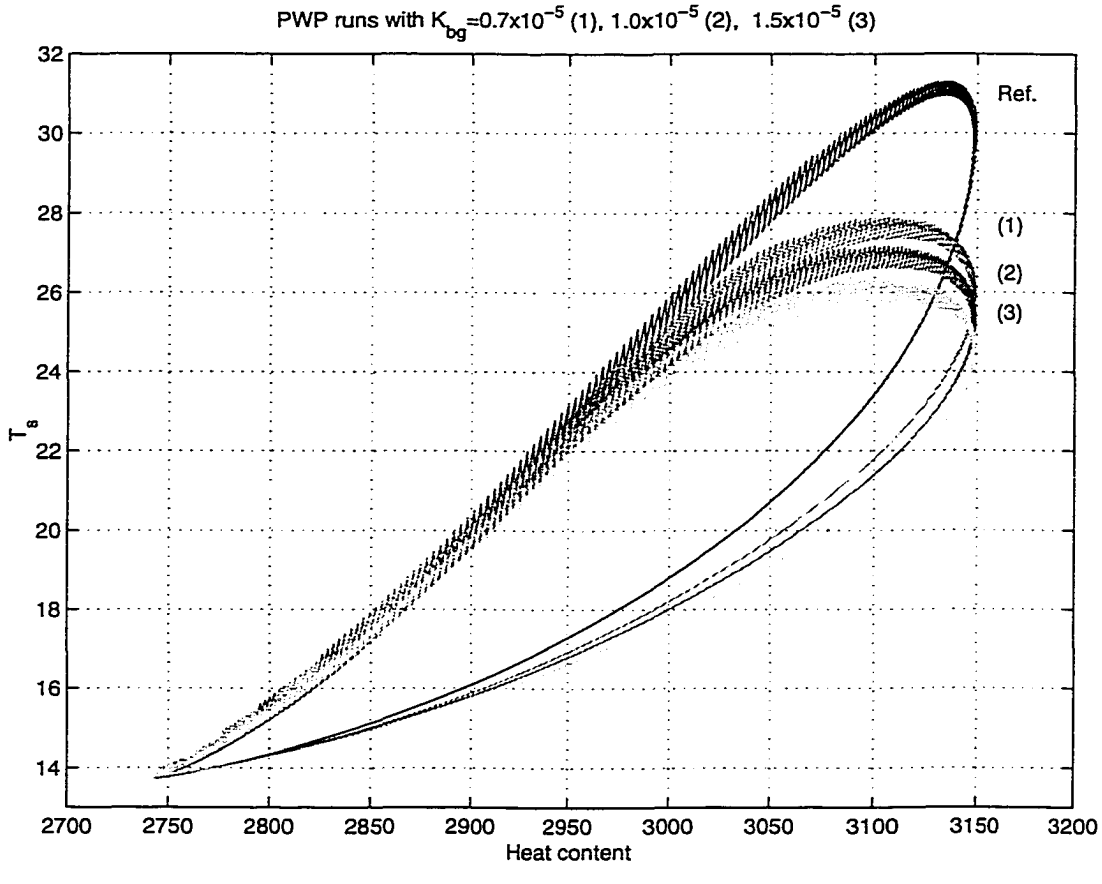

Fig. 5.5. Seasonal runs with the PWP model for three different background diffusivity values: $0.7 \times 10^{-5} m^2 s^{-1}$ (1), $1 \times 10^{-5} m^2 s^{-1}$ (2), and $1.5 \times 10^{-5} m^2 s^{-1}$ (3). Also shown for comparison is the reference ($K_{bg} = 0$ (top) case).

The PWP model was amended with an idealized heaving routine with a prescribed single representative amplitude and period/frequency. The 1-D equations for temperature and currents at each grid-point are

$$\frac{\partial T}{\partial t} + W\frac{\partial T}{\partial z} = -\frac{1}{\rho_0 C_p}\frac{\partial I}{\partial z} - \frac{\partial}{\partial z}\left(\overline{w'T'}\right), \tag{5.7}$$

$$\frac{\partial U}{\partial t} - fV + W\frac{\partial U}{\partial z} = -\frac{\partial}{\partial z}\left(\overline{w'u'}\right), \tag{5.8}$$

$$\frac{\partial V}{\partial t} + fU + W\frac{\partial V}{\partial z} = -\frac{\partial}{\partial z}\left(\overline{w'v'}\right), \tag{5.9}$$

where

$$W = \frac{\partial Z}{\partial t} = \begin{cases} 2\pi\left(\frac{A_w}{T_w}\right) cos\left(\frac{2\pi}{T_w}t\right) & |z| \geq h, \\ \frac{|z|}{h} 2\pi\left(\frac{A_w}{T_w}\right) cos\left(\frac{2\pi}{T_w}t\right) & |z| < h. \end{cases} \tag{5.10}$$

and

$$Z = Z(\rho = const., t), \tag{5.11}$$

so W is simply the prescribed rate of change of an isopycnal's depth with time. A_w denotes the representative amplitude of the internal wave, T_w is the period of the wave, and h is the ML depth.

Figure 5.6 is an isopycnal plot of depth versus time for a 24-hour period, and shows a typical output from the modified PWP model. Heaving is performed with the same amplitude and period below the mixed layer, in accordance with observations, and is attenuated from its constant value at the base of the ML to

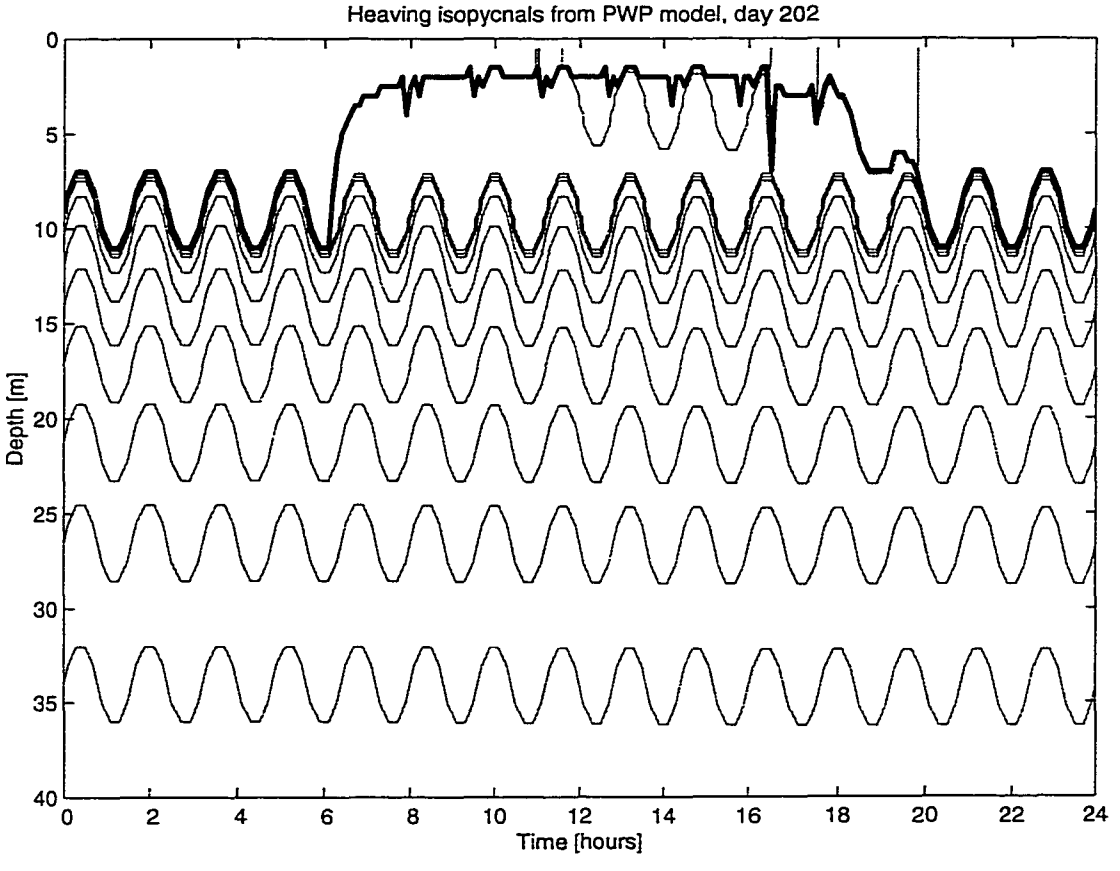

Fig. 5.6. One-day (year-day 202) modified PWP model output showing heaving isopycnals (thin lines) and mixed layer depth (thick black line).

zero at the surface. This seems to be a good first order representation of the non-breaking wave field below the mixed layer. Changes in horizontal current due to waves are not considered, as $\partial W/\partial z = 0$ at the ML depth and below, and constant within the ML, where U and V are represented only by averaged for the mixed layer values. Moreover, the 1-D model has no horizontal variability, hence no horizontal advection is supported or considered.

To explore the mean effect of heaving on entrainment, model runs with different internal wave amplitudes and periods, and different amplitude–period ratios, were performed. The range considered for A_w is from 2 to 5 metres, and the range for T_w is from 0.4 to 2.4 hours, corresponding to a 0.4–2.5 cph frequency range.

5.3.2 Seasonal runs with different heaving parameters

The PWP model with heaving, as described above, was run over a seasonal cycle, and forced with the same idealized forcing as before (the forcing is shown on Fig. 5.2). Because the net yearly-mean heat flux is zero, the curve of sea-surface temperature versus heat content forms a closed loop. Regardless of the mixed layer dynamics in the heating season, at the end of the winter the model ocean achieves a maximum mixed layer depth, resetting its properties. This serves as a good reference point from which model runs with different heaving parameters can be compared in the way they influence the evolution of the sea-surface temperature, especially in the summer months. The initial temperature profile used for these seasonal runs is

Z [m]	T(z) [deg.C]
0.0	16.5
-50.0	16.2
-70.0	14.5
-200.0	13.5

with a linear interpolation between these points. However, the particular initial profile and/or the deep ocean stratification turn out to be unimportant and do not affect the results of this study, as will be shown later.

The latitude chosen for the model runs is 30 degrees N so the model is run in subtropical conditions, characterized by a shallow summer mixed layer and a large seasonal variation in sea-surface temperature. The effects of ML dynamics on SST are thus amplified, making it a favourable setup for exploring the effects of heaving on entrainment.

We will adopt the maximum change (from a reference case) in SST at the end of summer $\Delta T_s^{\max}$ as a criterion for comparison of different heaving runs with a reference, no-heaving, case. This is in accordance with Martin (1985) and others, who used this criterion in their sensitivity studies of the effect of background diffusivity.

Figure 5.7 presents typical results from the first set of experiments, where the internal wave period was fixed and the wave amplitude was varied. All three loops converge in the winter to a point with maximum ML depth and minimum SST of about 14°C. The top curve is the reference case with no heaving. Its sea-surface temperature peaks at about 31°C at the end of summer. The middle curve

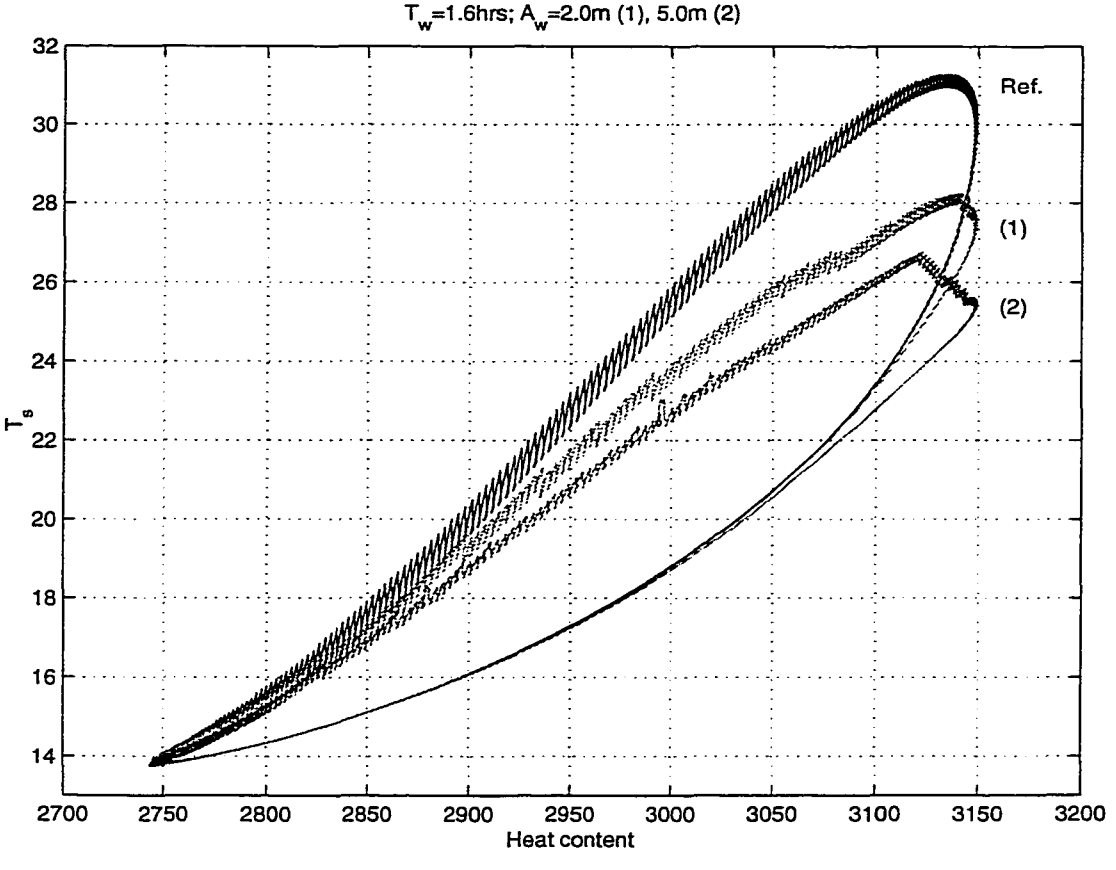

Fig. 5.7. Seasonal runs with a modified PWP model for two different amplitudes of isopycnal heaving: $A_w = 2.0m$ (1), and $A_w = 5.0m$ (2), with a fixed wave period T_w of 1.6 h. Those are compared to the reference (top) no-heaving case.

— a model run with heaving with 2 m amplitude — has a markedly lower SST maximum, peaking at about 28°C. Increasing the wave amplitude to 5 metres leads to further decrease in the maximum SST (bottom curve). The systematic differences between the three loops arise during conditions of net heating. The runs with heaving diverge from the reference case, suggesting a mean additional entrainment, hence incorporating colder water from below and lowering the SST throughout the summer months. With a fixed wave period, increasing the amplitude of the heaving leads to more entrainment and lower SST. This can also be seen on Figure 5.8 presenting ML depth time series from these two runs. In both panels, the solid black lines depict the daily range of ML depth for the reference case. Compared to it, the nighttime, seasonal mixed layer for a heaving run with $A_w = 2.0m$ (top panel) is slightly deeper during the spring shallowing while the shallow seasonal thermocline is being established; there are also episodic deepenings that entrain colder water into the ML throughout the summer. As the seasonal SST maximum is achieved around days 250-255, it is significant that the ML in the heaving case starts to deepen well before that time, thus causing a lower SST maximum for the year. The mixed layer depth for the heaving run with $A_w = 5.0m$ (bottom panel) exhibits very similar features, but in a more pronounced way. The systematically deeper nighttime ML during the spring months and at mid-year is more evident, and the deepening before the seasonal SST maximum is attained starts even earlier and is more emphasized.

In the next set of experiments, typical results of which are presented in Figure 5.9, we fix the amplitude at 2 metres, and vary the heaving period. Again, the top curve is the reference case with no heaving. The curve labeled (1) is a

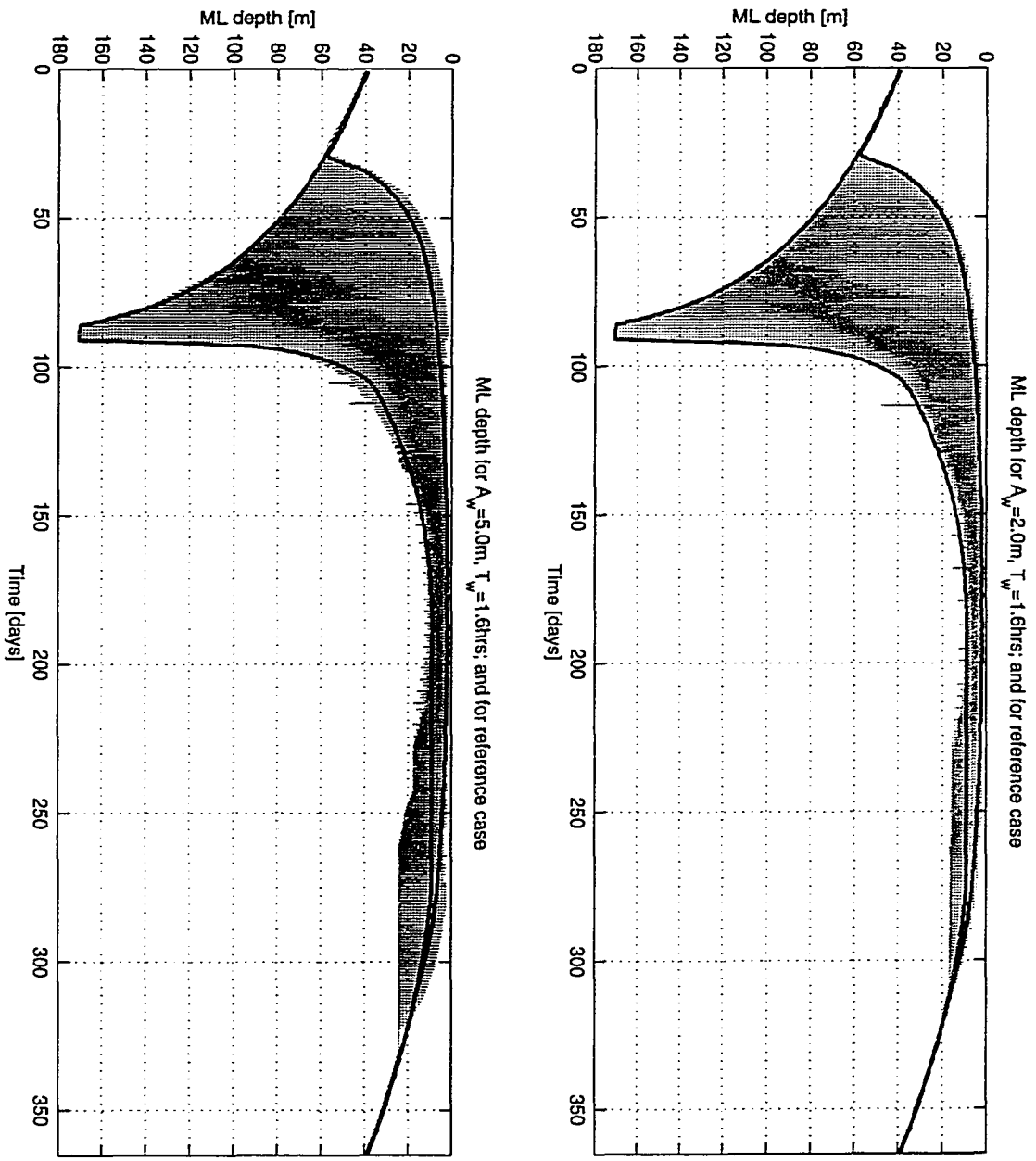

Fig. 5.8. Mixed layer depth from a modified PWP model for two different amplitudes of isopycnal heaving: $A_w = 2.0m$ (top panel), and $A_w = 5.0m$ (bottom panel), with a fixed wave period T_w of 1.6 h. Those are compared to the mixed layer depth (daily range) for the reference case.

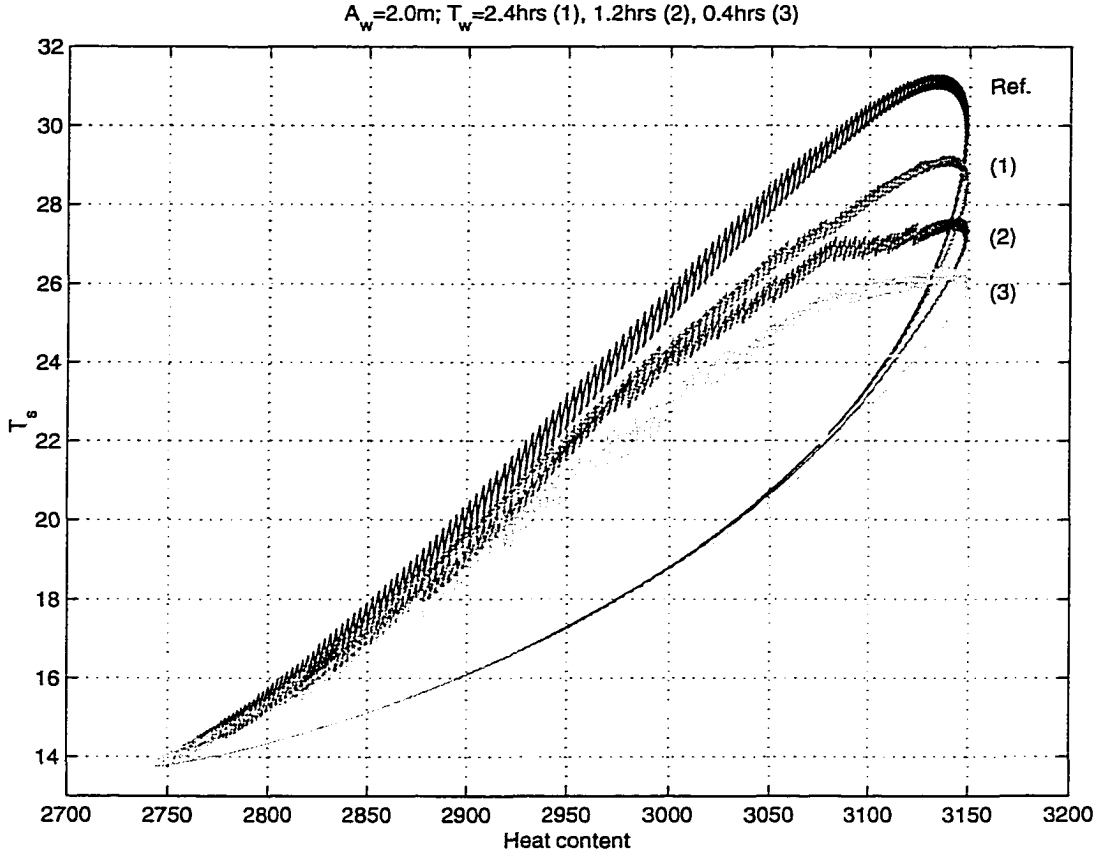

Fig. 5.9. Seasonal runs with a modified PWP model for three different periods of isopycnal heaving: $T_w = 2.4\ h$ (1), $T_w = 1.2\ h$ (2), and $T_w = 0.4\ h$ (3), with a fixed wave amplitude of A_w of $2.0m$. Those are compared to the reference (top) no-heaving case.

model run with heaving, with a period of 2.4 h. The SST maximum is at about 29°C, lower than the reference case. Decreasing the wave period to 1.2 h leads to further decrease of the maximum SST (curve (2)). Curve (3), with the lowest maximum sea-surface temperature of about 26°C, is a result of a model run with the shortest period, 0.4 h, of the three. Again, the systematic differences between the three loops arise during conditions of net heating. With a fixed wave amplitude, decreasing the period of the heaving leads to more entrainment and lower SST.

Figure 5.10 presents ML depth time series from the heaving runs with $T_w = 1.2\ h$ (top panel), and $T_w = 0.4\ h$ (bottom panel). As in Fig. 5.8, the solid black lines depict the daily range of ML depth for the reference case. The ML for the heaving runs exhibits the same features as described before. Decreasing the wave period emphasizes the extra deepening, especially the deepening before the seasonal SST maximum is established.

The results from these sets of experiments suggest that heaving might have a significant mean effect on entrainment, and lower the sea-surface temperature in the summer in a systematic way. In order to try to understand what exactly happens when heaving is present, we take a detailed look at a three-day period, days 200–202, in the summer.

5.3.3 A detailed look at a three-day period in the summer

It was demonstrated in the previous section that a model run with heaving results in the sea-surface temperature diverging from the reference SST in a systematic way, under conditions of net ocean heating. But how does heaving cause this? Let us consider a three-day period, from day 200 to 202 (i.e. 3 days in the

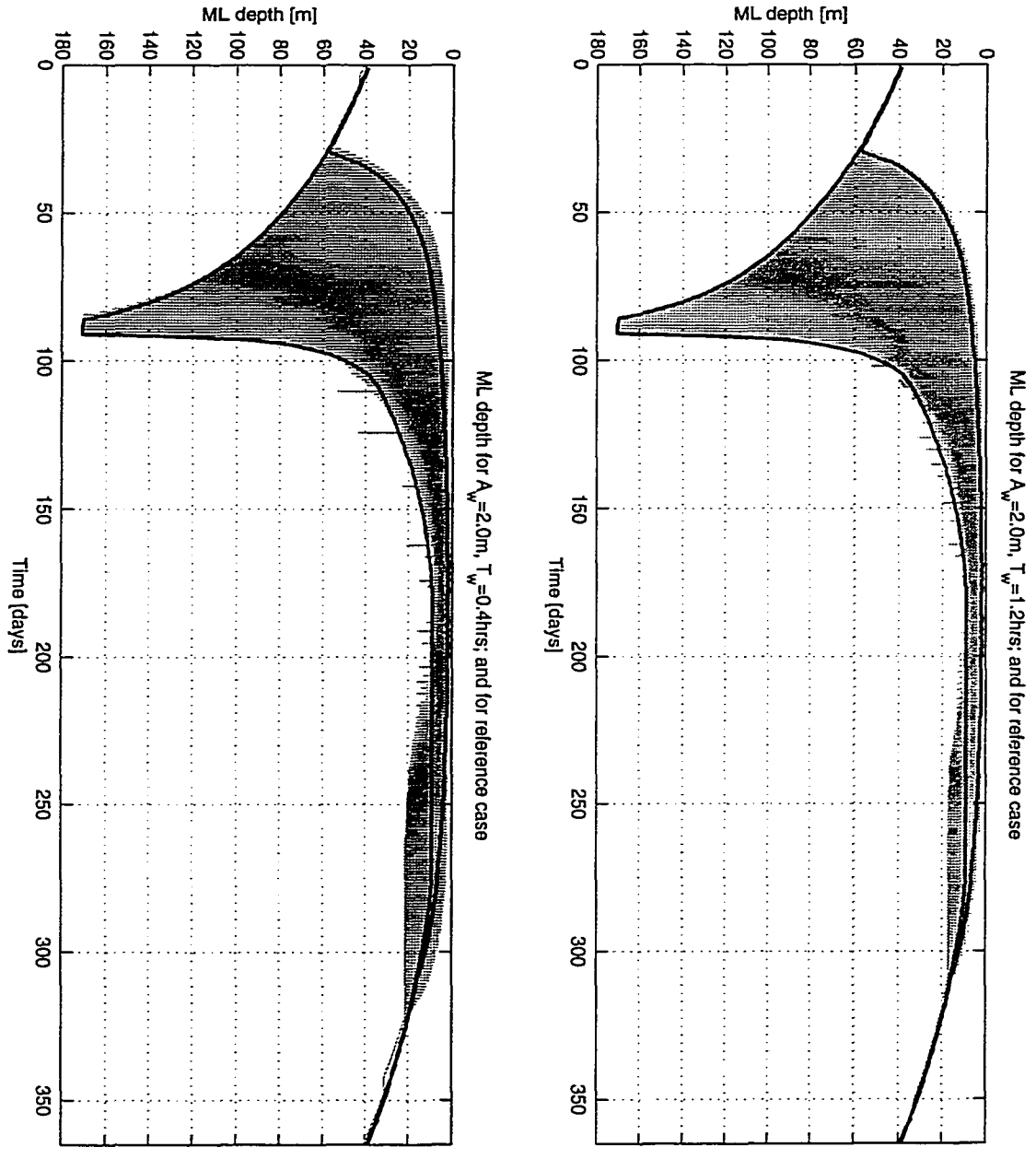

Fig. 5.10. Mixed layer depth from a modified PWP model for two different periods of isopycnal heaving: $T_w = 1.2\ h$ (top panel), and $T_w = 0.4\ h$ (bottom panel), with a fixed wave amplitude A_w of 2.0 m. Those are compared to the mixed layer depth (daily range) for the reference case.

second half of July). The last temperature and currents profiles from the reference model output, before the start of day 200, were given as an initial condition to a model with the same time-step and vertical resolution, but with heaving with an amplitude of 2 metres and a period of 1.6 h. The heaving model was run for 3 days, then the temperature profiles were averaged over the heaving period, for both the reference and the heaving runs. The resulting contour plots of mean temperature as a function of depth and time are presented in Figure 5.11. As the mixed layer depth is of the order of 10 metres during this period, only the top 20 metres of the model ocean are showed. The top panel is the reference case. There is a relatively strong summer thermocline at a depth of about 9 metres, and each diurnal cycle is clearly visible. The sea-surface temperature steadily increases due to the net daily heating and reaches a maximum of $26.7^{\circ}C$ at noon on the third day. The bottom panel shows temperature contours for the heaving case. The thermocline appears more diffuse and a bit warmer e.g. at a depth of 9 metres. The SST does not increase so rapidly, in fact the first diurnal peak is not resolved by the pseudo-color scheme, in contrast with the reference case. By noon on the third day the SST is almost a half degree lower indicating entrainment due to heaving.

Let us now examine an even more revealing plot — of the mean temperature difference between the two cases. The difference of $T_{\text{heav.}} - T_{ref.}$ is presented in Figure 5.12. The first temperature difference profile was subtracted from all the other profiles as well, to make the reference, background field exactly zero, shown in the figure in orange. Both cases were subject to the same net heating, so all temperature differences emerging with time must be due to the different patterns of entrainment. As constructed, a positive difference (color-coded with a red palette)

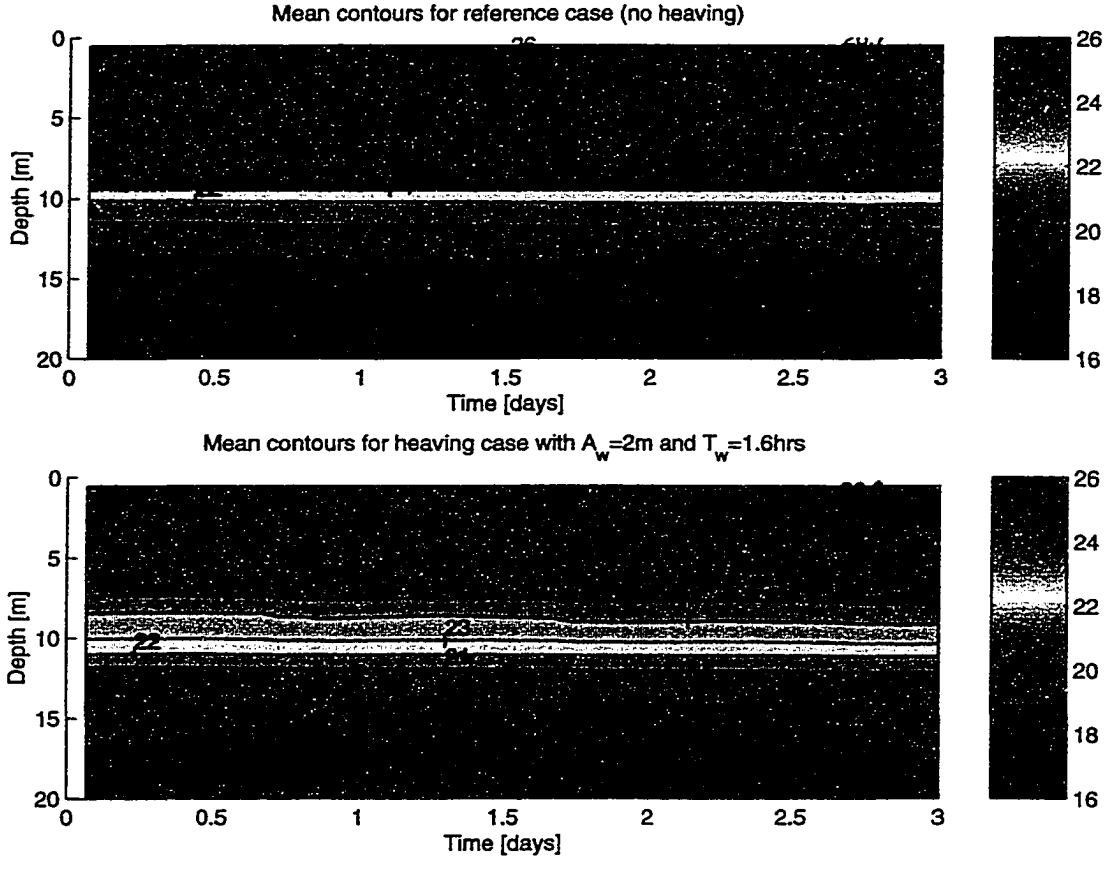

Fig. 5.11. Contour plots of depth versus time, for days 200-202. Top panel: mean (over a heaving period) temperature contours for the reference case (no heaving). Bottom panel: mean temperature contours for a heaving case with an amplitude of 2 metres and a period of 1.6 hours. The plots show the upper 20 metres of model ocean.

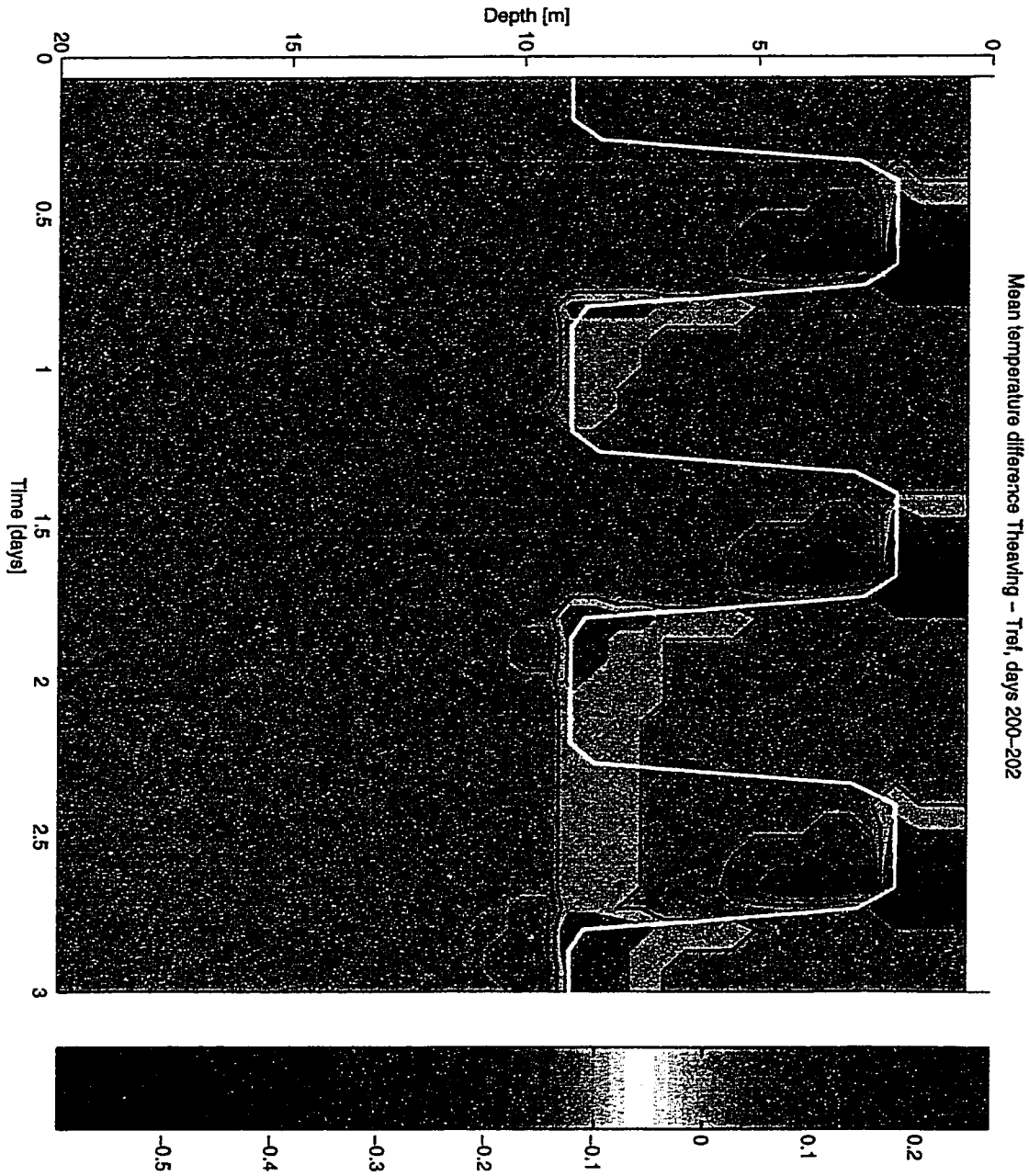

Fig. 5.12. Contour plot of depth versus time, for days 200-202, of the mean temperature difference (over a heaving period) between the reference case (no heaving) and a heaving case with an amplitude of 2 metres and a period of 1.6 hours. The plot shows the upper 20 metres of model ocean. The mixed layer depth for the reference case is shown in white.

indicates warmer water in the heaving case, and a negative difference (color-coded with a blue palette) indicates colder water in the heaving case. The mixed layer depth for the reference case is also shown for comparison.

From the first day, at daytime a characteristic pattern emerges, indicating that in the heaving case there is colder (than the reference) water within the mixed layer, and warmer (that the reference) water below it, in the diurnal thermocline. At night the daytime shallow diurnal thermocline is destroyed, and with it the pattern disappears, to reappear on the following day. In the seasonal thermocline the analogous colder–warmer "dipole" is established and maintained, getting stronger with time, suggesting that differences between the reference case and the heaving case increase. This pattern is characteristic of entrainment of colder water into a deepening mixed layer.

Physically, the entrainment due to heaving can be explained as follows. As the non-breaking internal waves pass through the thermocline, they periodically move the ML base up and down, thus stretching and compressing the mixed layer. Let us suppose that the mixed layer is stable, i.e. no deepening occurs. When such a layer is stretched, it becomes even more stable, as evident from the simple dynamic stability criterion in the PWP model involving the bulk Richardson number: $Rb = (g\alpha h\Delta T/\Delta \mathbf{u}^2)$, where h is the ML depth. However, when this mixed layer is compressed, there might be times when it will become unstable (the closer to marginal stability before compressing the ML is, the more likely is this to happen) and subsequently deepen, entraining colder water from below. Therefore the mean effect of heaving is likely to be net deepening and entrainment, and we saw this in the model results.

Since the diurnal thermocline is destroyed each night, it is likely that, in the heaving run, there will not be any important memory retained about the shallow daytime stratification and accumulated SST differences with respect to the reference case. This would imply that it is the seasonal thermocline — the strongly stratified layer between the daily maximum ML depth and the relatively weakly stratified ocean below it — that is more important (along with seasonal ML depth variability) for establishing any systematic differences due to entrainment from heaving. Figure 5.13 presents a comparison between a heaving run (curve (1) from Fig. 5.7) with $A_w = 2.0\ m$ and $T_w = 1.6\ h$ and a run with the same heaving parameters, but with heaving switched off between the hours of 8:00am and 4:00pm local time each day, when a shallow diurnal thermocline is maintained. The resulting $\mathcal{H} - T_s$ loops do not differ significantly from each other, suggesting the relative unimportance of daytime entrainment from heaving.

5.3.4 Heaving number

Heaving with a given amplitude and period results in lower sea-surface temperatures, the maximum seasonal SST difference between it and the reference case being $\Delta T_s^{\max}$. The larger the amplitude and/or the shorter the period, the larger $\Delta T_s^{\max}$ is. However, $\Delta T_s^{\max}$ does not increase linearly with heaving amplitude/period; instead the increments get smaller as if the SST difference becomes less sensitive to the entrainment from heaving.

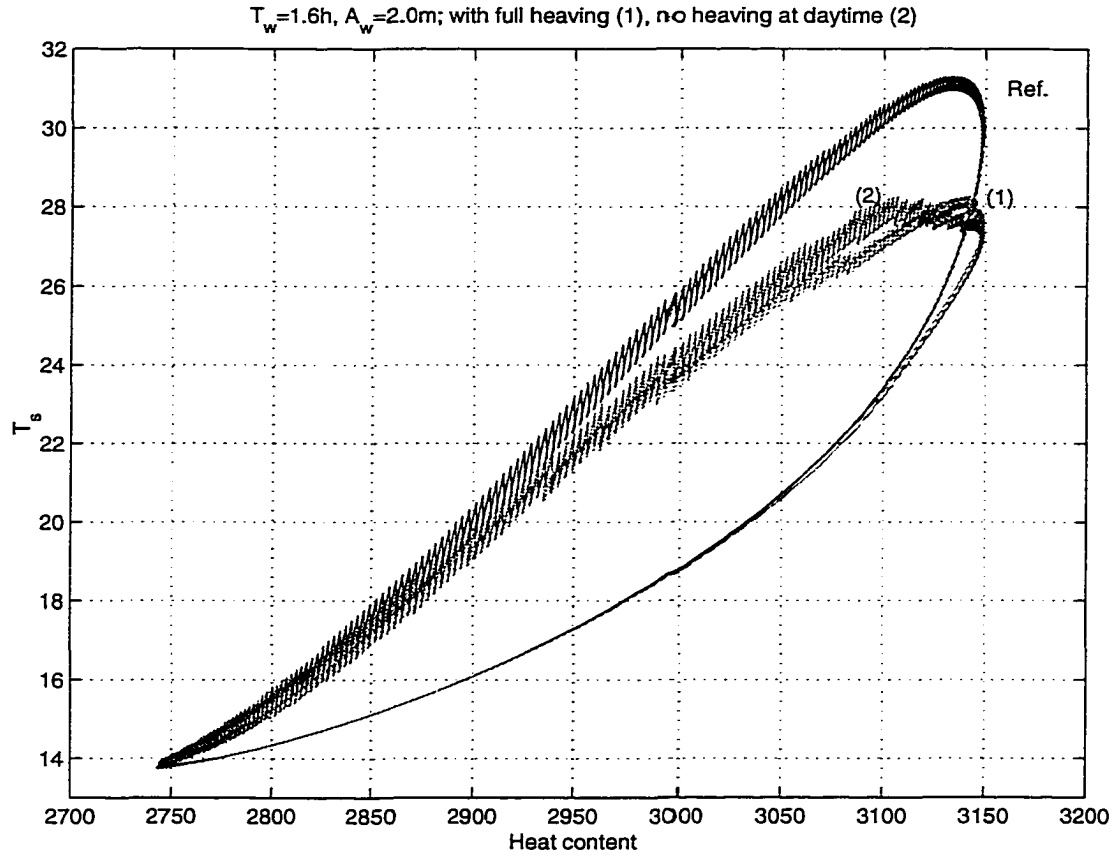

Fig. 5.13. Seasonal runs with a modified PWP model for a heaving with A_w = 2.0 m and T_w = 1.6 h: original run with continuous heaving (1) and a run with heaving switched off from 8:00am to 4:00pm each day (2). The no-heaving case is also shown for reference.

Combining these results, let us introduce a non-dimensional number to characterize heaving — a heaving number R_{H}:

$$R_{\mathrm{H}} = \frac{A_{\mathrm{w}} T_{\mathrm{D}}}{\overline{h_{\mathrm{sh}}} T_{\mathrm{w}}} \tag{5.12}$$

where T_{D} is the diurnal period; A_{w} and T_{w} are the internal wave (heaving) amplitude and period, respectively; $\overline{h_{sh}}$ is the average seasonal mixed layer depth when a shallow seasonal thermocline is maintained ($\overline{h_{sh}}$ is averaged over days 121–270).

As we are trying to relate heaving to entrainment and to changes in SST, $\overline{h_{sh}}$ is a relevant scale as the larger it is, the less sensitive the SST is to additional entrainment from heaving. $\overline{h_{sh}}$ reflects the atmospheric forcing and the processes, like heaving, that influence ML dynamics. It averages about 16 m for our case. It is not dependent on the initial profile, or on the deep ocean stratification. This is because the shallow seasonal thermocline is established each year from a "clean slate" (Stommel *et al.*1969) on top of a deep mixed layer. Indeed, model runs with different initial and deep stratifications (not shown) confirm this, yielding identical $\overline{h_{sh}}$ for the same forcing and heaving. The deep stratification only changes the maximum ML depth, and therefore the minimum SST, for the year.

Support for R_{H}, as introduced, to characterize heaving also comes from non-dimensionalizing the temperature equation (5.7). Scaling temperature with $\overline{\Delta T_{sh}}$ — the average seasonal temperature difference at the base of the ML; time with T_{D} — the diurnal period; ML depth/length with $\overline{h_{sh}}$, and integrating $\int_{-h}^{0} dz$ over the mixed layer to obtain an equation for the nondimensional sea-surface temperature

T_s and the entrainment rate w_e (scaled with $\overline{h_{sh}}/T_D$), one obtains

$$\frac{dT_s}{dt} - w_e\frac{\Delta T}{h} + 2\pi R_H \frac{\Delta T}{h}\cos\left(2\pi\frac{T_D}{T_w}t\right) = \frac{Q}{\rho_0 C_p h} \tag{5.13}$$

so it is the heaving number R_H that multiplies the vertical advection term associated with heaving. However, the form of this term indicates that, in addition to R_H, heaving might also depend directly on the nondimensional frequency T_D/T_w. To check this, we present in Figure 5.14 results for ΔT_s^{max}, for 5 pairs of heaving runs. Each pair has the same R_H but different T_D/T_w. Four out of the five pairs show a decrease in ΔT_s^{max} (i.e. less entrainment) with an increase in heaving frequency. The fifth pair has the opposite tendency. However, the variability for a typical two-fold increase in T_D/T_w is 10 percent of ΔT_s^{max} or less. We therefore conclude that R_H alone is reasonably adequate for characterizing heaving in this idealized process study. R_H can be interpreted as a ratio of the total vertical upwards displacement by the waves in a day to $\overline{h_{sh}}$, or as $A_w/\overline{h_{sh}}$ times the number of heaving events in a day.

In order to produce a plot relating heaving to ΔT_s^{max}, the maximum seasonal SST difference between a reference case and a particular heaving case, we scale ΔT_s^{max} with $\overline{\Delta T_{sh}^{ref}}$ — the average seasonal temperature difference at the ML base for the reference case, thus obtaining a non-dimensional maximum SST difference denoted by $\zeta_{\Delta T} = \Delta T_s^{max}/\overline{\Delta T_{sh}^{ref}}$. In addition, to relate background diffusivity to ΔT_s^{max} from the PWP model runs with K_{bg} presented earlier, we

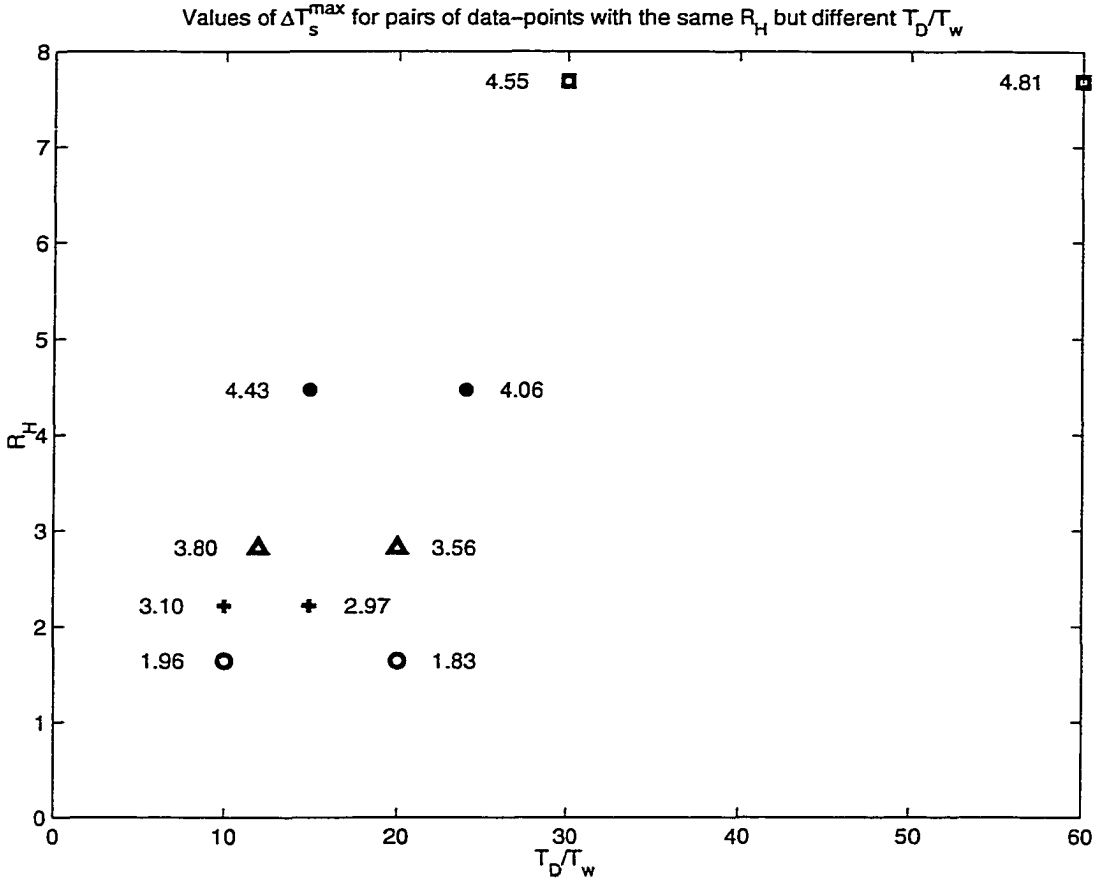

Fig. 5.14. Values of ΔT_s^{max} for pairs of data-points with the same heaving number R_H but different nondimensional frequency T_D/T_w. Pairs of points are denoted by the same symbol. Pairs: "o", $R_H = 1.64$; "+", $R_H = 2.22$; "△", $R_H = 2.82$; "*", $R_H = 4.47$; "□", $R_H = 7.69$.

scale K_{bg} to get a non-dimensional diffusivity

$$R_K = \frac{K_{bg} T_D}{\overline{h_{sh}}^2} \tag{5.14}$$

Figure 5.15 presents the results for the calculated $\zeta_{\Delta T}$ as a function of R_H and R_K for all cases considered. The top panel relates $\zeta_{\Delta T}$ to R_H. Typical heaving numbers then, from model runs, range from 1.5 to 11. For small R_H, up to about 3, the dependence appears to be linear, with a slope of $k_1 \approx 0.6$. Then, from $R_H = 3$ to about 8, one can crudely estimate a proportionality factor $k_2 \approx 0.1$. For heaving numbers larger than 8, $\zeta_{\Delta T}$ appears to be almost insensitive to R_H, so heaving does not result in a significant additional lowering of the SST. The bottom panel relates the non-dimensional diffusivity $\zeta_{\Delta T}$ to R_K. For the calculated values of R_K from 2×10^{-3} to 15×10^{-3}, $\zeta_{\Delta T}$ becomes less sensitive to the background diffusivity as R_K increases.

5.4 Parameterizing heaving for use in mixed layer models

Figure 5.15 related the heaving number R_H and the non-dimensional diffusivity R_K to the scaled maximum seasonal SST difference $\zeta_{\Delta T}$. Using these relationships, we will try to devise a way for ML models without heaving to account for it.

5.4.1 Heaving as an equivalent K_{bg}

$\zeta_{\Delta T}$ shares a similar range of values both as a function of R_H and as a function of R_K. Thus it is possible to calculate a correspondence between R_H and

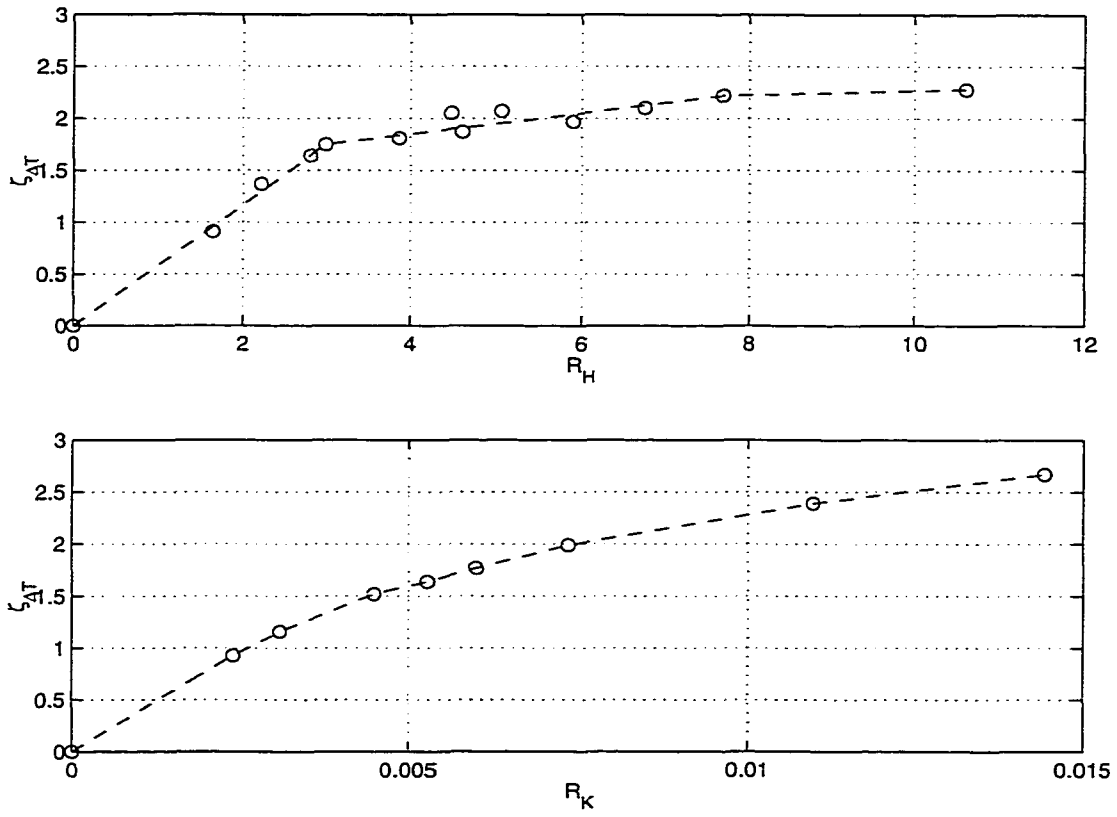

Fig. 5.15. Dependence of the scaled maximum seasonal SST difference $\zeta_{\Delta T}$ on the heaving number R_{H} (top panel), and on the scaled background diffusivity R_{K} (bottom panel), with corresponding interpolated values (dashed lines; in the top panel the dashed line indicates a crude piece-wise linear interpolation).

R_K such that for a given R_H there is a corresponding R_K producing the same $\zeta_{\Delta T}$. This is presented in the top panel of Fig. 5.16. Although there does not appear to be a simple analytical relation between the two, the crude piece-wise linearly interpolated relationship allows one, after estimating a heaving number R_H for a particular location, to obtain an equivalent background diffusivity that best "parameterizes" the heaving, for use in a model. This is done in the bottom panel of Fig. 5.16 where an average dimensional scaling factor to multiply R_K and obtain a dimensional background diffusivity is $1.33 \times 10^{-3} m^2 s^{-1}$, as estimated from model runs with K_{bg}. Subsequently, for a range in R_H from 1.5 to 11, one calculates equivalent K_{bg} in the range from $0.3 \times 10^{-5} m^2 s^{-1}$ to $1.3 \times 10^{-5} m^2 s^{-1}$. These values for K_{bg} certainly appear to be of the same order of magnitude as the background diffusivity values typically used in ML models. We need, however, to estimate characteristic heaving numbers for the locations/datasets that these models simulated so that we can estimate what fraction of the background diffusivities in these models could be attributed to heaving.

Martin (1985), Gaspar *et al.* (1988), Gaspar *et al.* (1990) all simulated OWS Papa data. Information about the internal wave field at Papa can be obtained from data from the MILE experiment in Aug–Sep 1977 near Papa. Dillon and Caldwell (1980) report high-frequency internal wave activity with frequencies from 2.5 cph to 4 cph. Davis *et al.* (1981a) quote a frequency peak at 3 cph from which we can take a typical wave period T_w of 1/3 h. From Levine *et al.* (1983) the amplitude of the internal waves varies from 0.7 to 2.5 metres, therefore we can take a typical A_w of 1–2 m. A typical averaged seasonal thermocline depth $\overline{h_{sh}}$ for Papa appears to be 20–25 metres (Martin 1985). Then a typical, or characteristic,

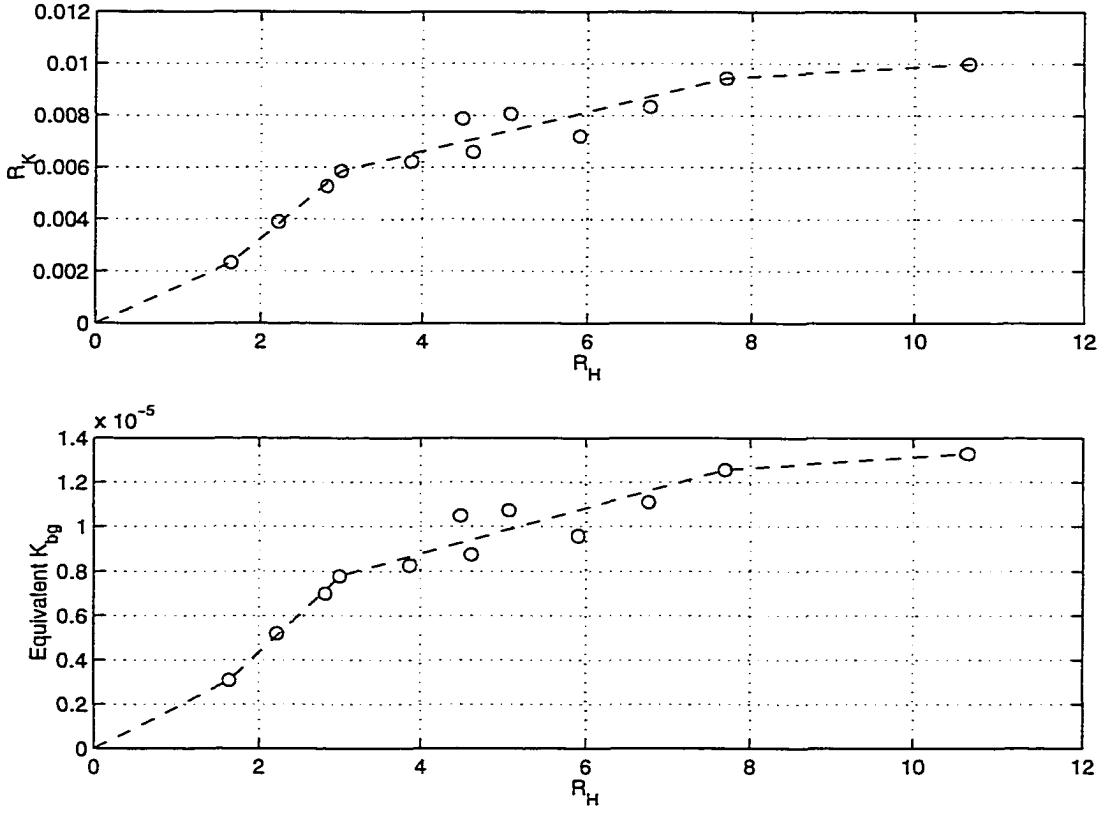

Fig. 5.16. Correspondence between the scaled background diffusivity R_K and the heaving number R_H (top panel), and equivalent background diffusivity K_{bg} (in $m^2 s^{-1}$) as a function of R_H (bottom panel), with corresponding interpolated values (dashed lines, indicating a crude piece-wise linear interpolation).

range at OWS Papa for R_H is 4–6. From the bottom panel of Fig. 5.16, this is equivalent to K_{bg} in the range $0.9 - 1.1 \times 10^{-5} m^2 s^{-1}$.

Kantha and Clayson (1994) simulated data from the LOTUS experiment in 1982 (Briscoe and Weller 1984). Estimates from data yield a range of A_w from 1 to 5 m, and a corresponding frequency range from 0.25 to 1 cph. A typical $\overline{h_{sh}}$ is about 20 metres. Taking T_w of 1–3 h, a characteristic range at LOTUS for R_H is 2–4. From the bottom panel of Fig. 5.16, this is equivalent to K_{bg} in the range $0.4 - 0.9 \times 10^{-5} m^2 s^{-1}$.

Judging from these estimates, it appears that heaving can explain a significant part of the need for background diffusivity as used in ML models.

5.4.2 Heaving as a correction to the dynamic stability criterion

Up to now we used the maximum seasonal SST difference ΔT_s^{max} between a reference case and a heaving or background diffusivity case as the chief indicator of how well or how poorly a model performs in simulating a particular dataset. This was in accordance with previous studies on models' sensitivity to K_{bg} which used ΔT_s^{max} as an indicator. In the previous section we related results from heaving runs to those from diffusivity runs, and proposed a correspondence between the two, whereby for a particular heaving characterized by R_H, an equivalent K_{bg} can be found that would produce the same ΔT_s^{max} when used in a model without heaving.

Going beyond ΔT_s^{max}, one might notice that the seasonal $\mathcal{H} - T_s$ loops from heaving and from K_{bg} model runs have some differences in the way SST evolves through the year despite sharing the same minimum and maximum SST. This

could be seen, for example, by comparing curve (1) from Fig. 5.7 with curve (1) from Fig. 5.5. The loop for the run with background diffusivity is "fatter" — with higher SST in the summer months before $T_s^{\max}$ and lower SST in the fall/winter months before $T_s^{\min}$. The loops from the MY model runs on Fig. 5.3 exhibit the same tendency, so this is not an artefact of the particular model used. Ideally, we would like to find a parameterization for heaving which will not only reproduce the correct $\Delta T_s^{\max}$ but also would match as closely as possible the seasonal SST variability from the heaving runs.

Recall that heaving causes an additional entrainment as it compresses the ML, making it less stable. Whereas the entrainment zone shear stress associated with $|\Delta \mathbf{u}|$ (the magnitude of the velocity jump at the ML base) is one of several available mechanisms which tend to cause entrainment, the only opposing influence on entrainment is that of the stable buoyancy jump Δb, with a velocity scale $(h\Delta b)^{1/2}$, or $(g\alpha\Delta T h)^{1/2}$ in our case. Heaving effectively decreases this scale, resulting in extra entrainment. Thus one other way to account for heaving in a model is to scale down the stability velocity scale $(h\Delta b)^{1/2}$ with a factor dependent on R_{H}. In our PWP model with its bulk Richardson number stability criterion $Rb = h\Delta b/\Delta \mathbf{u}^2 \geq Rb_{\mathrm{cr}}$, scaling down $(h\Delta b)^{1/2}$ will be equivalent to varying Rb_{cr}.

The top panel of Fig. 5.17 presents how the scaled maximum seasonal SST difference $\zeta_{\Delta T}$ varies with the critical Richardson number Rb_{cr}. For $Rb_{\mathrm{cr}} = 0.65$, $\zeta_{\Delta T} = 0$ because this is the critical value for Rb used in the original PWP model, without heaving. Increasing Rb_{cr} up to 4 covers the range for $\zeta_{\Delta T}$ that the heaving

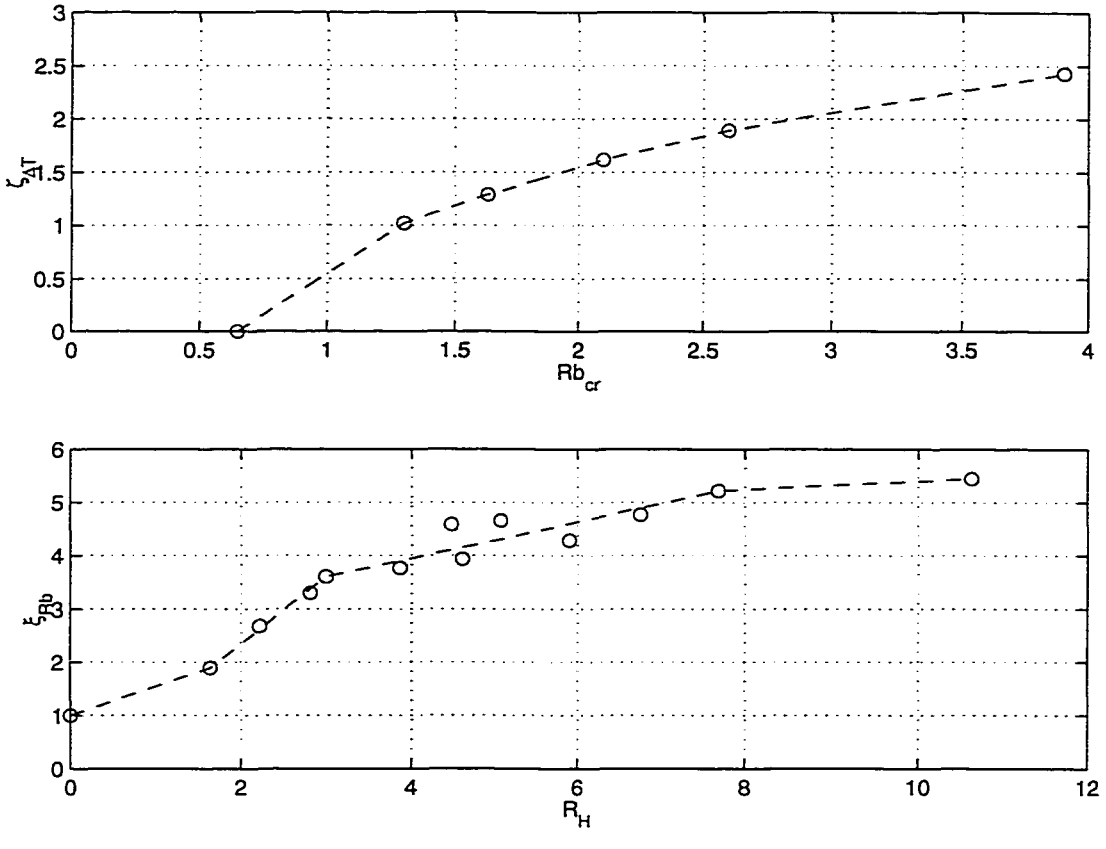

Fig. 5.17. Dependence of the scaled maximum seasonal SST difference $\zeta_{\Delta T}$ on the critical Richardson number Rb_{cr} (top panel), and a correspondence between the stability adjustment factor ξ_{Rb} and the heaving number R_H (bottom panel), with corresponding interpolated values (dashed lines; in the bottom panel the dashed line indicates a crude piece-wise linear interpolation).

and background diffusivity runs have. Let

$$\xi_{\mathrm{Rb}} = \frac{Rb_{\mathrm{cr}}}{0.65} \tag{5.15}$$

be an equivalent stability adjustment factor, dependent on R_{H}, with which to multiply $Rb_{\mathrm{cr}}^{\ ref} = 0.65$ from the reference model run in order to obtain $\Delta T_s^{\ \max}$ as in the heaving run. Using the data from the top panel of Fig. 5.15 we calculate the correspondence between R_{H} and ξ_{Rb}, as shown in the bottom panel of Fig. 5.17 along with a piece-wise linear interpolation. Quite large values ξ_{Rb} can be required in order to achieve $\Delta T_s^{\ \max}$ as in the heaving run, despite the relatively small changes to mixed layer depth h due to heaving, so model output does not seem very sensitive to the value of the critical bulk Richardson number.

In summary, then, for the PWP model a simple parameterization of heaving would be

$$Rb_{\mathrm{cr}} = 0.65\,\xi_{\mathrm{Rb}}, \tag{5.16}$$

where

$$\xi_{\mathrm{Rb}} = f(R_{\mathrm{H}}) \tag{5.17}$$

as shown in Fig. 5.17. For example, let us pick a heaving run with $R_{\mathrm{H}} = 3.0$. A corresponding K_{bg} run would have $K_{\mathrm{bg}} = 0.8 \times 10^{-5} m^2 s^{-1}$. From Fig. 5.17, to $R_{\mathrm{H}} = 3.0$ there corresponds a factor $\xi_{\mathrm{Rb}} = 3.6$, so the scaled critical Richardson number would be $Rb_{\mathrm{cr}} = 2.34$. Fig. 5.18 presents the respective seasonal $\mathcal{H} - T_s$

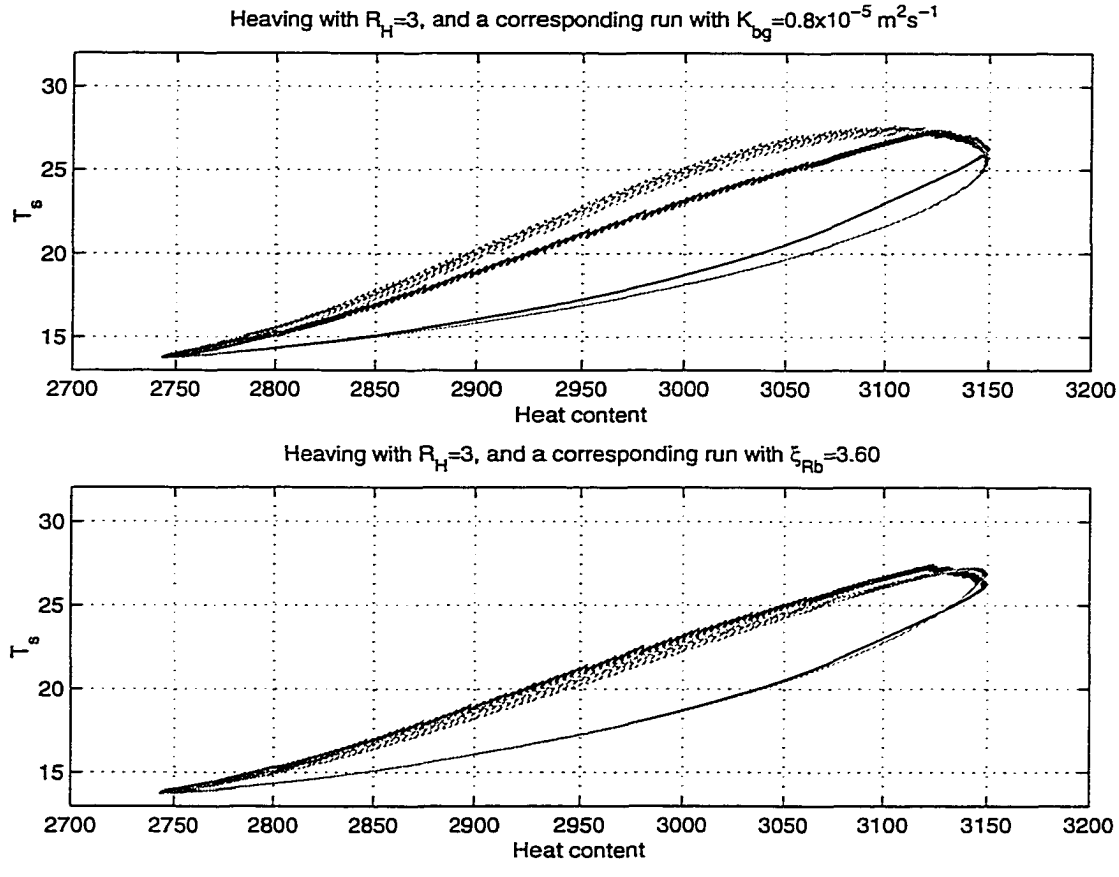

Fig. 5.18. A comparison between seasonal $\mathcal{H} - T_s$ curves for a heaving run (black line) with $R_H = 3.0$ and a diffusivity run with an equivalent background diffusivity of $K_{bg} = 0.8 \times 10^{-5} m^2 s^{-1}$ (top panel). The bottom panel shows a comparison between the same heaving run (black line) and an adjusted critical Richardson number run with the equivalent stability adjustment factor of $\xi_{Rb} = 3.6$.

loops. The K_{bg} run is compared to the heaving run in the top panel, and the curves for the heaving and Rb_{cr} runs are plotted in the bottom panel. Evidently the latter is a better approximation, overall, of the evolution of SST in the heaving run. It also seems more physically appealing given the mechanism by which heaving results in more entrainment.

5.5 Summary and conclusions

Mixed layer models are sensitive to the value of background diffusivity K_{bg} used below the mixed layer. Increasing K_{bg} leads to a deeper ML and lower sea-surface temperature. A typical value used is $1 \times 10^{-5} m^2 s^{-1}$. Models are most sensitive to K_{bg} during summer months — with a shallow ML, and a sharp temperature jump at the ML base. This sensitivity suggests that it is important to establish whether K_{bg} represents mixing processes in the thermocline or is a proxy for processes omitted from models.

One such process is isopycnal heaving in the thermocline due to non-breaking internal waves. Seasonal model runs incorporating idealized heaving show that heaving can produce maximum SST differences ΔT_s^{max} at the end of summer similar to those from a model without heaving but with a background diffusivity.

A detailed look at a three-day period in the summer months reveals that heaving causes additional entrainment of colder water into the ML, thus systematically lowering SST in comparison to a reference, no heaving case. A heaving number R_H to characterize heaving is proposed.

A correspondence between heaving and K_{bg} model runs is calculated, and it is suggested that a parameterization of heaving for use in ML models could involve a heaving number dependent background diffusivity. Equivalent background diffusivity values are calculated for the sites/datasets that previous ML model studies with K_{bg} simulated, showing that the internal wave heaving can explain a significant part of the need for K_{bg} in ML models.

Equivalent K_{bg} runs, despite matching the minimum and maximum seasonal SST for the heaving run, have a somewhat different SST variability in between. Thus a different scheme for parameterizing heaving is presented, involving scaling down the stability velocity scale $(h\Delta b)^{1/2}$. The resulting seasonal $\mathcal{H} - T_s$ curves appear to better simulate, in comparison to the respective equivalent background diffusivity runs, the seasonal evolution of SST from the heaving runs.

In conclusion, the results of this study suggest that heaving can have a considerable effect on mixed layer dynamics, and can explain a significant part of the need for background diffusivity in mixed layer models.

Chapter 6

Outlook

Upper ocean dynamics controls the evolution of sea-surface temperature which in turn influences the surface heat fluxes driving the atmosphere and the ocean. Chemical and biological processes are also sensitive to the variability of the mixed layer and the efficiency of the turbulent transport in the vertical. We therefore need good models of the upper ocean. These require, fundamentally, an understanding of the different physical processes involved and of the way they influence the variability of important parameters such as sea-surface temperature. In this study I have considered three processes that might influence mixed layer dynamics — the effects of the nonlinearity of the equation of state, the role of Langmuir circulation in the deepening of the mixed layer, and the mean effect of isopycnal heaving on ML entrainment.

Including the nonlinearity of the equation of state in ML models leads to a net buoyancy flux and a compensating buoyancy loss via cabbeling; these can be represented simply in terms of the area under the seasonal cycle of sea-surface temperature versus oceanic heat content. The sea-surface temperature, however, does not appear to be significantly affected. The inclusion of a nonlinear equation of state is thus relatively unimportant from the point of view of global variability except when a model uses buoyancy as a state variable instead of temperature and salinity separately. This would result in a spurious buoyancy input.

Langmuir circulation has been long believed to play a crucial role in establishing and maintaining the surface mixed layer. The present study finds some evidence that LC can, under strong wind forcing, overcome the stable stratification at the base of the mixed layer and deepen the ML even when the velocity shear at its base is too small to cause entrainment. This will clearly be very important in the spring months when a new shallow seasonal mixed layer is being established, as strong wind forcing can, via LC, delay the formation of the seasonal thermocline, and in general affect ventilation rates and water mass formation by affecting the evolution of the mixed layer. It is also implied that, in the summer months, strong synoptic forcing could lead to deepening of a shallow mixed layer across a relatively strong thermocline, significantly affecting sea-surface temperature variability. Understanding Langmuir circulation and including or parameterizing its effect in models is therefore important and should lead, in general, to more entrainment and lower sea-surface temperatures.

Isopycnal heaving due to non-breaking internal waves periodically stretches and compresses the mixed layer. An idealized modelling study of this process, simulating heaving by isopycnal motion with a representative internal wave amplitude and a representative internal wave period superimposed on the other variability, shows that heaving can have a mean effect on mixed layer entrainment by causing ML deepening at times when the mixed layer is compressed. The seasonal lowering of the sea-surface temperature, as a consequence of these deepening events, is significant in the spring and summer months, especially at relatively large values of the heaving number R_{H}, i.e. at locations where (i) there is a large seasonal range of surface temperatures reflecting the establishment of a shallow seasonal

mixed layer, (ii) the internal wave amplitude is large, or (iii) the internal wave period is short. Therefore the process of isopycnal heaving appears to be important for sea-surface temperature variability, and this would require including it or parameterizing it in models. Parameterizing heaving in a model by an equivalent background diffusivity K_{bg} below the mixed layer shows that values for K_{bg} typically used in ML models to account for or parameterize the effects of missing or unresolved processes may, to a large extent, be a proxy for heaving. Of course, in situations when there is, for example, a strong shear below the mixed layer, and other processes such as internal wave breaking are active, the required compound background diffusivity representing all these processes may include heaving as only a small part of the total value.

What should we do next in mixed layer modelling?

The dynamics of the mixed layer is sensitive to the surface fluxes that drive it and to the way solar radiation is absorbed in the ocean. Thus one important issue concerns obtaining better, more accurate, measurements of turbulent and radiative fluxes across the ocean-atmosphere interface. Advances in ocean optics are also required to better understand and parameterize oceanic absorption of solar radiation. Better estimates of surface fluxes and light absorption will help differentiate between model errors due to erroneous forcing and errors due to missing or inadequate physics in models.

The upper ocean is, inherently, a nonlinear system. In general, it would respond differently, in a mean sense, if forced by heat and momentum fluxes with some degree of temporal averaging, versus forcing by surface fluxes with the same

mean, but in which the full natural temporal variability has been preserved. A striking example of this involves the characteristic diurnal variability of solar radiation. Model output suggests that the seasonal sea-surface temperature obtained from a model forced with daily-averaged surface fluxes is much different from that from a model resolving the diurnal variability — in the former the seasonal mixed layer remains deep, the surface temperature is much lower as diurnal restratification due to strong solar heating at midday does not occur, and heat cannot be trapped in a shallow daytime layer to cause the sea-surface temperature to increase more rapidly. This sensitivity to resolving the diurnal variation of buoyancy forcing implies that models should either include this variability by employing a small-enough time-step, or parameterize its effect in a suitable way if, as may be in oceanic or coupled general circulation models, time-steps of the order of an hour are not feasible. Analogously for wind forcing, there is some indication that resolving the synoptic variability is important in getting a good agreement in a mean sense between model output and observations. Episodic wind storms, not resolved when forcing a model with daily or monthly wind averages, may cause a rapid ML entrainment and change the sea-surface temperature significantly, affecting its seasonal evolution. Highly-variable wind forcing may also affect profoundly the timing of the seasonal restratification. Further work on the issue of including or accounting for the temporal variability of the forcing in models seems to be needed.

A revealing test of a numerical model's success is a comparison of its output with actual oceanic observations. However, a model could give a good agreement with data for the wrong reasons. As instrumentation and data-acquisition techniques improve, we therefore need to obtain more high-quality data, with better

vertical resolution in the upper ocean in order to test the internal parameterization schemes used. Combined temperature (and salinity where important) and horizontal current profiles provide an opportunity to go beyond simulating the sea-surface temperature or temperature profiles by permitting the testing of the model's parameterizations, as well as allowing indirect validation through analysis of the output.

Finally, and perhaps most importantly, we need to continue the work towards identifying and including pertinent physical processes in mixed layer models. Ultimately, a good model is one that has all the right physics in it.

References

Archer, D., S. Emerson, T. Powell, and C. Wong, 1993: Numerical hindcasting of sea surface pCO_2 at weathership station Papa, *Prog. Oceanogr.*, **32**, 319–351.

Baines, P., 1973: The generation of internal tides by flat-bump topography, *Deep-Sea Res.*, **20**, 179–205.

Baines, P., 1982: On internal tide generation models, *Deep-Sea Res.*, **29**, 307–338.

Batchelor, G., 1967: *An introduction to fluid dynamics*, Cambridge University Press, London and New York, 615 pp.

Bell, T., 1975: Topographically generated internal waves in the open ocean, *J. Geophys. Res.*, **80**, 320–327.

Blackadar, A., 1962: The vertical distribution of wind and turbulent exchange in a neutral atmosphere, *J. Geophys. Res.*, **67**, 3095–3102.

Boussinesq, J., 1903: *Théorie analytique de la chaleur*, Vol. 2, Gaithier–Villars, Paris.

Bowers, C., J. Price, R. Weller, and M. Briscoe, 1986: Data tabulations and analysis of diurnal sea surface temperature variability observed at LOTUS, *Tech. Rep. WHOI-86-5*, 51 pp., Woods Hole Oceanographic Institution, Woods Hole, Masachusetts.

Brainerd, K., and M. Gregg, 1993: Diurnal restratification and turbulence in the oceanic surface mixed layer 1. Observations, *J. Geophys. Res.*, **98**(C12), 22,645–22,656.

Brekhovskikh, L., V. Goncharov, V. Kurtepov, and K. Nangolnykh, 1972: Resonant excitation of internal waves by nonlinear interaction of surface waves, *Izv. Acad. Sci. SSSR Atmos. Oceanic Phys.*, **8**, 112–117.

Briscoe, M., 1975: Preliminary results from the tri-moored internal wave experiment (IWEX), *J. Geophys. Res.*, **80**, 3872–3884.

Briscoe, M., and R. Weller, 1984: Preliminary results from the Long-Term Upper-Ocean Study (LOTUS), *Dyn. Atmos. Oceans*, **8**, 243–265.

Burenkov, V., and A. Vasilkov, 1987: Characteristics of internal waves in the upper thermocline near the Mascarene Ridge, *Oceanology*, **27**, 138–141.

Cox, C., and H. Sandstrom, 1962: Coupling of internal and surface waves in water of variable depth, *J. Oceanogr. Soc. Jap.*, **20**, 499–513.

Craik, A., 1977: The generation of Langmuir circulations by an instability mechanism, *J. Fluid Mech.*, **81**, 209–223.

Crawford, G., 1993: Upper ocean response to storms – a resonant system, Ph.D. thesis, University of British Columbia, Vancouver, Canada.

D'Alessio, S., K. Abdella, and N. McFarlane, 1998: A new second-order turbulence closure scheme for modeling the oceanic mixed layer, *J. Phys. Oceanogr.*, **28**, 1624–1641.

Davis, R., R. de Szoeke, D. Halpern, and P. Niiler, 1981*a*: Variability in the upper ocean during MILE. Part I: The heat and momentum balances, *Deep-Sea Res.*, **28A**(12), 1427–1451.

Davis, R., R. de Szoeke, and P. Niiler, 1981*b*: Variability in the upper ocean during MILE. Part II: Modelling the mixed layer response, *Deep-Sea Res.*, **28A**(12), 1453–1475.

Deardorff, J., 1983: A multi-limit mixed-layer entrainment formulation, *J. Phys. Oceanogr.*, **13**, 988–1002.

Denman, K., and M. Miyake, 1973: Upper layer modification at Ocean Station Papa: observations and simulations, *J. Phys. Oceanogr.*, **3**, 185–196.

Dillon, T., and D. Caldwell, 1980: High-frequency internal waves at Ocean Station P, *J. Geophys. Res.*, **85**(C6), 3277–3284.

Dobson, F., and S. Smith, 1988: Bulk models of radiation at sea, *Quart. J. R. Meteor. Soc.*, **114**, 165–182.

Ellison, T., and J. Turner, 1959: Turbulent entrainment in stratified flows, *J. Fluid Mech.*, **6**, 423–448.

Elsberry, R., and R. Garwood, 1978: Sea-surface temperature anomaly generation in relation to atmospheric storms, *Bull. Amer. Meteor. Soc.*, **59**, 786–789.

Elsberry, R., and S. Raney, 1978: Sea surface temperature response to variations in atmospheric wind forcing, *J. Phys. Oceanogr.*, **8**, 881–887.

Foster, T., 1972: An analysis of the cabbeling instability in sea water, *J. Phys. Oceanogr.*, **2**, 294–301.

Galperin, B., L. Kantha, S. Hassid, and A. Rosati, 1988: A quasi-equilibrium turbulent energy model for geophysical flows, *J. Atmos. Sci.*, **45**, 55–62.

Gargett, A., and G. Holloway, 1984: Dissipation and diffusion by internal wave breaking, *J. Mar. Res.*, **42**, 15–27.

Garrett, C., and E. Horne, 1978: Frontal circulation due to cabbeling and double diffusion, *J. Geophys. Res.*, **83**, 4651–4656.

Garrett, C., and W. Munk, 1975: Space-time scales of internal waves: a progress report, *J. Geophys. Res.*, **80**, 291–297.

Garrett, C., and W. Munk, 1979: Internal waves in the ocean, *Annual Review of Fluid Mechanics*, **11**, 339–369.

Garrett, C., R. Outerbridge, and K. Thompson, 1993: Interannual variability in Mediterranean heat and buoyancy fluxes, *J. Climate*, **6**, 900–910.

Garwood, R., 1977: An oceanic mixed layer model capable of simulating cyclic states, *J. Phys. Oceanogr.*, **7**, 455–468.

Gaspar, P., 1988: Modelling the seasonal cycle of the upper ocean, *J. Phys. Oceanogr.*, **18**, 161–180.

Gaspar, P., Y. Gregoris, and J.-M. Lefevre, 1990: A simple eddy kinetic energy model for simulations of the oceanic vertical mixing: Tests at station Papa and LOTUS site, *J. Geophys. Res.*, **95**, 16,179–16,193.

Gaspar, P., Y. Gregoris, R. Stull, and C. Boissier, 1988: Long-term simulations of upper ocean vertical mixing using models of different types, in *Small-scale turbulence and mixing in the ocean*, vol. 46 of *Elsevier Oceanography Series*, edited by J. Nihoul, and B. Jamart, pp. 169–184, Elsevier, Amsterdam; New York.

Gill, A. E., 1982: *Atmosphere-Ocean Dynamics*, Academic Press, 662 pp.

Gill, A., and J. Turner, 1976: A comparison of seasonal thermocline models with observation, *Deep-Sea Res.*, **23**, 391–401.

Huppert, H., and J. Miles, 1969: Lee waves in a stratified flow. 3. Semi-elliptical obstacle, *J. Fluid Mech.*, **35**, 481–496.

Ivanoff, A., 1977: Oceanic absorption of solar energy, in *Modelling and Prediction of the Upper Layers of the Ocean*, edited by E. B. Kraus, pp. 47–71, Pergamon Press.

Jerlov, N., 1976: *Marine optics*, Elsevier Oceanography Series, Elsevier, Amsterdam, 231 pp.

Kantha, L., and C. Clayson, 1994: An improved mixed layer model for geophysical applications, *J. Geophys. Res.*, **99**, 25,235–25,266.

Käse, R., and R. Clarke, 1978: High frequency internal waves in the upper thermocline during GATE, *Deep-Sea Res.*, **25**, 815–825.

Keller, J., and W. Munk, 1970: Internal wave wakes of a body moving in a stratified fluid, *Phys. Fluids*, **13**, 1425–1431.

Kilmatov, T., and V. Kuzmin, 1991: Effect of cabbeling in the mixing of sea water and its seasonal manifestation on the Pacific ocean subarctic front, *Izvestiya Atm.Oc.Phys.*, **27**, 628–631.

Kolmogoroff, A., 1941: Energy dissipation in locally isotropic turbulence, *Doklady AN SSSR*, **32**, 19–21.

Kraus, E., 1972: *Atmosphere-ocean interaction*, Clarendon Press, Oxford.

Kraus, E., and J. Turner, 1967: A one-dimensional model of the seasonal thermocline. II. The general theory and its consequences, *Tellus*, **XIX**, 98–105.

Krauss, W., 1972*a*: On the response of a stratified ocean to wind and air pressure, *Deut. Hydrogr. Z.*, **25**, 49–61.

Krauss, W., 1972*b*: Wind-generated internal waves and inertial-period motions, *Deut. Hydrogr. Z.*, **25**, 241–250.

Kronenburg, C., 1985: Wind-induced entrainment in a stably stratified fluid, *J. Fluid Mech.*, **145**, 253–273.

Langmuir, I., 1938: Surface motion of water induced by wind, *Science*, **87**, 119–123.

Large, W., and G. Crawford, 1995: Observations and simulations of upper-ocean response to wind events during the Ocean Storms experiment, *J. Phys. Oceanogr.*, **25**, 2831–2852.

Large, W., J. McWilliams, and S. Doney, 1994: Oceanic vertical mixing: A review and a model with a nonlocal boundary layer parameterization, *Reviews of Geophysics*, **32**, 363–403.

Large, W., J. McWilliams, and P. Niiler, 1986: Upper ocean thermal response to strong autumnal forcing of the Northeast Pacific, *J. Phys. Oceanogr.*, **16**, 1524–1550.

Large, W., and S. Pond, 1982: Sensible and latent heat flux observations over the ocean, *J. Phys. Oceanogr.*, **12**, 464–482.

LeBlond, P., 1966: On the damping of internal gravity waves in a continuously stratified ocean, *J. Fluid Mech.*, **25**, 121–142.

Leibovich, S., 1977*a*: Convective instability of stably stratified water in the ocean, *J. Fluid Mech.*, **82**, 561–581.

Leibovich, S., 1977*b*: On the evolution of the system of wind drift currents and Langmuir circulations in the ocean. Part I. Theory and averaged current, *J. Fluid Mech.*, **79**, 715–743.

Leibovich, S., 1983: The form and dynamics of Langmuir circulations, *Annual Review of Fluid Mechanics*, **15**, 391–427.

Leonov, A., and Y. Miropolsky, 1973: Resonant excitation of internal gravity waves in the ocean by atmospheric pressure fluctuations, *Izv. Acad. Sci. SSSR Atmos. Oceanic Phys.*, **9**, 480–485.

Levine, M., R. de Szoeke, and P. Niiler, 1983: Internal waves in the upper ocean during MILE, *J. Phys. Oceanogr.*, **13**, 240–257.

Li, M., and C. Garrett, 1993: Cell merging and the jet/downwelling ratio of Langmuir circulation, *J. Mar. Res.*, **51**, 737–769.

Li, M., and C. Garrett, 1997: Mixed layer deepening due to Langmuir circulation, *J. Phys. Oceanogr.*, **27**, 121–132.

Li, M., K. Zahariev, and C. Garrett, 1995: Role of Langmuir circulation in the deepening of the ocean surface mixed layer, *Science*, **270**, 1955–1957.

Macdonald, A., J. Candela, and H. Bryden, 1994: An estimate of the net heat transport through the Strait of Gibraltar, in *Coastal Estuarine Studies*, vol. 46, edited by P. Violette, AGU, Washington, D.C.

Magaard, L., 1973: On the generation of internal gravity waves by a fluctuating buoyancy flux at the sea surface, *Geophys. Fluid Dyn.*, **5**, 101–111.

Martin, P., 1985: Simulation of the ocean mixed layer at OWS November and Papa with several models, *J. Geophys. Res.*, **90**, 903–916.

Martin, P., 1986: Testing and comparison of several mixed-layer models, *Tech. Rep. NORDA 143*, 30 pp., Naval Research Laboratory, Stennis Space Center, Mississipi.

McComas, C., and F. Bretherton, 1977: Resonant interactions of oceanic internal waves, *J. Geophys. Res.*, **82**, 1397–1412.

McDougall, T., 1984: The relative roles of diapycnal and isopycnal mixing on subsurface water mass conversion, *J. Phys. Oceanogr.*, **14**, 1577–1589.

Mellor, G., and T. Yamada, 1974: A hierarchy of turbulence closure models for planetary boundary layers, *J. Atmos. Sci.*, **31**, 1791–1806.

Mellor, G., and T. Yamada, 1982: Development of a turbulence closure model for geophysical fluid problems, *Rev. Geophys. Space Phys.*, **20**, 851–875.

Millero, F., and A. Poisson, 1981: International one-atmosphere equation of state for sea-water, *Deep-Sea Res.*, **28A**, 625–629.

Mofjeld, H., and J. Lavelle, 1984: Setting the length scale in a second order closure model of the unstratified bottom boundary layer, *J. Phys. Oceanogr.*, **14**, 833–839.

Munk, W., 1981: Internal waves and small-scale processes, in *Evolution of physical oceanography*, edited by B. Warren, and C. Wunsch, pp. 264–291, MIT Press, Cambridge, Massachusetts.

Nansen, F., 1902: Oceanography of the North Pole basin, in *Scientific results of the Norwegian North Polar expedition. 1893–1896*, p. 427pp.

Nesterov, S., 1972: Resonant interaction of surface and internal waves, *Izv. Acad. Sci. SSSR Atmos. Oceanic Phys.*, **8**, 252–254.

Niiler, P. P., 1975: Deepening of the wind-mixed layer, *J. Mar. Res.*, **33**, 405–422.

Niiler, P. P., and E. B. Kraus, 1977: One-dimensional models of the upper ocean, in *Modelling and Prediction of the Upper Layers of the Ocean*, edited by E. B. Kraus, pp. 143–172, Pergamon Press.

Nurser, A., 1996: A review of models and observations of the oceanic mixed layer, *Tech. Rep. ID-14*, 247 pp., Southampton Oceanography Centre, Southampton, UK.

Olbers, D., 1976: Non-linear energy transfer and the energy balance of the internal wave field in the deep ocean, *J. Fluid Mech.*, **74**, 375–379.

Orlanski, I., and K. Bryan, 1969: Formation of the thermocline step structure by large-amplitude internal gravity waves, *J. Geophys. Res.*, **74**, 6975–6983.

Orlanski, I., and B. Ross, 1973: Numerical simulation of the generation and breaking of internal gravity waves, *J. Geophys. Res.*, **78**, 8808–8826.

Paulson, C., and J. Simpson, 1977: Irradiance measurements in the upper ocean, *J. Phys. Oceanogr.*, **7**, 952–956.

Phillips, O., 1977: *The dynamics of the upper ocean*, 2nd edition, Cambridge University Press, 336 pp.

Pinkel, R., 1975: Upper ocean internal wave observations from Flip, *J. Geophys. Res.*, **80**, 3892–3910.

Pinkel, R., and S. Anderson, 1992: Towards a statistical description of finescale strain in the thermocline, *J. Phys. Oceanogr.*, **22**, 773–793.

Plueddemann, A., J. Smith, D. Farmer, R. Weller, W. Crawford, R. Pinkel, S. Vagle, and A. Gnanadesikan, 1996: Structure and variability of Langmuir circulation during the Surface Waves Processes Program, *J. Geophys. Res.*, **101**, 3525–3543.

Plueddemann, A., R. Weller, M. Stramska, and T. Dickey, 1995: Vertical structure of the upper ocean during the Marine Light Mixed Layers experiment, *J. Geophys. Res.*, **100**, 6605–6619.

Pollard, R., 1977: Observations and theories of Langmuir circulations and their role in the near surface mixing, in *A voyage of discovery: George Deacon 70th anniversary volume*, edited by M. Angel, pp. 235–251, Pergamon, New York.

Pollard, R., P. Rhines, and R. Thompson, 1973: The deepening of the wind-mixed layer, *Geophys. Fluid Dyn.*, **3**, 381–404.

Pollard, R., and K. Thomas, 1989: Vertical circulation revealed by diurnal heating of the upper ocean in late winter. Part I: Observations, *J. Phys. Oceanogr.*, **19**, 269–278.

Polyanskaya, V., 1969: The generation of subsurface waves by a plane pressure front moving at constant velocity, *Izv. Acad. Sci. SSSR Atmos. Oceanic Phys.*, **5**, 608–611.

Pomphrey, G., J. Meiss, and K. Watson, 1980: Description of nonlinear internal wave interactions using Langevin methods, *J. Geophys. Res.*, **85**, 1085–1094.

Price, J. F., 1979*a*: Observations of a rain-formed mixed layer, *J. Phys. Oceanogr.*, **9**, 643–649.

Price, J. F., 1979*b*: On the scaling of stress-driven entrainment experiments, *J. Fluid Mech.*, **90**, 509–529.

Price, J., C. Mooers, and J. van Leer, 1978: Observation and simulation of storm-induced mixed-layer deepening, *J. Phys. Oceanogr.*, **8**, 582–599.

Price, J., R. Weller, C. Bowers, and M. Briscoe, 1987: Diurnal response of sea surface temperature observed at the Long-Term Upper-Ocean Study (34°N, 70°W) in the Sargasso Sea, *J. Geophys. Res.*, **92**(C13), 14,480–14,490.

Price, J., R. Weller, and R. Pinkel, 1986: Diurnal cycling: observations and models of the upper ocean in response to diurnal heating, cooling, and wind mixing, *J. Geophys. Res.*, **91**, 8411–8427.

Reed, R., 1977: On estimating insolation over the oceans, *J. Phys. Oceanogr.*, **7**, 482–485.

Richman, J., and C. Garrett, 1977: The transfer of energy and momentum by the wind to the surface mixed layer, *J. Phys. Oceanogr.*, **7**, 876–881.

Schudlich, R., and J. Price, 1992: Diurnal cycles of current, temperature, and turbulent dissipation in a model of the equatorial upper ocean, *J. Geophys. Res.*, **97**, 5409–5422.

Simpson, J., and T. Dickey, 1981: Alternative parameterizations of downward irradiance and their dynamical significance, *J. Phys. Oceanogr.*, **11**, 876–882.

Skyllingstad, E., and D. Denbo, 1995: An ocean large eddy simulation of Langmuir circulations and convection within the surface mixed layer, *J. Geophys. Res.*, **100**, 8501–8522.

Smith, J., R. Pinkel, and R. Weller, 1987: Velocity structure in the mixed layer during MILDEX, *J. Phys. Oceanogr.*, **17**, 425–439.

Smith, J., 1992: Observed growth of Langmuir circulation, *J. Geophys. Res.*, **97**, 5651–5664.

Smith, S., 1980: Wind stress and heat flux over the ocean in gale force winds, *J. Phys. Oceanogr.*, **10**, 709–726.

Smith, S., 1988: Coefficients for sea surface wind stress, heat flux, and wind profiles as a function of wind speed and temperature, *J. Geophys. Res.*, **93**, 15,467–15,472.

Spiegel, E., and G. Veronis, 1960: On the Boussinesq approximation for a compressible fluid, *Astrophys. J.*, **131**, 442–447.

Stommel, H., K. Sanders, W. Simmons, and J. Cooper, 1969: Observations of the diurnal thermocline, *Deep-Sea Res.*, **16**, 269–284.

Stramma, L., P. Cornillon, R. Weller, J. Price, and M. Briscoe, 1986: Large diurnal sea surface temperature variability: Satellite and in situ measurements, *J. Phys. Oceanogr.*, **16**, 827–837.

Stull, R., 1976: The energetics of entrainment across a density interface, *J. Atmos. Sci.*, **33**, 1260–1267.

Tabata, S., 1965: Variability of oceanographic conditions at Ocean Station "P" in the northeast Pacific Ocean, *Trans. Royal Soc. Canada*, **III**, 367–418.

Taylor, G., 1916: Conditions at the surface of a hot body exposed to the wind, *Brit. Adv. Com. Aero. Rep. Memor.*, p. 272.

Thorpe, S., 1966: On wave interactions in a stratified fluid, *J. Fluid Mech.*, **24**, 737–751.

Thorpe, S., 1973: Experiments on instability and turbulence in a stably stratified shear flow, *J. Fluid Mech.*, **61**, 731–751.

Thorpe, S., 1975: The excitation, dissipation, and interaction of internal waves in the deep ocean, *J. Geophys. Res.*, **80**, 328–338.

Thorpe, S., 1985: Small-scale processes in the upper ocean boundary layer, *Nature*, **318**, 519–522.

Tomczak, M., 1966: Winderzeugte interne wellen, insbesondere im periodenbereich oberhalb der trägheitsperiode, *Deut. Hydrogr. Z.*, **19**, 1–21.

Tomczak, M., 1967: Über den einfluss fluktuierender windfelder auf ein stetig geschichtetes meer, *Deut. Hydrogr. Z.*, **20**, 101–129.

Weller, R., and A. Plueddemann, 1996: Observations of the vertical structure of the oceanic boundary layer, *J. Geophys. Res.*, **101**, 8789–8806.

Weller, R., and J. Price, 1988: Langmuir circulation within the oceanic mixed layer, *Deep-Sea Res.*, **35**, 711–747.

Witte, E., 1902: Zur theorie der stromkabbelungen, *Gaea, Köln*, pp. 484–487.

Woods, J. D., 1980: Diurnal and seasonal variation of convection in the wind–mixed layer of the ocean, *Quart. J. R. Meteor. Soc.*, **106**, 379–394.

Woods, J. D., and W. Barkmann, 1986: The response of the upper ocean to solar heating. I: The mixed layer, *Quart. J. R. Meteor. Soc.*, **112**, 1–27.

Woods, J. D., W. Barkmann, and A. Horch, 1984: Solar heating of the oceans – diurnal, seasonal and meridional variation, *Quart. J. R. Meteor. Soc.*, **110**, 633–656.

Yelland, M., and P. Taylor, 1996: Wind stress measurements from the open ocean, *J. Phys. Oceanogr.*, **26**, 541–558.

Zahariev, K., and C. Garrett, 1997: An apparent surface buoyancy flux associated with the nonlinearity of the equation of state, *JPO*, **27**, 362–368.